CALIFORNIA INSTITUTE OF TECHNOLOGY

EARTHQUAKE ENGINEERING RESEARCH LABORATORY

PROBABILISTIC ROBUST CONTROL: THEORY AND APPLICATIONS

BY

B. SCOTT MAY

REPORT NO. EERL 97-08

PASADENA, CALIFORNIA

1997

A REPORT ON RESEARCH PARTIALLY SUPPORTED BY A SUBCONTRACT FROM THE UNIVERSITY OF MINNESOTA UNDER NSF GRANT CMS-9503370 AND THE EARTHQUAKE RESEARCH AFFILIATES PROGRAM OF CALTECH UNDER THE SUPERVISION OF JAMES L. BECK

Probabilistic Robust Control: Theory and Applications

Thesis by
B. Scott May

In Partial Fulfillment of the Requirements
for the Degree of
Doctor of Philosophy

California Institute of Technology
Pasadena, California

(Defended July 18, 1997)

Acknowledgements

Writing a thesis is hard work, and I have several people to acknowledge who helped out in one way or another. First, I'd like to thank my committee, who, through their lively discussions, helped to make the thesis better. The committee consisted of Tom Caughey, John Hall, Bill Iwan, John Doyle, and Jim Beck. In particular, John Doyle's outside perspective on the civil engineering aspects of the work was appreciated.

I'd like to thank my advisor, Jim Beck, for going a little outside his established field and making the thesis possible. Also, my thanks go to the the National Science Foundation for their financial support.

And finally, I have several people I'd like to thank for making the whole process more enjoyable. First, my office mates, Dave, Anders, and Mike, who provided a steady source of discussion and distraction. Second, my training partner John, who provided a steady source of trash talking (when he wasn't too far behind to be heard). And finally, Vicki, who helped to keep me happy, focused, and on track.

Abstract

In this work, the development of a probabilistic approach to robust control is motivated by structural control applications in civil engineering. Often in civil structural applications, a system's performance is specified in terms of its reliability. In addition, the model and input uncertainty for the system may be described most appropriately using probabilistic or "soft" bounds on the model and input sets. The probabilistic robust control methodology contrasts with existing $\mathcal{H}_\infty/\mu$ robust control methodologies that do not use probability information for the model and input uncertainty sets, yielding only the guaranteed (i.e., "worst-case") system performance, and no information about the system's probable performance which would be of interest to civil engineers.

The design objective for the probabilistic robust controller is to maximize the reliability of the uncertain structure/controller system for a probabilistically-described uncertain excitation. The robust performance is computed for a set of possible models by weighting the conditional performance probability for a particular model by the probability of that model, then integrating over the set of possible models. This integration is accomplished efficiently using an asymptotic approximation. The probable performance can be optimized numerically over the class of allowable controllers to find the optimal controller. Also, if structural response data becomes available from a controlled structure, its probable performance can easily be updated using Bayes's Theorem to update the probability distribution over the set of possible models. An updated optimal controller can then be produced, if desired, by following the original procedure. Thus, the probabilistic framework integrates system identification and robust control in a natural manner.

The probabilistic robust control methodology is applied to two systems in this thesis. The first is a high-fidelity computer model of a benchmark structural control laboratory experiment. For this application, uncertainty in the input model only is considered. The probabilistic control design minimizes the failure probability of the benchmark system while remaining robust with respect to the input model uncertainty. The performance of an optimal low-order controller compares favorably

with higher-order controllers for the same benchmark system which are based on other approaches. The second application is to the Caltech Flexible Structure, which is a light-weight aluminum truss structure actuated by three voice coil actuators. A controller is designed to minimize the failure probability for a nominal model of this system. Furthermore, the method for updating the model-based performance calculation given new response data from the system is illustrated.

Contents

List of Figures

List of Tables

Chapter 1

Introduction

1.1 Objective

A useful question to ask when analyzing the performance of a civil engineering structure is

*What is the **probable performance** of the structure?*

Civil engineers, building owners, and insurance companies often define the performance of a particular structure using its *reliability*, which is the probability that the response of the structure remains within a specified "safe" region over a time interval of interest (typically the desired lifetime of the building). The reliability of a structure is used throughout this thesis to evaluate the performance of civil engineering systems.

The uncertainties that are inherent in the models developed for the structural system and its disturbance should be addressed in a probabilistic manner in order to achieve an estimate of the structure's *probable performance*. The structural model can be constructed using traditional analysis tools. However, this model is necessarily uncertain, as it is a simplified, finite-order mathematical representation of a complex physical system. Through application of Bayesian system identification techniques, first-principles modeling, or other methods, a probability model can be assigned to this model uncertainty, so the relative probabilities of the uncertain models can be considered when evaluating the performance.

The environmental disturbances that may act on the structure during its lifetime are also uncertain. The disturbances are often described by stochastic processes, where the probability models for the processes are assigned using a combination of statistical data and first-principles modeling of the underlying causes of the processes.

Once the *probable performance* of a system has been determined, a second question that can be asked is

> *For this structural system, how can its performance be improved given a set of allowable improvements that could be made to the system?*

This is the prototypical question of control system design, and requires optimizing a measure of the system performance over the class of permissible controllers. In this case, the performance measure is the probable performance of the uncertain system, and the controller class is the set of possible improvements that could be made to the structure. Examples of the types of *improvements* that could be considered include optimizing the structural design, selecting the dimensions and material properties of passive energy dissipating elements, and designing a feedback control loop for an active element in the system.

The above questions, and hence the objective, are different from the typical questions asked in control analysis and synthesis, and are the appropriate questions to ask for structural engineering applications. The objective of the probabilistic robust control research is to answer these questions by

> *developing a consistent probability-based approach for the analysis and design of controllers for uncertain structural systems.*

The analysis methods that are developed in this thesis can be used to estimate the failure probability for an uncertain system. This failure probability can then be used as a control-design objective function, and probability-based controller design requires minimizing the calculated failure probability. After illustrating the concepts using a simple system, the controller design method is applied to two structural

control problems. The first is a "benchmark" computer model of a laboratory system, and the second is a flexible laboratory structure.

The method that is developed for *probabilistic robust control* will be seen to have certain advantages over existing techniques. For one, obtaining the probable robust performance of the system adds an "extra dimension" to the robust analysis of uncertain systems, as probability information about the uncertainties can be included in the analyses. Second, probabilistic performance measures, such as the system's failure probability, can be used, which are often of interest in civil engineering applications. Finally, descriptions of the probabilities of the uncertain models in the performance analysis and controller design can be updated in a simple fashion. This allows for updating the performance analysis and the control design in the presence of new data from the system, hence combining system identification and robust control under this probabilistic formulation.

1.2 Motivation and background

1.2.1 Structural control

Passive, semi-active, and active methods of vibration control in civil engineering structures are currently receiving much interest (Housner et al. 1994; Soong 1990), as evidenced by the increasing number of conference sessions, workshops (Housner and Masri 1993; Housner 1992; Housner and Masri 1990), special journal issues (Housner et al. 1997; Spencer 1997), and even an entire conference (Housner et al. 1994) devoted to the topic of structural control. These control methods seek to reduce the vibration response of a structure to dynamic loading events such as earthquakes or high winds.

Structural control objectives can be divided into *serviceability* and *life safety* categories. The serviceability objective is to minimize the disruption in service of a structure during a dynamic loading event. In this case, either the disturbance is sufficiently large, the structure is sufficiently flexible, or the equipment housed in the structure is sufficiently sensitive to render the structure unusable for (at least) the

duration of the event. In general, when determining a structure's serviceability, the disturbances that are considered are not so large that the integrity of the structure or the safety of the occupants are threatened. One application where serviceability might not be met would be in a flexible high-rise structure where the occupants experience discomfort during episodes of high wind. In addition, measures of a structure's overall economic performance are often included in the serviceability objective. For the economic performance, determining damage to non-structural components such as building cladding and interior components is of interest. Damage to non-structural components during a dynamic loading event can be equally as expensive as structural damage, and hence also undesirable from an owner's or insurer's perspective.

The life-safety objective is to minimize the threat of physical harm to a structure's occupants by preventing collapse, while perhaps allowing a significant level of damage to the structure's load-bearing members as well as its non-structural components. Life safety can be threatened by extreme dynamic disturbances such as large earthquakes or very high winds.

Under earthquake excitations, where the events are infrequent, unpredictable, and of relatively short duration, the control design objectives could include improving life safety for the occupants by reducing the risk of structural collapse during severe earthquakes, and reducing the level of structural and non-structural damage during more moderate events.

The application of active control to structures under earthquake excitation is considered for structural control examples throughout this thesis. The objective that is used will be to reduce the level of structural damage to improve the structure's performance during an earthquake, consequently improving life safety.

1.2.2 Uncertainty in modeling

Engineers construct parameterized models of physical systems in order to predict and describe their behavior. In civil engineering, these models are typically finite-order ordinary differential equations, although they may be linear or nonlinear, and

have two or three spatial dimensions. The models can be created from first-principles modeling, such as from finite element modeling (Cook et al. 1989) or matrix structural analysis methods (Sack 1989), or from system identification techniques (Beck 1996; Söderström and Stoica 1989). The goal of any modeling method is to choose a model from within a model class that is being used to model the system, where that model minimizes some measure of fit between the measured and predicted response of the system.

Regardless of their origins in theory, the model is at some level an approximation of the physical system's performance. Many of the model parameters used to describe the system are uncertain. Non-parametric modeling error exists as well, which accounts for the differences between any model within the assumed model class and the physical system that the models represent. When the modeling errors are significant (or the performance demands of the system are very stringent), the model uncertainty should be addressed when attempting to analyze the physical system's behavior.

For control of structures during earthquakes, the response of the structure is difficult to model accurately for several reasons. The structural response levels due to forced or ambient vibration field tests, which are used to calibrate a mathematical model of the structure, are orders of magnitude smaller than the vibration levels encountered during even a moderate earthquake. The natural periods of the building (and hence its stiffness) are typically observed to decrease quite significantly with increasing input amplitude, although linear models of the building response are generally appropriate at both excitation levels (provided the excitation is not so large that the structural members begin to yield). As a further complication, at the high vibration levels caused by major earthquakes, the building response evidences significant nonlinear behavior as the structural members yield and eventually deteriorate in an often unpredictable manner. The presence of significant uncertainty in the building models presents a compelling argument for including the model uncertainty in the analysis and control design methods that are used.

1.2.3 Norm-bounded robust control

With current linear robust analysis methods, such as $\mathcal{H}_\infty$ and μ analysis techniques (Zhou et al. 1996), uncertainty sets and inputs that are bounded by operator norms are considered. These analysis methods yield the "worst-case" performance of a particular system. This worst-case performance is usually realized only by a single member of the uncertain model set, as well as by the particular input signal that yields the most pessimistic value of the performance measure. No information results from the μ-analysis methods regarding the likelihood that this worst-case model will describe the system's "true" performance, or the likelihood that the worst-case input will ever occur in practice.

Modern norm-bounded robust control methods have two limitations when applied to determining the performance of a structure. The first is that the robust analysis yields only the worst-case performance of the system, with no information as to the probability that this will be the actual system performance. Hence, the worst-case may be overly conservative for most of the models in the uncertainty set. The second limitation is that the model uncertainty may be more naturally described using "soft" (or probabilistic) bounds, rather than the "hard" bounds that result from using the operator norms. One large advantage of the norm-bounded approach is that it is well established and is generally computationally efficient. In addition, recent advances in robust-$\mathcal{H}_2$ analysis (Paganini 1996) allow for a less conservative class of inputs to be considered, where the input signals must satisfy a statistical test for white noise, rather than the single-frequency $\mathcal{H}_\infty$ worst-case input (Doyle et al. 1992). This technique might be promising for robust analysis of civil engineering systems, where white noise, which is perhaps colored by a linear filter, is often used to model the input.

Several examples exist of the application of robust control methods to control of large structures under earthquake excitations. See Yang et al. (1994) for $\mathcal{H}_\infty$ and sliding mode control for a laboratory test structure, Smith and Chase (1994) for $\mathcal{H}_\infty$ control of structures with time-varying uncertainties, and Yoshida and Watanabe (1994) for $\mathcal{H}_\infty$ and μ-synthesis control design for a building model.

1.2.4 Probabilistic robust control

A probabilistic approach to the robust analysis of an uncertain system is able to address the probable system performance, rather than the worst case, while still considering model uncertainty and allowing the use of soft bounds on the model uncertainty sets, if desired. By computing the *probable* performance of the system, the highly unlikely members of the uncertain model class that indicate bad performance will not dominate the overall calculated performance. However, if the bad models that do exist have significant probability associated with them, they would have a strong influence on the probable performance.

In addition, a probabilistic interpretation of the model uncertainty class can be used to provide an "added dimension" (a probabilistic one) to the model uncertainty class and for the interpretation of the calculated performance. In this manner, models within the class of possible models that are more likely to predict the behavior of the system receive more weight in the performance calculation, and models that are quite unlikely receive less weight.

Finally, a probabilistic approach to robust control permits the incorporation of data obtained from the system in order to update the probability over the model uncertainty set. For example, the original probability distributions for the uncertain model class can be quantified using first-principles modeling and engineering judgment. Then, Bayesian system identification (system ID) techniques can be applied to response data from the system to update the probabilistic description of the uncertain models (Beck 1996; Beck and Katafygiotis 1998).

The probabilistic stability of an uncertain system has been investigated previously by Stengel and Ray (1991), using Monte Carlo methods to estimate the probability of instability given parametric uncertainty in a system. Marrison and Stengel (1995) then developed a method for controller synthesis design based on numerical optimization of the performance that is estimated from the Monte Carlo methods.

Spencer et al. (1994) and Field et al. (1995) have investigated methods to compute the reliability of an uncertain system. In addition, controller design methods

that use this reliability as an objective function have been investigated by Spencer and Kaspari (1994a) and Spencer and Kaspari (1994b).

1.3 Thesis organization

The current chapter has introduced and motivated the probabilistic robust control problem. In addition, some of the current work in structural control, norm-bounded robust control, and probabilistic approaches to robust control have been highlighted.

The second chapter introduces the analysis theory for determining the probable performance of an uncertain structural system, which is then used as the objective function for control design in Chapter 3. A simple example is used throughout the chapter to highlight the various points of the theory.

In Chapter 3, the controller design optimization problem is presented. The simple example is continued here to illustrate the design methodology. Also included in this chapter is a method for updating the performance calculation (and hence the controller design) using response data from the system. In addition, an alternative formulation of the performance calculation in discrete time is developed, which provides another method for computing the reliability of the system and allows for the design of controllers with dynamics.

The fourth chapter describes the application of the probabilistic robust control methodology to a benchmark structural control problem. The chapter describes the benchmark problem and the controllers that are designed for the system.

Chapter 5 focuses on the application of the control methodology to the Caltech flexible structure. A detailed description of the laboratory structure and the system identification used to develop a model for the system are presented. Controllers are designed for this system using the probable robust performance objective function.

The final chapter provides conclusions, analysis of the impact of the work, and several suggested directions for further research of the probabilistic robust control methodology.

Chapter 2

Probabilistic robust analysis theory

2.1 Introduction and preliminary material

2.1.1 Chapter overview

This chapter outlines the basic elements of the theory that has been developed for the probabilistic robust analysis portion of the probabilistic robust control methodology. The elements of the theory that are discussed in the following four sections are

- the probabilistic performance objective,
- the description of the model uncertainty,
- the calculation of the probabilistic performance for an uncertain system.

Chapter 3 will discuss how to optimize this performance over the class of controllers that might be considered for the system. The primary performance measure used in this chapter and the next is the system reliability. In addition, $\mathcal{H}_2$ and $\mathcal{H}_\infty$ performance measures, which are the measures most commonly used in the controls community, are also considered and are shown for comparison with the reliability-based performance measure.

2.1.2 Illustrative example

A simple example will be used in this chapter and the next to illustrate the basic principles of probabilistic robust control theory. This example is a finite element

model of a two-story special-moment-resisting-frame (SMRF) building that is "designed" to satisfy the lateral drift guidelines under earthquake loads found in the 1994 Uniform Building Code (UBC). The design drift level is $0.03/Rw = 0.0025$, where $R_w = 12$ for a SMRF building. A schematic of a single bay of this two-story steel-frame structure is shown in Figure 2.1. A summary of the model used to approximate this example building is given in this chapter, while a more detailed explanation of the design procedure is located in Appendix A.

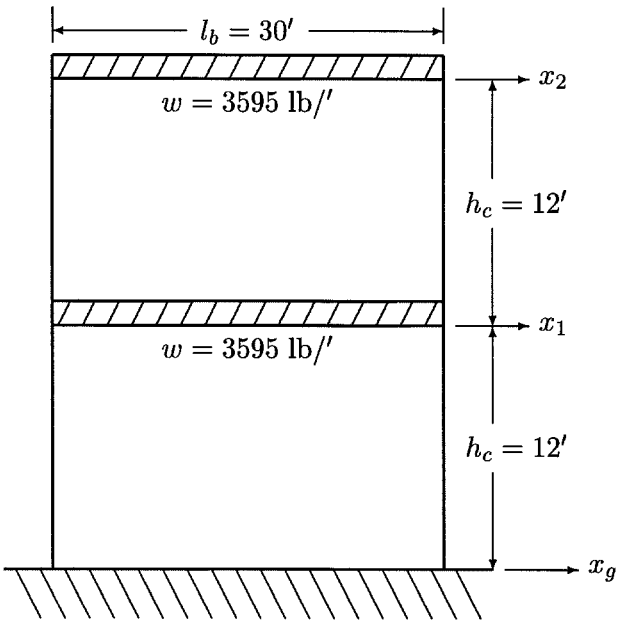

Figure 2.1 Two-story steel frame building.

In summary, the design procedure requires first estimating the vertical load on the building from its own weight and assuming typical loading conditions, then estimating the lateral forces that might occur during a "typical" earthquake, next approximating the distribution of moments in the beams and columns at the connections using a simple analysis technique such as the portal method. Finally, the beam and column moments of inertia necessary to provide adequate inter-story

drift performance can be selected. A subsequent analysis is then performed to ensure that the selected moments of inertia satisfy the lateral drift requirement, and the design is repeated if necessary. The steps followed in this procedure are detailed in Appendix A. The beam and column moments of inertia are shown in Table 2.1, along with the inter-story drift ratio under the design static lateral load. Note that the inter-story drift ratios are identical for the two stories, which was the goal of the design procedure. This was done so the drift response in each story would be comparable, which leads to a more interesting performance analysis.

Table 2.1 Beam and column moments-of-inertia for two-story example.

Floor	I_b	I_c	φ
	(in^4)	(in^4)	(drift ratio)
1	1347	754	1.12×10^{-3}
2	1306	1219	1.12×10^{-3}

A schematic representation of the 2DOF model corresponding to this two-story structure is pictured in Figure 2.2. Linear viscous damping at two percent of critical for each mode is chosen to approximate the damping, and so the model response can be expressed using classical normal modes (Caughey and O'Kelly 1965). This value is chosen as a typical value for the damping ratio that is used for modeling steel-frame buildings, which tend to be lightly damped. The mass, damping, and stiffness matrices for the reduced-order model of the example are provided in Appendix A, and the periods, damping ratios, and modeshape components are given in Table 2.2. Note that later in this chapter these model parameters will be considered uncertain, but for now they are considered known and treated as "nominal" parameters.

2.1.3 Representation of linear systems

This section describes some of the notation that is used throughout the thesis to describe dynamical systems in general and linear systems in particular. The input-output relationships of a dynamical system are often represented with a block dia-

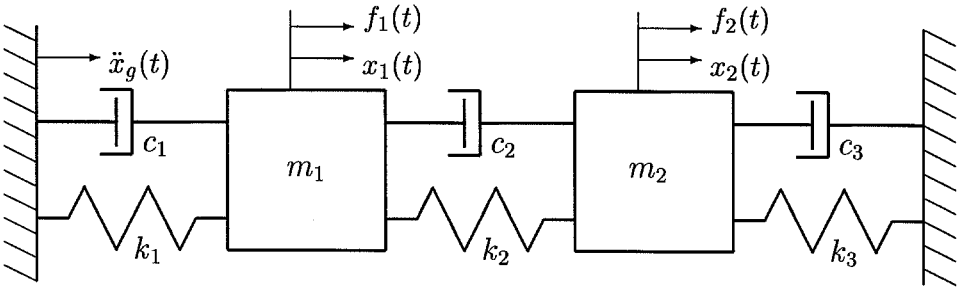

Figure 2.2 Representation of 2DOF system.

Table 2.2 Modal properties for two-story example.

Mode	Period	Frequency	Damping	Modeshape[a]	
	(sec.)	(Hz)	(%)	$\phi_1^{(r)}$	$\phi_2^{(r)}$
1	0.542	1.84	2.0	0.448	0.894
2	0.153	6.56	2.0	0.894	−0.448

[a] $\phi_i^{(r)}$ represents the i^{th} component of the r^{th} modeshape vector.

gram such as the one shown in Figure 2.3, where the inputs to the system are given by the vector w and the system outputs are given by y.

To simplify notation throughout this thesis, no distinction will be made between the time domain representation of a stable linear system and its Laplace or frequency domain representation. For example, in the time domain, let G represent the state-space system given by the first-order linear differential equation

$$G := \left[\begin{array}{c|c} A & B \\ \hline C & D \end{array}\right] = \left\{\begin{array}{l} \dot{x} = Ax + Bw \\ \\ y = Cx + Dw. \end{array}\right\} \tag{2.1}$$

where w is an exogenous disturbance and y is the vector of output variables. In the

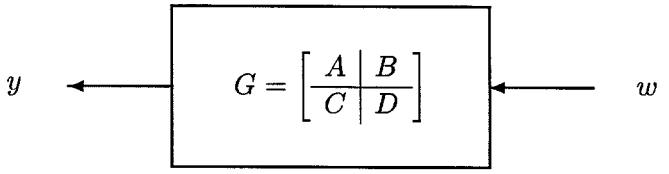

Figure 2.3 Linear system representation.

Laplace domain, G is the transfer function given by

$$G := \left[\begin{array}{c|c} A & B \\ \hline C & D \end{array}\right] = C(sI - A)^{-1}B + D. \tag{2.2}$$

Given this notation, w and y will typically represent members of the Lebesgue space $\mathcal{L}_2(0, \infty)$ in their time-domain incarnation, or members of the Hardy space $\mathcal{H}_2$ in the frequency domain[1] ($\mathcal{H}_2$ is the space of functions that are bounded in the square integrable sense on the imaginary axis, with analytic continuation into the right half plane).

2.2 Performance measure

2.2.1 Definition of "performance"

The *performance* of a civil engineering structure is a measure of that structure's effectiveness in satisfying its design objectives, where the performance is quantified using the system's predicted response quantities. Numerous performance measures are possible, such as estimates of the system's maximum response to a set of specified inputs or its mean-square response to random excitation. The response quantities that are generally used to calculate the performance of a structure are the relative drift ratios between stories, the absolute acceleration at different points in the structure, and the magnitude of the base shear between the structure and its foundation.

[1]This convention is also adopted in Doyle et al. (1989) and other locations in the modern robust control literature.

Structural engineers interested in the behavior of buildings during earthquakes are typically interested in whether the structure will collapse, cause harm to the occupants, or experience significant economic loss due to an earthquake. Hence, performance variables are selected that can be used to quantify the existence or extent of these types of damage. Under seismic excitation, excessive inter-story drift has been observed to correlate strongly with damage in structures, and this is the response quantity that is used in the performance analyses contained in this thesis.

The performance can be defined as the probability that the system does not exceed a specified level of response when subjected to random excitation. This performance measure is termed the structural *reliability*. While difficult to compute, the reliability of a structure is of great interest to structural engineers (and others). The reliability calculation (or its complement, the failure probability) is the main focus of this section, although some of the other performance measures mentioned above will be examined as well.

2.2.2 Reliability-based performance measures

The system's performance can be measured probabilistically by considering its *reliability*. The reliability of a system is defined as the probability that the system response will remain satisfactory when the system is subject to excitation(s) from a class of possible excitations.

For a building subject to dynamic excitation, *satisfactory performance* occurs when the response level of the building does not exceed the failure level for any *failure mode*. A failure mode is defined as the level of response that indicates that the building has suffered significant damage, perhaps caused harm to the occupants, or even collapsed. The probability that the response of the system does not exceed these maximum levels over a time period of interest is the reliability. Note that in this thesis, the complement of the reliability, termed the *failure probability*, will be used as the performance measure. This is done to simplify the representation of the performance, as small failure probabilities can be displayed using scientific notation,

while high reliabilities (i.e., reliability very close to one) require many decimal places for representation.

A response variable that correlates strongly with structural damage is the inter-story drift ratio. In general, significant structural damage occurs when the inter-story drift ratio exceeds 2-3% of the story height. The reliability calculation requires computing the probability that this inter-story drift ratio remains less than its maximum value. Other potential failure modes in buildings include exceeding the maximum allowable base shear and exceeding acceptable absolute acceleration levels.

Failure modes that are defined in terms of mean-square response quantities are typically fatigue-related, and are hence a function of the total energy absorbed by the building. These failure modes are of primary interest when the building is subjected to wind, traffic, or other forms of persistent excitation. Fatigue-related failure modes are generally less of a problem for (relatively) short-duration earthquake excitations than the other possibilities for failure.

The region in response variable space where failure is defined to occur is the *failure region*, the complement of this region is the *safe region*, and the boundary between these two regions is the *failure surface*. An illustration of a three-dimensional failure surface is shown in Figure 2.4, which corresponds to the ∞-norm on z_i, where z_i represents the response quantities used to monitor the system performance for failure mode i. The β_i's represent the failure threshold for each of the N_f failure modes $i \in \{1, 2, \ldots, N_f\}$. The safe region is defined by

$$\mathcal{S} := \left\{ \max_i (|z_i(t)|) \leq \beta_i,\ i \in \{1, \ldots, N_f\} \text{ for } t \in [0, T] \right\}. \tag{2.3}$$

Calculating the reliability requires determining the probability that the response variables are in the safe region. The reliability is denoted by

$$\mathcal{P}_R := \mathcal{P}(\mathcal{S}|\boldsymbol{\Theta}), \tag{2.4}$$

where the probability that the response is in the safe region is conditional on a

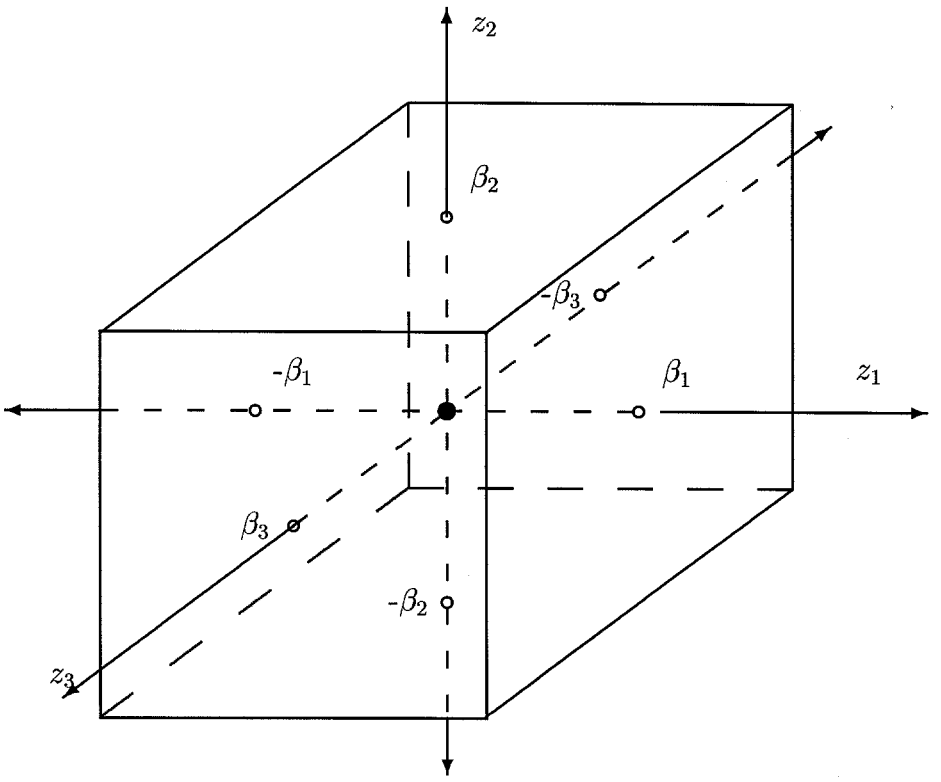

Figure 2.4 Safe region in response-variable space.

particular model or class of models for the system. The model or class of possible models chosen for the system is represented symbolically by Θ, and the conditioning of the reliability on the model(s) is represented by $\mathcal{P}_R(\cdot|\Theta)$. Note that the failure probability is given by

$$\mathcal{P}_F := 1 - \mathcal{P}_R. \tag{2.5}$$

2.2.3 Reliability for first-passage type failures

A particular class of failures, termed "first-passage" failures, arises when calculating the probability that the dynamic response of the system remains within a "safe"

region over a specified interval. The reliability of such a system is denoted by

$$\mathcal{P}_R(\mathcal{S}|\Theta) := \mathcal{P}\left\{x(t) \in \mathcal{S},\ \forall\, t \in (0,T]|\Theta\right\}, \tag{2.6}$$

and its failure probability is given by one minus the reliability. Under the simplifying assumptions that the process is stationary and Gaussian, and that the displacement of the process is independent of its velocity, a simple expression can be found to approximate this reliability.

In general, the classic "first-passage" problem has no known exact solution for a dynamic system subject to random excitation (Lin 1976; Lin and Cai 1995). Hence, an approximate solution must be used. The approximation chosen is based on threshold-crossing theory, developed originally by Rice (1944), and also explained in Lin (1976) for scalar processes and Veneziano et al. (1977) for vector-valued processes crossing a polyhedral region. The threshold-crossing rate, termed the "out-crossing rate," estimates the mean rate at which a random process crosses a specified boundary in the outward direction.

The failure probability approximation from the out-crossing rate requires treating the failures as independent arrivals of a Poisson process, which is a reasonable assumption under broad-band excitation when the out-crossing rate is small. Under the Poisson approximation, $\mathcal{P}(\mathcal{F}|\Theta)$ is the probability that at least one failure occurs during the time interval $(0,T]$, assuming an unfailed system initially, so

$$\mathcal{P}(\mathcal{F}|\boldsymbol{\theta}) \simeq 1 - \exp\left[-\int_0^T \nu_\beta(\boldsymbol{\theta},t)\mathrm{d}t\right], \tag{2.7}$$

where $\nu_\beta(\boldsymbol{\theta},t)$ is the mean out-crossing rate of the threshold level β. The notation of a lowercase $\boldsymbol{\theta}$ is used to denote probabilities conditional on a particular model, while Θ will be used when a class of possible models is considered to describe the system (this distinction is significant when the performance over the uncertain model set is considered).

For the applications in this thesis, the random process of interest for the reliability calculation is the response of a structure to an uncertain input. By using a

linear model to represent the structural system, modeling the input as a stationary Gaussian process, and considering the stationary response of the system, (2.7) can be greatly simplified. Then, $\nu_\beta(\boldsymbol{\theta}, t) = \nu_\beta(\boldsymbol{\theta})$ is independent of time and the failure probability is approximated by

$$\mathcal{P}(\mathcal{F}|\boldsymbol{\theta}) \simeq 1 - \exp\left[-\nu_\beta(\boldsymbol{\theta})T\right], \tag{2.8}$$

which, for $\nu_\beta(\boldsymbol{\theta})T \ll 1$, yields

$$\mathcal{P}(\mathcal{F}|\boldsymbol{\theta}) \simeq \nu_\beta(\boldsymbol{\theta})T. \tag{2.9}$$

To compute the out-crossing rate, the additional assumption is made that the displacement and velocity of the response quantity of interest are independent. This assumption can be shown to be satisfied for the linear systems of interest in the absence of dynamic feedback control, but it may be violated in the general case of dynamic compensation. So, for a scalar-valued Gaussian process where the random variable $X(t)$ and its derivative $\dot{X}(t)$ are independently and normally distributed with means of zero and variances of σ_x and $\sigma_{\dot{x}}$, respectively, the average number of outward crossings per unit time of the threshold β is (Rice 1944; Lin 1976)

$$\begin{aligned} \nu_\beta &= \int_0^\infty \dot{x} f_{X\dot{X}}(\beta, \dot{x}) d\dot{x} + \int_{-\infty}^0 \dot{x} f_{X\dot{X}}(-\beta, \dot{x}) d\dot{x} \\ &= 2\int_0^\infty \dot{x} f_{X\dot{X}}(\beta, \dot{x}) d\dot{x}, \end{aligned} \tag{2.10}$$

where

$$f_{X\dot{X}}(x, \dot{x}) = \left(\frac{1}{\sqrt{2\pi}\sigma_x} \exp[-\frac{x^2}{2\sigma_x^2}]\right)\left(\frac{1}{\sqrt{2\pi}\sigma_{\dot{x}}} \exp[-\frac{\dot{x}^2}{2\sigma_{\dot{x}}^2}]\right) \tag{2.11}$$

for the independent variables x and $\dot{x}$. Evaluating the integral,

$$\nu_\beta = \frac{\sigma_{\dot{x}}}{\pi\sigma_x} \exp\left[-\frac{1}{2}\frac{\beta^2}{\sigma_x^2}\right], \tag{2.12}$$

where the dependence on $\boldsymbol{\theta}$ is implicit. For vector processes, the out-crossing rate

can be obtained by integrating the joint probability density function of the vector response evaluated at each failure surface for all velocities with components pointing outward from that surface, then summing this quantity over all the failure surfaces. See Veneziano et al. (1977) for a more detailed explanation of how this can be done for polyhedral failure surfaces in $\mathbb{R}^N$ and an uncorrelated Gaussian process. Unfortunately, when the response variables are correlated, this vector out-crossing requires a difficult integration even for low-dimensional failure surfaces. To simplify the calculation, an upper bound on the composite failure probability, which adds the probabilities for each failure mode together and neglects the correlation between the failure modes, is used herein.

2.2.4 Norm-based performance measures

Many computational techniques have been developed for analysis of linear systems using the induced $\mathcal{H}_2$ and $\mathcal{H}_\infty$ norms on transfer functions (Zhou et al. 1996; Doyle et al. 1992). When considering linear systems, these methods can be used as an alternative to the probabilistic performance measures described above.

The first norm-bounded performance measure considered is the $\mathcal{H}_2$ norm, which is a measure of the expected output variance of a linear system excited by "white" input. The $\mathcal{H}_2$ norm is defined in the frequency domain for a stable transfer function $G(s)$ as

$$\|G\|_{\mathcal{H}_2} := \left(\frac{1}{2\pi}\int_{-\infty}^{\infty} \mathrm{Tr}\left[G^*(j\omega)G(j\omega)\right] d\omega\right)^{1/2}, \tag{2.13}$$

where Tr[·] denotes the *trace* of a matrix and $(\cdot)^*$ its complex conjugate transpose.

The $\mathcal{H}_2$ performance is easily computed for a linear, time-invariant system $G(s) = C(sI - A)^{-1}B$ from the solution of a standard Lyapunov equation (Doyle et al. 1989)

$$AR + RA' + Q = 0, \tag{2.14}$$

so $\|G\|_{\mathcal{H}_2} = (\mathrm{Tr}[CRC'])^{1/2}$. Note that $R := E[z(t)z(t)']$ is the stationary covariance

matrix of the state variable $z(t)$ for a unit-magnitude white-noise input $w(t)$.

The second performance measure is the $\mathcal{H}_\infty$ norm of the system transfer function, which measures the worst possible output variance of the system given an input of bounded variance or bounded energy. Note that this is a different class of inputs than the one used for the failure-probability and $\mathcal{H}_2$ performance measures, so the analysis results should be treated differently. For single-input single-output systems, the $\mathcal{H}_\infty$ norm can be shown to be the peak of the transfer function in the frequency domain (Doyle et al. 1992). In the multi-input multi-output case, this generalizes to

$$\|G\|_{\mathcal{H}_\infty} := \sup_\omega \sigma_{max}\left[G(j\omega)\right], \tag{2.15}$$

where $\sigma_{max}[\cdot]$ is the maximum singular value of the argument. If w, z are signals in $\mathcal{L}_2(0,\infty)$, the $\mathcal{H}_\infty$ norm of G is given by

$$\|G\|_{\mathcal{H}_\infty} := \sup_{\|w\|_2=1} \|Gw\|_2. \tag{2.16}$$

This norm is somewhat more difficult to compute than the $\mathcal{H}_2$ norm. Bounds on the $\mathcal{H}_\infty$ norm of the system are computed using the Hamiltonian matrix H associated with the system G, where H is given by

$$H := \begin{bmatrix} A & \gamma^{-2}BB' \\ -C'C & -A' \end{bmatrix}. \tag{2.17}$$

According to a theorem given in (Doyle et al. 1992; Zhou et al. 1996), $\|G\|_{\mathcal{H}_\infty} < \gamma$ if and only if H has no $j\omega$-axis eigenvalues. So, an iterative procedure to compute $\|G\|_{\mathcal{H}_\infty}$ proceeds by assuming a γ, testing whether H has any $j\omega$-axis eigenvalues for that γ, then scaling γ until a strictly imaginary eigenvalue is found. Estimates of the $\mathcal{H}_\infty$ norm of a system can thus be obtained to an arbitrary precision (Doyle et al. 1992; Zhou et al. 1996; Balas et al. 1994).

The above norms are the typical ones used in classical (e.g., $\mathcal{H}_2$, LQR/LQG) and modern (e.g., $\mathcal{H}_\infty$, μ) control theory. Analysis techniques have also been developed

based on the $\mathcal{L}_1$ or l_1 norms, where

$$\|\hat{G}\|_{\mathcal{L}_1} = \sup_{\|u\|_\infty=1} \|Gu\|_\infty \tag{2.18}$$

and l_1 is the 1-norm of a response sequence in discrete time. At present, these are not as widely used due to difficulties in computing the induced transfer function norms.

2.3 Performance of "nominal" example structure

2.3.1 Overview

The performance of the two-story structural example is calculated using the performance measures described above and the nominal system parameters that are given in Section 2.1.2 and Appendix A. The first performance measure is the reliability of the system with respect to the inter-story drift failure mode. The reliability is estimated using the out-crossing rate approximation, and failure is defined to occur when the maximum inter-story drift exceeds 2% of the story height. The second measure computes the expected variance of the interstory-drift ratio in each floor via the $\mathcal{H}_2$ norm. Finally, the so-called "worst-case" performance is calculated for this system using the $\mathcal{H}_\infty$ norm.

For illustration, plotted in Figure 2.5 is the simulated response of the first-story inter-story drift ratio of the model, when the model is subject to computer-generated Gaussian-white input (0.01 second time step). The input has zero mean and a variance of 20% g (g is the gravitational acceleration constant, 386.4 in/sec^2), and has a flat spectrum. The 20% g level is a typical ground acceleration level that would be used to model a moderate-sized far-field earthquake, although in practice the frequency content would not be uniform, and the 10 second duration of the input is also representative for the strong shaking portion the earthquake. The simulation was run for 10 seconds prior to the record that is displayed in order to allow the transient response to die out. The dashed lines in the figure represent the failure

level for the inter-story drift ratio, noting that failure can occur in either direction.

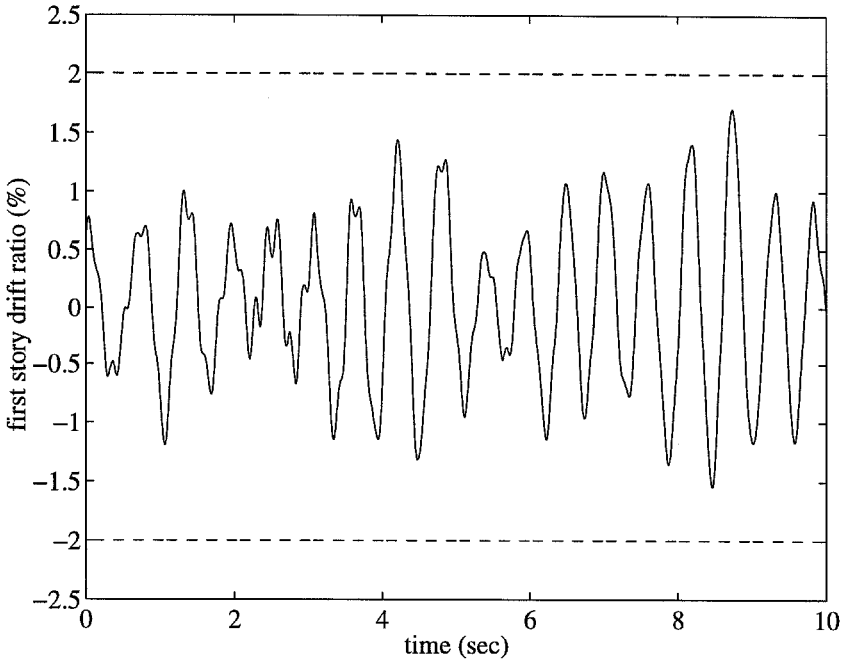

Figure 2.5 Simulated response of 2DOF example to white noise.

2.3.2 Nominal reliability-based performance

The reliability of the system with respect to the inter-story drift failure mode is defined as the probability that the computed inter-story drift ratios in both the 1^{st} or 2^{nd} stories of the building model do not exceed the failure levels at any point during the time interval of interest. The uncertain excitation for the system is modeled as Gaussian white noise with zero mean and standard deviation of 20% g, as discussed previously.

The reliability is computed on the basis of the out-crossing rate approximation (2.7) and (2.12) over a 10 second interval. The failure level for the inter-story drift ratio is $\beta = 2.0\%$. For (2.12), the standard deviations of the inter-story displacements and velocities are needed, and these can be obtained from the solution of

the Lyapunov equation (2.14), where A is the state matrix given by (A.13) and $Q = BWB'$, where W is $(0.2\ \text{g})^2$. The variance of the performance variables can be determined through a judicious choice for C in (A.12), such that the output variables are the inter-story drifts and their velocities, as in (A.14). Then, the quantities of interest are found by CRC', where $R := E[z(t)z(t)']$ is the solution to (2.14). For the model parameters given here and in Appendix A, the nominal failure probability for this system is found to be 7.4% (and hence its reliability is 92.6%).

The failure surface in this example is two-dimensional, since the response for each of the two performance variables must be considered (i.e., the inter-story drift ratio in each floor). Although these variables are correlated, the failure probability is added for each failure mode to simplify the calculation. Hence, this simplification provides an upper bound on the estimate of the failure probability.

2.3.3 $\mathcal{H}_2$ performance

For the $\mathcal{H}_2$ performance of the system, the $\mathcal{H}_2$ norm is calculated for the inter-story drifts. The $\mathcal{H}_2$ norm of the linear system G is given by (2.13), where R is the solution to the standard time-invariant Lyapunov equation given by (2.14), $Q = BWB'$, and $W = (0.2\ \text{g})^2$ for this system. Since the $\mathcal{H}_2$ performance is defined only in terms of the drift ratios (and not their velocities), C in this case is given by

$$C = \frac{1}{h_c}\begin{bmatrix} 1 & 0 & 0 & 0 \\ -1 & 1 & 0 & 0 \end{bmatrix}\begin{bmatrix} \Phi \\ 0 \end{bmatrix}, \tag{2.19}$$

as contrasted to C from (A.14).

For the nominal parameters defined for this system (i.e., the model parameters described above and in Appendix A), the $\mathcal{H}_2$ norm of the drift ratio is 0.76% of the story height.

2.3.4 Nominal $\mathcal{H}_\infty$ performance

The $\mathcal{H}_\infty$ norm of the inter-story drifts is also computed for this example problem. The $\mathcal{H}_\infty$ drift level performance is found to be 1.60% of the story height, which

corresponds to the "worst" possible 2-norm of the inter-story drift ratio given an input w in $\mathcal{L}_2(0,\infty)$ with $\|w\|_2 \leq 0.2$ g. The specific input that causes the $\mathcal{H}_\infty$ bound to be realized is a pure sinusoidal input at a frequency equal to the dominant resonant mode of the system (the frequency is the damped natural frequency of the first mode). The value of 1.60% for $\mathcal{H}_\infty$-norm of the the inter-story drift ratio indicates that, for this 2-norm bounded input and failure level of 2% for the inter-story drift, the system is guaranteed to never fail. Note that this input class is clearly much different than the one used for the failure probability and $\mathcal{H}_2$ performance calculations. The $\mathcal{H}_\infty$ results are provided merely for comparison.

2.4 Model uncertainty description

2.4.1 Sources of model uncertainty

Overview

Models of physical systems can never be certain in the sense that they cannot perfectly predict the future behavior of the system. The sources of discrepancy between the measured and predicted response (termed the "prediction error"–see Söderström and Stoica 1989) of a physical system generally can be sorted into two categories,

- model uncertainty,
- modeling error.

The *model uncertainty* relates to errors and uncertainty in selecting the "best" model from within the class of possible models used to describe the system. When selecting a model for a physical system from a class of possible models, the model that best agrees with the engineer's present state of knowledge of the system is selected. That model and the parameters associated with it, however, typically are uncertain, as the engineer's knowledge is often incomplete.

The *modeling error* is the inherent error in approximating a real system with a simplified mathematical representation of that system, and accounts for the remain-

ing difference between the "best" model within the model class and the observed behavior of the physical system. These two sources of error are described in the following sections, along with the uncertainty associated with the input.

Parametric model uncertainty

The class of possible models considered herein for structural engineering applications are finite-order ordinary differential equations, where the system can be approximated with (possibly nonlinear) springs, masses, and dissipative elements (e.g., linearly-viscous dashpots). The parameters for the models in this class typically are determined either through finite-element models that are composed of mechanics-of-materials models of the individual members (beams, columns, etc.) of the structure (Sack 1989; Cook et al. 1989), or through a modal identification procedure, such as the one described by Beck (1996) and Beck (1978), which distills the measured dynamical response of the building into the responses from each of several classical normal modes of vibration (Caughey and O'Kelly 1965).

Sources of parametric uncertainty in the construction of finite-element models for buildings are the material properties that are assumed in the creation of the structural model, as these properties may vary from member to member in the structure, or the damping ratio that is chosen to represent linear viscous damping in the structure. In addition, the connectivity conditions between members may be uncertain, as well as the interaction between the structure and its foundation. In general, the greatest source of uncertainty is in modeling the damping of the structure.

If the model class is the class of linear modal models of the system, such as in Beck (1996), the modal parameters that are identified (modal frequencies, damping ratios, and modeshape components) can be viewed as the most probable parameters, and the covariance of these parameter estimates can be obtained to describe their uncertainty.

Modeling (non-parametric) uncertainty

In a prediction-error setting, the non-parametric modeling error accounts for the difference between the predicted output from a parameterized model of a system and that system's actual output. Hence, the modeling error includes unmodeled dynamics and unmodeled nonlinearities in the system as well as sensor noise. Clearly this term is linked to the parametric model error of the previous section, as the most accurate models within a specific class lead to the smallest error between the measured and predicted outputs, and hence the smallest modeling error.

Typically, all modeling error is described by a "sensor noise" term in the modeled equations of motion. This may be misleading, since often in structural engineering applications, the actual modeling error is much more significant than the sensor noise in the instruments that are used to measure the structure's response. Instruments with 12-bit or even 16-bit precision are quite common for measuring vibrations in civil engineering structures, yielding root-mean-square sensor noise levels of $\ll 1\%$, while the difference between the measured output and the predicted output is typically on the order of several percent of the measured response. The unmodeled dynamics of the system typically include non-structural components, variations in the details of beam-column connections, and soil-structure interaction. These components often behave very non-linearly under earthquake excitation, even if the structural members do not yield.

Uncertainty in inputs

For civil engineering structures, the excitation is usually more uncertain than the model. For example in earthquake applications, the magnitude, duration, and frequency content of the ground motion are difficult quantities to model, and are hence quite uncertain. They can be parameterized to some extent by modeling the local site conditions, such as the proximity of the structure to a fault, local soil conditions, and general seismicity of the region. Any description of the performance should take the potential variations in the input into account.

For earthquake applications, in order to simulate the response of the system

to an earthquake, the stationary portion of the strong motion of an earthquake is typically described by a Kanai-Tajimi stochastic model (Kanai 1957; Tajimi 1960; Clough and Penzien 1975). The stationary model for the input is fairly standard in earthquake engineering applications, and represents the most intense and damaging portion of the ground motion, which is typically fairly uniform in frequency content and magnitude. For the Kanai-Tajimi model, a Gaussian white noise process is passed through a second-order linear filter. The filter parameters, as well as the magnitude of the Gaussian input, can be taken as uncertain variables.

More realistic ground motion models can also be developed that include nonstationarities in the amplitude and frequency content (see, for example, Papadimitriou 1990). However, that lies beyond the scope of this thesis. Herein, only the stationary response of the system to the stationary input filter is considered for the performance analysis and control design.

2.4.2 Modeling model uncertainty

Probabilistic model uncertainty

The calculation of the probable performance of an uncertain system requires computing the performance over the class of possible models for the system. This measures the system's probable performance for the set of possible models, termed the *performance over models.* In order to consider the uncertainty described in the previous section when computing the performance, the uncertainty should be modeled as well. This is accomplished by specifying probabilities of the uncertain models.

The probability distributions assigned to the set of possible models for the system are used to quantify the relative plausibility of each model, where the plausibility of a model is determined by its ability to predict the future response of the system. These probabilities are specified based on the modeler's present state of knowledge of the system (Beck 1996; Jeffreys 1961). The knowledge can be a combination of theoretical modeling, system identification using previous response data, and "engineering judgment."

Selection of model probabilities

The selection of the probabilistic models for the model uncertainty can be addressed in a variety of fashions. One approach is for the modeler to assume *a priori* probability distributions on the model parameters. A second possibility is to invoke maximum entropy principles (Jaynes 1978) in order to select a probability distribution that maximizes the engineers *uncertainty* in the model. In other words, if the engineer constructs the best possible model of the system, then the remaining uncertainty should be maximized in some sense. Otherwise a model with less uncertainty could have been created.

For modal models constructed from system identification of the dynamic response data, the mean and variance of the modal parameters can be calculated from the data (Beck 1996). A probability model, such as Gaussian-distributed parameter uncertainty, can then be fit to the mean and variance of the parameters that are identified to obtain the probabilities for the models within the model class.

Furthermore, the output error (model error) can be modeled as a random process with an associated probability distribution, and this probability distribution can then be parameterized with parameters which are themselves uncertain, hence returning to the parameterized uncertainty problem. For example, the prediction error is typically modeled as a Gaussian process, and the mean and variance of that process are parameters which are assigned *a priori* based on engineering judgment, estimated from response data, or are themselves assigned probability distributions (Box and Tiao 1973).

2.4.3 Model uncertainty for the two-story example

Uncertainty in the model of the two-story system can be treated with two methods, depending on whether a finite element model or a modal model is used for the example. For the finite element model, the mass, stiffness, and damping parameters used to construct the M, K, and C matrices of the building model (A.7) are allowed to vary, and for the modal model (A.11), the frequencies ω_i, damping ratios ζ_i, and modeshape vectors $\phi^{(i)}$ are considered uncertain.

Each modeling method has its advantages and disadvantages. Uncertainty at the finite-element-model level has a more physical interpretation, as variations in the member properties can be considered explicitly. Uncertainty at the modal model level is easier to consider when using response data to identify modal parameters or to update their estimates using Bayesian system identification techniques.

Consider uncertainty in the modal model parameters of the two-story example that were given in Table 2.2. To illustrate the model uncertainty, the natural frequencies and damping ratios are now allowed to vary, so

$$\tilde{\omega}_i = \omega_i(1 + w_{\omega_i}\delta_{\omega_i}) \tag{2.20a}$$

$$\tilde{\zeta}_i = \zeta_i(1 + w_{\zeta_i}\delta_{\zeta_i}), \tag{2.20b}$$

while the modeshapes are assumed to remain certain in order to simplify the calculations. The nominal parameter values are given in Table 2.2 for ω_i and ζ_i, $i \in \{1, 2\}$, while $\tilde{\omega}_i$, $\tilde{\zeta}_i$ represent the uncertain values. The factors w_{ω_i}, w_{ζ_i} are weights on the standardized random variables δ_{ω_i}, δ_{ζ_i}. For this example, the δ's are chosen to be zero-mean Gaussian-distributed random variables. The probability density functions (PDFs) for $\tilde{\omega}_1$, $\tilde{\omega}_2$ and $\tilde{\zeta}_1$, $\tilde{\zeta}_2$ are shown in Figure 2.6. Note that using Gaussian variables allows a finite probability that the frequency and damping could be negative, but the probability is negligible for the parameters in this example and is ignored. All the w_{ω_i}'s and w_{ζ_i}'s are equal to 0.1 in this case. The natural frequencies are assigned the same coefficient of variation, and the two damping ratios are assumed to have the same mean and variance, which is why their PDFs are identical in the figure.

As a next step in the modeling of the uncertainty, beyond the scope of this simple demonstration (and this thesis), variations in the modeshape components could be considered as well. For an additional level of complexity, the uncertainty could also be treated at the physical model level, where the stiffness and damping parameters for the model are uncertain, so these quantities would then have a direct physical interpretation in terms of the components of the structure.

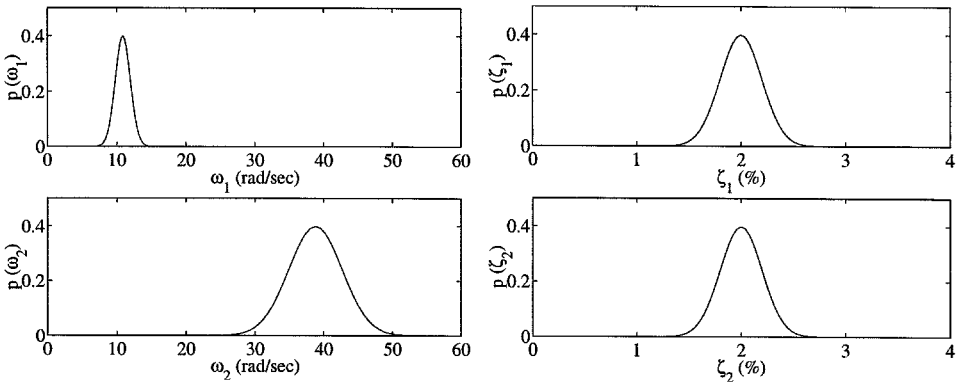

(a) Frequencies (b) Damping ratios

Figure 2.6 Uncertain parameter PDFs for 2DOF system.

The next section discusses how the probabilistic performance of a system with uncertainty can be estimated.

2.5 Probabilistic robust analysis

2.5.1 Robust performance as probability-over-models

The idea of probabilistic robust analysis is to compute the probable performance of the physical system over the set of possible inputs and the class of possible models that could be used to describe the system. Contrast this with the current robust analysis paradigm (Zhou, Glover, and Doyle 1996), which defines robust analysis as the worst-case performance over the sets of possible system models and inputs. This "worst" model used as the basis for the robust analysis may be a highly unlikely member of the set of possible models, so the analysis result may be unnecessarily conservative and hence misleading.

This section explains how the "performance" of the uncertain system is determined probabilistically by calculating the performance over the possible model set.

2.5.2 Robust reliability

The total failure probability, as implied by the total probability theorem[2], is given by integrating the probability of failure which is conditional on a particular model weighted by the probability assigned to that model, over all the possible models,

$$\mathcal{P}(\mathcal{F}|\Theta) := \int_{\Theta} \mathcal{P}(\mathcal{F}|\boldsymbol{\theta}) p(\boldsymbol{\theta}|\Theta) d\boldsymbol{\theta}, \tag{2.21}$$

where Θ represents the class of possible models considered for the system and $\boldsymbol{\theta} \in \Theta$ represents a particular model within the class of possible models. The quantity $p(\boldsymbol{\theta}|\Theta)$ is the *probability* of the particular model parameterized by $\boldsymbol{\theta}$, given the set of all possible models Θ and the modeler's present knowledge of the system.

This total probability integral typically cannot be solved analytically, so numerical approximations are necessary. In addition, an efficient approximate solution method for this integral (2.21) is necessary if numerous uncertain parameters are considered. Furthermore, the analysis result from (2.21) is needed for each iteration of the controller design optimization (see Chapter 3 for the controller design procedure), so the solution to (2.21) must also be obtained efficiently to enable this optimization.

2.5.3 Probable $\mathcal{H}_2$ performance

Similar to the robust reliability calculation discussed above, the "probable robust $\mathcal{H}_2$" performance can also be solved through application of the total probability theorem. First, let $\mathcal{Q}(\boldsymbol{\theta})$ represent the $\mathcal{H}_2$ performance of the system described by the parameters $\boldsymbol{\theta}$, then

$$\mathcal{Q}(\Theta) := \int_{\Theta} \mathcal{Q}(\boldsymbol{\theta}) p(\boldsymbol{\theta}|\Theta) d\boldsymbol{\theta}, \tag{2.22}$$

which, recognizing (2.22) as the expected value of $\mathcal{Q}(\boldsymbol{\theta})$ (Papoulis 1965), can be thought of as the "expected $\mathcal{H}_2$ performance" over the uncertain model set Θ.

[2]This theorem is easily derived from the axioms of probability, (Papoulis 1965; Beck 1996).

2.5.4 Computing the probable robust performance

Space-gridding numerical integration techniques

A variety of numerical integration techniques exist that require gridding the domain of integration along each dimension of the integrand. The integration techniques, such as those based on the trapezoidal rule, Simpson's rule, or Gaussian quadrature, are generally simple to implement and reliable, provided sufficient divisions of the domain are taken for each dimension of the integrand. See Press et al. (1992), for example, for an overview of these techniques. The computation time required to evaluate the integral grows exponentially with the dimension of the integrand by these methods (i.e., exponentially with the number of uncertain parameters in the model), which is unacceptable for high-dimensional integrands and a difficult obstacle even for low-order ones when the controller optimization is performed.

Asymptotic approximation

The method of asymptotic approximation to classical reliability integrals has been studied extensively by Breitung (1989, 1991). An asymptotic approximation has also been applied recently to dynamic linear systems under stochastic excitation by Papadimitriou et al. (1997). This method is used herein for the evaluations of the total failure probability. The method fits a second order surface to the log of the integrand, in the region of the integrand with the greatest contribution to the probability integral (Papadimitriou et al. 1997). Hence, the method requires an optimization over the uncertain parameter space to find the "design point(s)," or maximum (maxima) of the integrand. Multiple maxima may be considered if several regions of the integrand have a large contribution to the integral. Unfortunately, the surface over which the optimization is performed to find the design point(s) is nonlinear and (possibly) non-convex. The asymptotic approximation is based on Laplace's method (Breitung 1994) for integrals of the form

$$I = \int_{\Theta} e^{l(\boldsymbol{\theta})} d\theta, \tag{2.23}$$

and involves fitting a Gaussian-type surface to the "design point," or maximum, of the integrand in (2.21). In this application, an $l(\theta)$ of the form

$$l(\boldsymbol{\theta}) = \log \mathcal{P}(\mathcal{F}|\boldsymbol{\theta}) + \log p(\boldsymbol{\theta}|\boldsymbol{\Theta}), \tag{2.24}$$

can be chosen. Then, the integral (2.21) can be approximated by

$$\mathcal{P}(\mathcal{F}|\boldsymbol{\Theta}) \simeq (2\pi)^{n/2} \frac{\mathcal{P}(\mathcal{F}|\boldsymbol{\theta}^*)p(\boldsymbol{\theta}^*|\boldsymbol{\Theta})}{\sqrt{\det L(\boldsymbol{\theta}^*)}}, \tag{2.25}$$

where $\boldsymbol{\theta}^*$ maximizes (2.24) (and so the integrand of (2.21)), and $L(\boldsymbol{\theta}^*)$ is the Hessian of $l(\boldsymbol{\theta})$ evaluated at $\boldsymbol{\theta}^*$. See Papadimitriou et al. (1997) for the details of this derivation, and for an explanation of how it could be applied to the case when multiple maxima exist in (2.24).

Since the asymptotic approximation requires an optimization to find the maximum of the integrand of (2.21), denoted by $\boldsymbol{\theta}^*$, the computation time required for the approximation has an upper bound that grows exponentially with the number of uncertain parameters. The method appears to be efficient, however, for the civil engineering applications examined herein, indicating that the optimization for these systems is well behaved. An investigation into the behavior of the optimization for a larger class of civil engineering applications would be a good subject for further study of this method.

Monte Carlo integration

One advantage of the Monte Carlo method for approximating (2.21) is that the required solution time depends only on the desired accuracy of the solution, and not on the dimension of the integral. Of course, civil engineering systems typically have a high reliability (since that is the design goal), so many samples may be required for an accurate approximation from the Monte Carlo method. A variance reduction technique, such as importance sampling, could improve the efficiency of the Monte Carlo method significantly in this case (Press et al. 1992; Papadimitriou et al. 1997), although this requires either some prior knowledge of the distribution

of the integrand of (2.21), or an optimization to find the maximum (or maxima) of the integrand (as per the asymptotic expansion method).

2.5.5 Comments on norm-bounded robust analysis methods

An extensive framework exists for evaluating the performance of uncertain linear systems using modern robust analysis techniques based on the $\mathcal{H}_\infty$ norm of the system and the structured singular value "μ" (Zhou et al. 1996; Balas et al. 1994). These *hard-bounded* approaches[3] describe only the performance of the "worst" model and input within the set of possible models and inputs, and hence could be quite conservative with respect to the performance of the actual system. At the present time, no probabilistic information on the model uncertainty can be incorporated into the analysis by these methods, and the robust analysis result does not have a natural probabilistic or reliability interpretation.

2.5.6 Robust analysis of the 2DOF example

The total probability of failure for the 2DOF example is obtained by synthesizing the methods of the Sections 2.2 and 2.4. Based on the total probability theorem (2.21), an integral of the failure probability for a particular model (from Section 2.2), weighted by the probability of that model (from Section 2.4), over the set of all possible models yields the total failure probability. This probability is conditional on the class of possible models, $\boldsymbol{\Theta}$.

The primary method used to calculate the total reliability integral (2.21) for the 2DOF example is through an asymptotic expansion about the region of the integrand with the greatest contribution to the probability integral (Papadimitriou et al. 1997), then applying (2.25) to find the total reliability. The maximum of the integrand, $\boldsymbol{\theta}^*$, is found using the Nelder and Mead nonlinear simplex method (Press et al. 1992; The MathWorks, Inc. 1994a). This optimization method is not particularly efficient, but it does not require knowledge of the derivative of the

[3] *Hard-bounded* because hard bounds are placed on both the limits of the uncertain model sets and the level of the input.

objective function, and the MATLAB routine generally performed well. Monte Carlo integration is also considered to provide an independent check of the analysis results.

The asymptotic approximation to (2.21) yields a probabilistic failure probability of 21.1%, requiring approximately 2 minutes of CPU time[4]. For the Monte Carlo integration, using 5000 samples the estimated failure probability is found to be 21.3%. The Monte Carlo estimate has a standard deviation in the failure probability estimate of 0.5%, and also requires about 2 minutes of CPU time. The total failure probability for the uncertain system differs so significantly from that for the nominal system (which is 7.4%) because the failure probability from (2.7) depends strongly on the value of the damping ratio. This can be seen in Figure 2.7, where the failure probability is plotted against ζ for the 2DOF system with $\zeta_1 = \zeta_2 = \zeta$ and the nominal-model values of the frequencies. This strong dependence is a concern when using the inter-story drift reliability as a performance measure, because the damping ratio is typically the most uncertain quantity, so in all cases using the inter-story drift reliability as the performance measure, the computed performance will depend strongly on a parameter that is quite uncertain. This nonlinear dependence of the failure probability on the damping parameter, for the inter-story drift failure mode and a white input, indicates either that the failure probability (or its complement the reliability) may not be the best performance measure for this case, or that the uncertainty in ζ should be handled differently, perhaps by providing performance levels for various values of the damping ratio.

The expected $\mathcal{H}_2$ performance can also be computed for the uncertain system through application of (2.22). The expected $\mathcal{H}_2$ performance (i.e., the standard deviation of the inter-story drift ratios) is found to be 0.78% using the asymptotic approximation method and 0.79% with standard deviation of 4×10^{-3}% using 5000 samples for the Monte Carlo integration. In Figure 2.8, the $\mathcal{H}_2$ norm of the system is plotted against the damping ratio ζ. As is evident from this figure, the $\mathcal{H}_2$ performance is less sensitive to ζ than the failure-probability-based performance.

The "expected" $\mathcal{H}_\infty$ performance is computed by again applying the total prob-

[4]The CPU time is provided as a gauge of the computational effort, and is measured using MATLAB to perform the required computations on a DEC/Alpha 3000 Workstation.

ability theorem to obtain the expected performance of the uncertain system. This is provided as an analogy to $\mathcal{H}_\infty$based performance analysis methods, and for comparison with the results of the failure-probability and $\mathcal{H}_2$ analysis methods. The expected $\mathcal{H}_\infty$ performance is calculated to be 1.64% using the asymptotic approximation method and 1.68% from the Monte Carlo approximation (with a standard deviation on the result of 1.2×10^{-2}%). Again, the $\mathcal{H}_\infty$ performance measure assumes a different input class than the failure probability and $\mathcal{H}_2$ measures. Here, the expected $\mathcal{H}_\infty$ peformance "guarantees" that the system will not fail, but this is for 2-norm bounded input, rather than a Gaussian input whose variance is specified.

The results for the various performance measures that are computed for the 2DOF example system are summarized in Table 2.3.

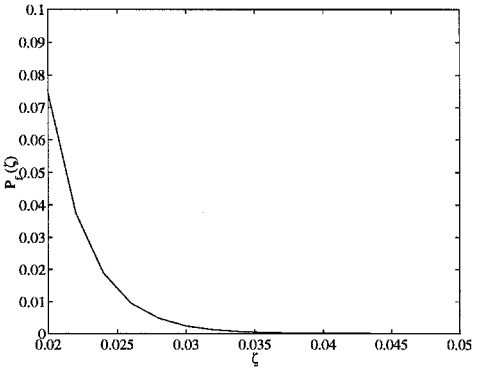

Figure 2.7 Nominal failure probability vs. damping ratio, ζ.

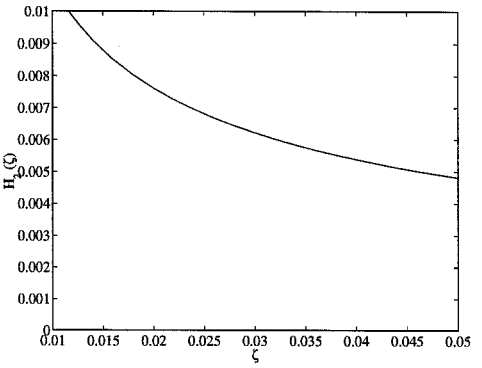

Figure 2.8 Nominal $\mathcal{H}_2$ performance vs. damping ratio, ζ.

Table 2.3 Performance measure summary for two-story example.

	Nominal Performance	Probabilistic Robust Performance	
		Asymptotic	Monte Carlo
Failure probability (%)	7.4	21.1	21.3
$\mathcal{H}_2$ performance (% drift)	0.62	0.78	0.79
$\mathcal{H}_\infty$ performance (% drift)	1.20	1.64	1.68

Chapter 3

Controller design for probabilistic performance objectives

3.1 Controller design

3.1.1 General concepts and methodology

Once the probable performance of an uncertain structural system has been determined from the methods of Chapter 2, the next step in the probabilistic robust control methodology is to attempt to improve this performance through feedback control. Structural control can use passive, semi-active, or fully active systems in order to improve the performance of a structure (Soong 1990; Housner et al. 1997). The choice of the particular control device and the sensor configuration determines the *controller class* that is to be considered for the system.

In this chapter, the controller design methodology is developed for an active structural control system. This design procedure uses the performance measures that are defined in the previous chapter as objectives for the design. The method can easily be applied to passive or semi-active structural control systems as well, although that is not explored herein.

The goal of the controller optimization is to find the optimal controller, ϕ^*, out of the class of possible controllers, Φ, that minimizes the cost function $J(\phi, \Theta)$. Here, Θ again represents the set of possible models for the system, and the cost function

represents the performance of the composite structure and actuator system. Hence,

$$J(\phi^*, \Theta) = \min_{\phi \in \Phi} J(\phi, \Theta), \tag{3.1}$$

where

$$J(\phi, \Theta) := P(\mathcal{F}|\phi, \Theta, \mathcal{D}) \tag{3.2}$$

may be determined by including the controller parameters in the evaluation of (2.21). In general, the optimal solution ϕ^* requires a nonlinear optimization over Φ, which can be conducted using a variety of existing numerical methods (see Pierre 1986 or Press et al. 1992, for example). The solution techniques that are used for the applications in this thesis are the unconstrained optimization algorithms that exist in MATLAB (The MathWorks, Inc. 1994a), such as the Nelder and Mead (Press et al. 1992) nonlinear simplex algorithm (MATLAB function fmins()) for the multi-variable optimizations and a combined golden-section-search and parabolic interpolation (Press et al. 1992) for single-variable optimizations (MATLAB function fmin()).

The optimization performed for (3.1) is subject to constraints on the controller, such as a limit on the available actuator effort or a penalty on the expected energy used by the controller. These constraints can either be imposed as boundaries on the possible controller set or as a penalty function incorporated into the design objective of (3.1). The latter approach allows for the use of unconstrained optimization methods and is adopted for the controller optimizations performed in this thesis.

One comment on the controller class is that any parameterized controller could be considered for the control design problem, such as an output-feedback controller with a state estimator or a nonlinear controller. A practical limit exists on the controller class that depends on the speed of the computer and number of uncertain parameters used to describe the system. In addition, the efficiency of the optimization routines that are used for both the search for the "design point" in the asymptotic approximation to (2.21) as well as the controller optimization for (3.1)

influence the feasible problem size. Note that for the probabilistic robust control design, the integration to determine "total performance" from Section 2.5 must be performed for each function evaluation in the optimization. Hence, the solution time has an upper bound that grows exponentially with the product of the number of uncertain parameters and the number of parameters in the control law.

3.1.2 More linear system representation

The generalized equations of motion for a linear system given by (2.1) can be augmented such that the inputs are the exogenous disturbance, sensor noise, and modeling error, which are all grouped into w, and the control input, u,

$$\begin{aligned} \dot{x} &= Ax + \begin{bmatrix} B_u & B_w \end{bmatrix} \begin{Bmatrix} u \\ w \end{Bmatrix} \\ \begin{Bmatrix} y \\ z \end{Bmatrix} &= \begin{bmatrix} C_y \\ C_z \end{bmatrix} x + \begin{bmatrix} 0 & D_{yw} \\ D_{zu} & 0 \end{bmatrix} \begin{Bmatrix} u \\ w \end{Bmatrix}, \end{aligned} \tag{3.3}$$

which is presented in block-diagram form in Figure 3.1. Here, the system output has been partitioned into the *measured outputs* y and the *performance variables* z. In (3.3), the assumption of no direct feed-through of $w \rightarrow z$ and $u \rightarrow y$ has been made (i.e., D_{zw} and D_{yu} are zero, as shown). This is not a very restrictive assumption, as the controller takes the measured output y as input, so feedback of u to the controller can be performed internally for the controller. In addition, direct feed-through of the disturbance w to z would cause the variance of the performance variables to be unbounded. If the performance variables are to include the modeling error by modeling the prediction error as a Gaussian process, their influence should be filtered using a frequency weighting function that rolls off at higher frequencies (Doyle et al. 1992).

For output-feedback control, u is a function of the measured output variable y and the disturbance input w. If the control law is linear, the controller can be

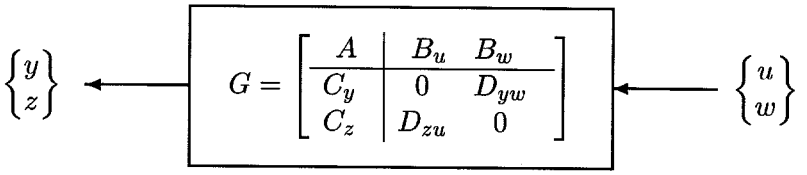

Figure 3.1 Linear system representation with control input u, disturbance w, measured outputs y, and performance variables z.

represented by

$$\begin{aligned} \dot{x}_c &= A_c x_c + B_{cy} y \\ u &= C_c x_c + D_c y \end{aligned} \tag{3.4}$$

where x_c is the controller state, which contains the "memory" of the controller[1]. In block-diagram form, this linear control system is shown in Figure 3.2.

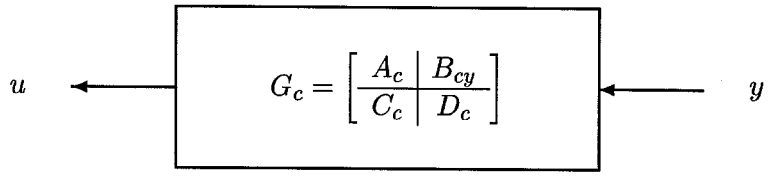

Figure 3.2 Representation of linear control system.

These two systems can be inter-connected to form the closed-loop system, where the measured outputs from the structural system become the inputs to the controller, and the outputs from the controller are input to the structure. This closed-loop system is shown in Figure 3.3, where the direction of the input-output arrows on the controller block have been reversed from the sense of Figure 3.2 to simplify the diagram.

The equations of motion for the closed loop system can be obtained for the

[1]A controller with state dimension of zero is called "memory-less."

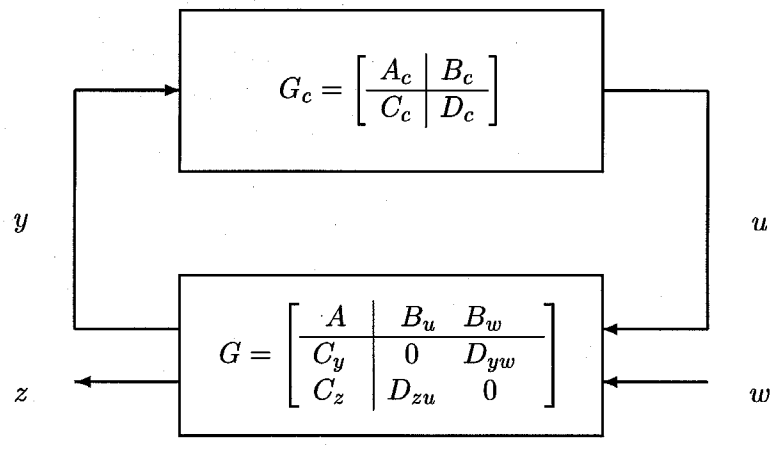

Figure 3.3 Closed-loop system.

system interconnection of Figure 3.3 from solving (3.3) and (3.4), and are given by

$$\begin{Bmatrix} \dot{x} \\ \dot{x}_c \end{Bmatrix} = \begin{bmatrix} A + B_u D_c C_y & B_u C_c \\ B_c C_y & A_c \end{bmatrix} \begin{Bmatrix} x \\ x_c \end{Bmatrix} + \begin{bmatrix} B_w + B_u D_c D_{yw} \\ B_c D_{yw} \end{bmatrix} w \tag{3.5}$$

$$z = \begin{bmatrix} C_z + D_{zu} D_c C_y & D_{zu} C_c \end{bmatrix} \begin{Bmatrix} x \\ x_c \end{Bmatrix} + \begin{bmatrix} D_{zu} D_c D_{yw} \end{bmatrix} w.$$

In order to have finite variance of the response, either $D_{zu} D_c D_{yw} = 0$ or w must be band-limited. For the examples worked out later in this chapter, the Gaussian input w will be passed through a low-pass linear filter. The state equations in (3.5) can easily be augmented to include this filter, but that is not presented here.

3.1.3 Performance measures

The reliability-based controller design seeks to minimize the failure probability of the composite structure/actuator system. As mentioned previously in Chapter 2, structural failure occurs when the inter-story drift in any story exceeds a specified fraction of the story height. In addition, the probability of actuator failure is incorporated into the performance objective, and the actuator is considered to have failed when the required actuator effort exceeds its allowable maximum. The controller

design procedure then searches over the set of possible controller parameter values to minimize this composite failure probability.

The failure probability can be computed on the basis of a single model of the system, termed the *nominal performance*, or for a whole set of possible models, termed the *robust performance*. The nominal performance is computed on the basis of (2.7), and the robust performance is determined by evaluating the total failure probability for the system, (2.21).

In addition, the $\mathcal{H}_2$-performance of the system is considered for the control design. The design seeks to minimize the $\mathcal{H}_2$-norm of the system, either for a nominal system, or for an uncertain one using (2.22) to compute the expected $\mathcal{H}_2$ performance.

3.2 Example control design for two-story building model

3.2.1 Controller class(es)

The probabilistic robust control design methodology is illustrated using the 2DOF system representing the two-story steel-frame building described in Appendix A. The sensor location is assumed to be the roof of the structure, allowing either the displacement, $x_2(t)$, velocity, $\dot{x}_2(t)$, or acceleration, $\ddot{x}_2(t)$, to be used as the measured output that is input to the controller, depending on the type of sensor that is used. The actuator is also located at the roof level, and provides the control force $u_2(t)$. In practice, this roof-level actuator could be implemented with an active-mass-driver (AMD) actuator, which is commonly used for structural control investigations (Spencer et al. 1997a; Soong 1990; Chung et al. 1989). Three controller classes are chosen to provide a comprehensive illustration of the probabilistic robust control design. These classes are chosen because they are each representative of controller classes that are common in classical control theory.

First, the simplest controller class is considered, which is the class of constant-gain output-feedback controllers. The control law consists of a single gain multiplying the measured output. This simple controller class permits graphical display of

the variation in performance with the feedback control gain.

A second class of controllers that is considered is the class of state-feedback controllers with constant gains, where the entire state of the system is assumed to be available as the controller input. In practice, the entire state may not be measurable, so a state estimator would be constructed. Note that in classical $\mathcal{H}_2$/LQG control theory (Franklin et al. 1994), the state estimator and state-feedback control design are separable for the optimal control design, and so they can be performed independently. For probabilistic robust control, however, separation of the estimator design and state-feedback design may lead to a sub-optimal controller. The estimator design problem is addressed further in Section 3.3.

The final class of controllers that is considered is the class of observer-based controllers. For this class, an optimal observer is designed to estimate the state using the measured output and the most probable model for the system. Then, the performance objectives that are based on the failure probability and the $\mathcal{H}_2$-norm of the system are used for the controller optimization using the estimated-state for feedback.

3.2.2 Constant-gain output feedback

For this example, as in the probabilistic robust analysis from Chapter 2, the interstory drift ratios remain the performance variables of interest. The maximum allowable interstory drift, as in Chapter 2, is again chosen to be 2% of the story height for the reliability-based controller design.

In the controller design optimization, some constraint or penalty is needed to limit the control effort and allow a solution. For the results presented herein, the "failure" probability of the actuator is included. In reality, the actuator "failure" corresponds to actuator saturation, at which point the linear control law breaks down. Actuator saturation is not necessarily detrimental to the performance of the system, particularly when the required actuator force exceeds the limiting force only rarely, as is the case for this example. In addition, various schemes have been proposed that optimize the performance of control systems in the presence of

actuator saturation. Explicit treatment of the actuator saturation is beyond the scope of the current work. So, to provide a constraint on the controller effort during the design optimization, u_2 is limited to 5% of the seismically effective weight of the building. This actuator force limit is chosen to be representative of the forces that are achieved by existing structural control applications. For example, the active mass driver for the laboratory structure constructed by Spencer et al. (1997a) can generate a maximum force of nearly 10% of the building mass, and in a large-scale experimental study (Soong 1990), up to 5% of the structure's mass is considered the maximum control force.

Note that the matrices C_z and D_{zu} from (3.3) are scaled by dividing each performance variable (i.e., the inter-story drifts d_1 and d_2 and the actuator force u) by its corresponding failure level. Then, for the failure probability calculations, $\|z\|_\infty \leq 1$ implies satisfactory performance given $E[ww'] = 1$. For the $\mathcal{H}_2$ performance analysis, the components of z are now dimensionless and weighted appropriately (i.e., the identity matrix can be used as the weighting matrix for the $\mathcal{H}_2$ control design).

Since the output feedback controller in this section is memory-less and contains no states, the control force u is given by

$$u = K_{of} y, \tag{3.6}$$

which is a constant gain multiplying the measured output. The closed-loop interconnection of (3.5) for this system can be represented with G_{clp}, where the performance variables include the inter-story drifts, drift velocities, and control input u

$$G_{clp} := \left[\begin{array}{c|c} A + B_u K_{of} C_y & B_w + B_u K_{of} D_{yw} \\ \hline C_z + D_{zu} K_{of} C_y & D_{zw} + D_{zu} K_{of} D_{yw} \\ K_{of} C_y & K_{of} D_{yw} \end{array}\right]. \tag{3.7}$$

Note that $\dot{u}$ is also needed to calculate the out-crossing rate for the reliability approximation (see (2.12)). It can be estimated from u using a linear filter with the

transfer function

$$G_{diff}(s) = \frac{s}{s/\omega_d + 1} \tag{3.8}$$

to approximate the derivative. This filter approximates the derivative of its input at frequencies well below the cut-off frequency ω_d.

Velocity output-feedback controllers are designed using several of the performance measures defined in Section 2.5. The controller design seeks the value for the controller parameter K_{of} that minimizes the performance objective, that is, the composite structure/actuator failure probability (Sections 2.2.3 and 2.5.2), or the expected $\mathcal{H}_2$ response of the system (Sections 2.2.4 and 2.5.3). The probable robust performance is calculated using the asymptotic approximation method (Section 2.5). The controller optimization is performed using the uncertain models described in Section 2.4.3. For comparison, a "nominal" model controller design is performed using the most probable parameters from the model uncertainty set. The controller parameters and the corresponding performance measures for the closed loop systems are displayed in Table 3.1.

Shown in Figure 3.4 is the relationship between the controller gain K_{of} and the performance for both the failure probability and $\mathcal{H}_2$ performance measures. The solid lines represent the robust performance measures for the uncertain models, while the dashed lines represent the performance values calculated for the nominal (most-probable) model. In both figures, the effect of the controller constraint on the performance measure can clearly be seen. For the failure probability controller, the actuator failure has a rather sudden affect on the performance due to the nonlinearity in the performance measure, and the optimal controller gain is very sensitive to the specified failure level. This sensitivity indicates that the specification of the composite performance objective should be studied in greater detail, as a future project.

For further comparison, position feedback and acceleration feedback control are considered, and the resulting controller designs and performance measures are given

Table 3.1 Velocity output feedback controller design for 2DOF example.

	Nominal-model Controller		Uncertain-model Controller	
Control Gain	$K_{\text{pf}_{\text{nom}}}$	$K_{\mathcal{H}_{2\text{nom}}}$	$K_{\text{pf}_{\text{rob}}}$	$K_{\mathcal{H}_{2\text{rob}}}$
	0.4769	0.3263	0.5519	0.3286
nominal P_f (%)	0.0290	0.1401	0.1002	0.1363
robust P_f (%)	0.4699	1.5143	0.3220	1.4868
nominal $\mathcal{H}_2$	0.3403	0.3348	0.3463	0.3348
robust $\mathcal{H}_2$	0.3430	0.3376	0.3488	0.3376

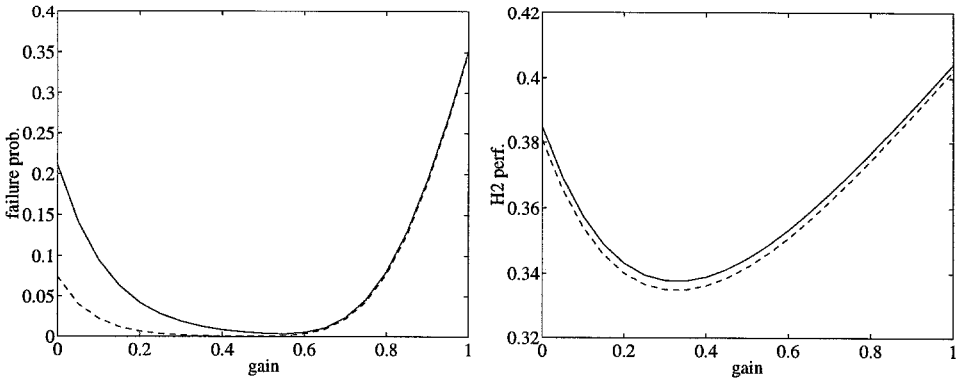

(a) Failure probability

(b) $\mathcal{H}_2$ performance

Figure 3.4 Failure probability and $\mathcal{H}_2$ performance with velocity output feedback for the nominal (dashed) and uncertain (solid) 2DOF system.

in Table 3.2 for position feedback control and in Table 3.3 for acceleration feedback control. In addition, the performance of these systems is plotted as a function of the controller gain for position feedback (Figure 3.5) and acceleration feedback (Figure 3.6).

The impact of the type of control can be understood intuitively by considering a second-order system. Direct velocity feedback increases the damping of the system, position feedback increases the stiffness, and acceleration feedback affects the effective inertia of the system. Velocity feedback has the most influence on the system performance, both for the failure probability and $\mathcal{H}_2$ performance measures. This is

due to a combination of factors: the existing damping ratio is small and can easily be increased with moderate control forces, and also because the response of the system is inversely proportional to the damping ratio. Both position-feedback control and acceleration-feedback control generate large control forces for comparable levels of vibration reduction, so they are not as effective, particularly the position-feedback controller, which achieves almost no reduction in response as compared to the uncontrolled system (Table 3.2).

Table 3.2 Position output feedback controller design for 2DOF example.

	Nominal-model Controller		Uncertain-model Controller	
Control Gain	$K_{\text{pf}_{\text{nom}}}$	$K_{\mathcal{H}_{2\text{nom}}}$	$K_{\text{pf}_{\text{rob}}}$	$K_{\mathcal{H}_{2\text{rob}}}$
	4.2338	0.1891	3.6554	0.1953
nominal P_f (%)	6.2416	7.3616	6.3469	7.3597
robust P_f (%)	19.6723	20.9497	19.1197	20.9462
nominal $\mathcal{H}_2$	0.4311	0.3806	0.4184	0.3806
robust $\mathcal{H}_2$	0.4356	0.3847	0.4228	0.3847

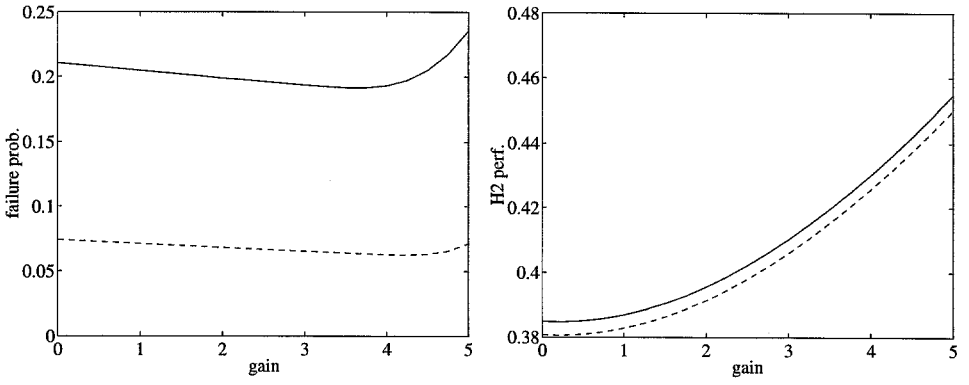

(a) Failure probability

(b) $\mathcal{H}_2$ performance

Figure 3.5 Failure probability and $\mathcal{H}_2$ performance with position output feedback for the nominal (dashed) and uncertain (solid) 2DOF system.

Table 3.3 Acceleration output feedback controller design for 2DOF example.

	Nominal-model Controller		Uncertain-model Controller	
Control Gain	$K_{\mathrm{pf_{nom}}}$	$K_{\mathcal{H}_{2\mathrm{nom}}}$	$K_{\mathrm{pf_{rob}}}$	$K_{\mathcal{H}_{2\mathrm{rob}}}$
	-3.47×10^{-2}	-2.40×10^{-5}	-3.42×10^{-2}	-2.58×10^{-5}
nominal P_f (%)	5.5794	7.2696	5.5829	7.2586
robust P_f (%)	18.2824	20.7744	18.1546	20.7542
nominal $\mathcal{H}_2$	0.4289	0.3804	0.4275	0.3804
robust $\mathcal{H}_2$	0.4338	0.3845	0.4323	0.3845

3.2.3 Constant-gain state feedback

The position and velocity at each floor can be fed back to the controller to provide full-state feedback, so $y \equiv x$, where x is the vector of nodal coordinates. Note that the nodal variables differ by a linear transformation from the "modal variables" that are used to form the state equations, (A.13), for the system described in Appendix A. To perform actual state feedback, the measured outputs are multiplied by the inverse of the modeshape matrix, as in (A.10).

The resulting controller gains for the nominal-model and uncertain-model controller designs using both the failure probability and $\mathcal{H}_2$ performance objectives are displayed in Table 3.4, where the gains as shown in the table multiply the measured *nodal* response of the system, rather than the modal state variables. The order of the gains in the table is that K_{x_1}, K_{x_2}, $K_{\dot{x}_1}$, and $K_{\dot{x}_2}$ multiply x_1, x_2, $\dot{x}_1$, and $\dot{x}_2$, in order. In the table, on the left, the feedback gains are subscripted by these values for easy reference. For each optimization, the initial guess that is used for the feedback-control gain vector is the controller resulting from a standard linear quadratic regulator design (Franklin et al. 1994; The MathWorks, Inc. 1995).

For the nominal-model design based on an $\mathcal{H}_2$ performance objective, the state-feedback problem is simply the linear quadratic regulator (LQR) design problem, which has a well-known analytic solution (Doyle et al. 1989; Franklin et al. 1994; The MathWorks, Inc. 1995). For the failure-probability-based performance objective for the nominal model design as well as for the probabilistic robust perfor-

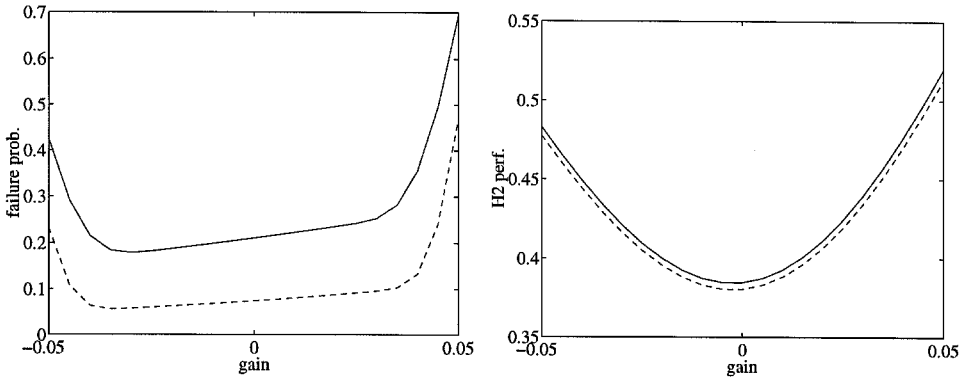

(a) Failure probability

(b) $\mathcal{H}_2$ performance

Figure 3.6 Failure probability and $\mathcal{H}_2$ performance with acceleration output feedback for the nominal (dashed) and uncertain (solid) 2DOF system.

mance measures, the controller optimization is carried out numerically. Note that the full-state feedback achieves only marginally better performance than the velocity output-feedback case. This is not surprising, as the position-feedback control in Table 3.2 has very little effect on the performance. Essentially, all that is gained in the full-state feedback case over the single-output velocity feedback is the freedom to choose the second velocity-feedback gain parameter, so the effective damping ratios of the two modes can be adjusted independently to minimize the performance objective.

3.3 Controllers with dynamics

3.3.1 Theory

In practice, the entire state may not be measurable, so a state estimator must be used, then the state-feedback controller in Section 3.2.3 can be used along with the state estimate. In classical linear control theory (Franklin et al. 1994), the state estimator and state feedback design problems are separable in the sense that the $\mathcal{H}_2$-optimal (dynamic) output-feedback controller is a combination of the optimal

Table 3.4 Full-state feedback controller design for 2DOF example.

	Nominal-model Controller		Uncertain-model Controller	
	$K_{\text{pf}_{\text{nom}}}$	$K_{\mathcal{H}_{2\text{nom}}}$	$K_{\text{pf}_{\text{rob}}}$	$K_{\mathcal{H}_{2\text{rob}}}$
Control Gains K_{x_1}	0.0545	0.0471	0.0533	0.0483
Control Gains K_{x_2}	0.2842	0.1705	0.2505	0.1765
Control Gains $K_{\dot{x}_1}$	0.1550	0.1194	0.1808	0.1177
Control Gains $K_{\dot{x}_2}$	0.4025	0.2699	0.4663	0.2731
nominal P_f (%)	0.0279	0.1344	0.0974	0.1306
robust P_f (%)	0.4540	1.4687	0.3101	1.4406
nominal $\mathcal{H}_2$	0.3398	0.3344	0.3458	0.3344
robust $\mathcal{H}_2$	0.3425	0.3372	0.3483	0.3372

state estimator and the optimal state-feedback controller. In general, for probabilistic robust control, the optimal dynamic output-feedback controller will not be a combination of an independently-designed state estimator and (constant-gain) state-feedback controller. However, a sub-optimal dynamic-feedback controller can be constructed that uses an $\mathcal{H}_2$-optimal estimator to estimate the state on the basis of the (most-probable) nominal system. Then, any of the previously-defined objective functions can be used for the control optimization, where the controller class is the set of gains multiplying the estimated state.

Consider the equations of motion for a linear system,

$$\dot{x} = A\ x + B_u\ u + B_w\ w + B_v\ v \tag{3.9}$$

$$y = C_y x \qquad\qquad + D_{yw} w + D_{yv} v \tag{3.10}$$

$$z = C_z x + D_{zu} u \qquad\qquad + D_{zv} v, \tag{3.11}$$

where x is the state of the system, y is the vector of measured outputs, z is the vector of performance variables, u represents the control inputs, w represents the external disturbances to the system and v is a combination of the sensor noise and modeling error. As shown, the performance variables z have a direct feed-through of the sensor noise/modeling error, v (henceforth simply called "noise"). In order to provide bounded signals for z when the noise is modeled as a Gaussian process,

v is low-pass filtered in practice.

Let $A = A_0 + \Delta A$ (and similarly for the other matrices in (3.3.1)), where A_0 is defined in terms of the most-probable parameter values, and the uncertainty in A is included in ΔA. The state estimator is designed on the basis of the most probable model of the system,

$$\begin{aligned} \dot{\hat{x}} &= A_0\hat{x} + B_{u0}u + L(y - \hat{y}) \\ \hat{y} &= C_0\hat{x} + D_{u0}u, \end{aligned} \tag{3.12}$$

where $\hat{x}$ is the estimated state, A_0, B_{u0}, C_0, and D_{u0} are the most-probable-model system matrices, $u = -K\hat{x}$ is the control force, and L is the $\mathcal{H}_2$-optimal/Kalman estimator gain.

As an extension of the estimator design, on-line identification of the parameters could be considered. In this case, the state of the estimator is augmented to include the model parameters as well as the states, using a nonlinear extended Kalman filter. This suggests a technique for adaptive (and probabilistic robust) control, and would be interesting topic for future work.

3.3.2 Application to 2DOF example

The estimator design based on the most probable model of the 2DOF example system is performed assuming $\Delta A = 0$, $\Delta C = 0$, $\Delta B_u = 0$, $D_{yw} = D_{zw} = \sigma_w I$, $D_{yv} = D_{zv} = \sigma_v I$. The control optimization is then performed for the failure probability and $\mathcal{H}_2$ performance objectives to find the optimal gains that multiply the estimated states. The controllers that are found and their calculated performance are given in Table 3.5. The controller gains multiply the estimated states, which are in terms of the modal coordinates. So, the gains $K_{\tilde{x}_1}$, $K_{\tilde{x}_2}$, $K_{\dot{\tilde{x}}_1}$, and $K_{\dot{\tilde{x}}_2}$ multiply $\tilde{x}_1$, $\tilde{x}_2$, $\dot{\tilde{x}}_1$, and $\dot{\tilde{x}}_2$, respectively, where the tilde is used to denote the modal state variables (i.e., so $\tilde{x}_1$ is the modal displacement for the first mode).

In order to compare their values to the full-state feedback from Table 3.4, the gains in Table 3.4 should be multiplied by the inverse of the modeshape transformation matrix, as is done for Table 3.6. As seen in Table 3.6, the controller gains

that are found for the full-state feedback are quite similar to those that use the state estimator for most of the controller designs, as would be expected. However, the state-estimator (SE) controller found using the robust failure probability performance objective differs significantly in most of the feedback parameters from that found for the full-state (FS) feedback case. However, the controller gain $K_{\dot{\tilde{x}}_1}$, which multiplies the modal velocity of the first mode, $\dot{\tilde{x}}_1$, is quite similar for the SE and FS controllers when they are designed using the same objective function. This is expected, as this feedback gain directly increases the damping of the first mode, which is the mode that dominates the displacement and velocity response of the system. Although not presented here, a brief numerical investigation into the sensitivity of the performance with respect to the different controller parameters has been done to demonstrate that the performance is not very sensitive to the other feedback gains. The differences in their values can largely be attributed to numerical inaccuracies from the controller optimization.

Table 3.5 Estimated-state feedback controller design for 2DOF example.

	Nominal-model Controller		Uncertain-model Controller	
	$K_{\mathrm{pf_{nom}}}$	$K_{\mathcal{H}_{2\mathrm{nom}}}$	$K_{\mathrm{pf_{rob}}}$	$K_{\mathcal{H}_{2\mathrm{rob}}}$
Control Gains $K_{\tilde{x}_1}$	0.3781	0.1730	2.2352	0.1747
Control Gains $K_{\tilde{x}_2}$	−0.0207	−0.0364	−0.0086	−0.0372
Control Gains $K_{\dot{\tilde{x}}_1}$	0.4891	0.2933	0.5005	0.2961
Control Gains $K_{\dot{\tilde{x}}_2}$	− 0.0304	−0.0275	0.0523	−0.0273
nominal P_f (%)	0.0403	0.2491	0.0901	0.2399
robust P_f (%)	0.5799	2.0411	0.4270	1.9902
nominal $\mathcal{H}_2$	0.0269	0.0261	0.0276	0.0261
robust $\mathcal{H}_2$	0.0271	0.0264	0.0279	0.0264

3.4 Pre- vs. Post-data controller

One major advantage of the probabilistic robust control methodology over existing robust control techniques is that it allows updating of the uncertainty description of

Table 3.6 Comparison between full-state (FS) feedback controller parameters and state-estimator (SE) controller parameters.

	Control Gains			
	$K_{\tilde{x}_1}$	$K_{\tilde{x}_2}$	$K_{\dot{\tilde{x}}_1}$	$K_{\dot{\tilde{x}}_2}$
FS $K_{\mathrm{pf}_{\mathrm{nom}}}$	0.2785	−0.0808	0.4293	−0.0451
SE $K_{\mathrm{pf}_{\mathrm{nom}}}$	0.3781	−0.0207	0.4891	−0.0304
FS $K_{\mathcal{H}_{2\mathrm{nom}}}$	0.1739	−0.0344	0.2956	−0.0145
SE $K_{\mathcal{H}_{2\mathrm{nom}}}$	0.1730	−0.0364	0.2933	−0.0275
FS $K_{\mathrm{pf}_{\mathrm{rob}}}$	0.2478	−0.0665	0.4979	−0.0512
SE $K_{\mathrm{pf}_{\mathrm{rob}}}$	2.2352	−0.0086	0.5005	0.0523
FS $K_{\mathcal{H}_{2\mathrm{rob}}}$	0.1794	−0.0371	0.2977	−0.0173
SE $K_{\mathcal{H}_{2\mathrm{rob}}}$	0.1747	−0.0372	0.2961	−0.0273

the system by incorporating response data. The probabilistic robust performance calculation that is described in Section 2.5 can be updated easily to incorporate new knowledge of the system. Then, if desired, the controller designs from Section 3.1 can be updated as well.

The *a priori* probability distribution $p(\boldsymbol{\theta}|\boldsymbol{\Theta})$ for the models within the set of possible models for the system can be updated when response data is available through the application of Bayes's theorem (Beck 1996; Beck 1989; Papoulis 1965). This yields the updated probability density for $\boldsymbol{\theta}$ that is then conditional on the data $\mathcal{D}$ as well as the model class $\boldsymbol{\Theta}$,

$$p(\boldsymbol{\theta}|\boldsymbol{\Theta},\mathcal{D}) = \frac{p(\mathcal{D}|\boldsymbol{\theta},\boldsymbol{\Theta})p(\boldsymbol{\theta}|\boldsymbol{\Theta})}{p(\mathcal{D}|\boldsymbol{\Theta})}, \tag{3.13}$$

where the denominator $p(\mathcal{D}|\boldsymbol{\Theta})$ serves to normalize (3.13) such that

$$\int_{\boldsymbol{\Theta}} p(\boldsymbol{\theta}|\boldsymbol{\Theta},\mathcal{D}) = 1. \tag{3.14}$$

This updated PDF for $p(\boldsymbol{\theta}|\boldsymbol{\Theta},\mathcal{D})$ then becomes the integrand in the probabilistic robust performance calculation, (2.21) or (2.22). This procedure is illustrated in Chapter 5 using a pre- and post-data model for the Caltech flexible structure.

In general, the *a priori* probability distribution $p(\boldsymbol{\theta}|\boldsymbol{\Theta})$ is likely to be fairly

broad, reflecting a lack of precise knowledge about the system. When response data becomes available, the PDF for $\boldsymbol{\theta}$ can be updated, and the peak of the PDF corresponds to the most probable values for the parameters in $p(\boldsymbol{\theta}|\boldsymbol{\Theta}, \mathcal{D})$. The local curvature of the PDF is related to the uncertainty in the parameter estimate, and is determined by sensor noise and model error, together with the sensitivity of the model response to changes in the model parameters.

When large amounts of data that pin down the model parameters precisely is available, the PDF $p(\boldsymbol{\theta}|\boldsymbol{\Theta}, \mathcal{D})$ becomes very peaked about its most-probable values (Beck 1996; Beck 1989). When this occurs, both the accuracy and the efficiency of the asymptotic approximation to the total probability integrals, (2.21) and (2.22), are improved significantly, as the peak of the integrand is then close to the peak of $p(\boldsymbol{\theta}|\boldsymbol{\Theta}, \mathcal{D})$, which is relatively easy to find.

3.5 Reliability of a linear system in discrete time

3.5.1 Introduction

In this section, bounds for the failure probability of a linear system excited by Gaussian-white noise are derived in discrete time, as an alternative to the continuous-time failure probability approximation shown in Section 2.2.3. The advantage of the discrete-time formulation is that bounds are obtained rather than an approximation for the failure probability. Furthermore, the discrete time formulation allows a simple method for introducing "memory" (i.e., dynamics) into the controller by multiplying delayed versions of the output by controller gains, in addition to the current output. Memory could be introduced similarly for a continuous-time system through the use of simple integrators taken from a Youla parameterization of the stabilizing controllers, but that is not examined here.

Failure is defined to occur when the system response exits a specified "safe" region in response-variable space for the first time. This represents a formulation of the "first-passage" problem in discrete time. The performance variables, i.e., the variables that determine the failure probability of the system, are linear combina-

tions of the state and controller variables. The system is assumed to be excited by a Gaussian-white random process, and the state-variable response is modeled as a Markov process.

3.5.2 System definition

Discrete-time system representation

Consider the state equations for a linear system in discrete time with linear output-feedback control,

$$\begin{aligned} x_{n+1} &= Ax_n + B_u u_n + B_w w_n \\ y_n &= C_y x_n + D_{yv} v_n \\ z_n &= C_z x_n + D_{zu} u_n \end{aligned} \tag{3.15}$$

where $u_n \in \mathbb{R}^{n_u}$ is the feedback control force,

$$u_n = -\sum_{i=0}^{m} K_i y_{n-i}. \tag{3.16}$$

In addition,

$n \in \{0, \ldots, N\}$	is the sequence of time indices of interest,
$x_n \in \mathbb{R}^{n_x}$	is the state vector (at time n),
$w_n \in \mathbb{R}^{n_w}$	is the excitation vector,
$y_n \in \mathbb{R}^{n_y}$	is the measured output vector,
$v_n \in \mathbb{R}^{n_y}$	is the output-error/measurement noise vector, and
$z_n \in \mathbb{R}^{n_z}$	is the performance variable vector.

The matrix $A \in \mathbb{R}^{n_x \otimes n_x}$ is the state-transition matrix, $B_u \in \mathbb{R}^{n_x \otimes n_u}$ and $B_w \in \mathbb{R}^{n_x \otimes n_w}$ determine the influence of the control input and the external excitation, $C_y \in \mathbb{R}^{n_y \otimes n_x}$ is the output matrix, $K_i \in \mathbb{R}^{n_u \otimes n_y}$ is the i^{th} control gain, multiplying the i^{th} output, and m is the total number of delays used by the controller. The

matrix D_{yv} scales the measurement noise, and is typically represented by a diagonal matrix. As is done for the continuous-time systems described in Section 3.1.2, no direct feed-through from the noise term, v_n, to the performance variables, z_n, is permitted. However, the noise can be filtered with a low-pass filter, and the filter states are then included in x_n. The performance variables are scaled using $C_z \in \mathbb{R}^{n_z \otimes n_x}$, $D_{zu} \in \mathbb{R}^{n_z \otimes n_u}$ such that $|z_n| = 1$ indicates a limit state has been attained at time step n, where $|\cdot|$ denotes the ∞-norm of the vector.

Inputs

The stochastic processes $\{w_n\}$ and $\{v_n\}$ are assumed to be zero-mean (and uncorrelated) Gaussian-white processes, with

$$\mathrm{E}[w_n w_m'] = W_n \delta_{mn} \tag{3.17}$$

$$\mathrm{E}[v_n v_m'] = V_n \delta_{mn} \tag{3.18}$$

$$\mathrm{E}[w_n v_m'] = 0. \tag{3.19}$$

Initial conditions

The initial state x_0 is assumed to be a zero-mean normally-distributed vector, with

$$R_0 := \mathrm{E}[x_0 x_0']. \tag{3.20}$$

Generalized representation of the linear system

First, consider the example of the memory-less controller. Let $A_0 := A - B_u K_0 C_y$, $B_0 := \begin{bmatrix} B_w & -B_u K_0 D_{yv} \end{bmatrix}$, $C_{z_0} := C_z - D_{zu} K_0 C_y$, and $D_{z_0} := \begin{bmatrix} 0 & -D_{zu} K_0 D_{yv} \end{bmatrix}$. Then the state-space representation of the system with the memory-less controller

is

$$
\begin{aligned}
x_{n+1} &= A_0 x_n + B_0 \left\{ \begin{matrix} w_n \\ v_n \end{matrix} \right\} \\
z_n &= C_{z_0} x_n + D_{z_0} \left\{ \begin{matrix} w_n \\ v_n \end{matrix} \right\}.
\end{aligned} \tag{3.21}
$$

The system with controller memory can be placed in a simpler form analogous to the memory-less case by wrapping the control feedback terms back into the state equation. Consider an augmented state vector $\tilde{x}_n$ and excitation vector $\tilde{w}_n$,

$$
\tilde{x}_n := \left\{ \begin{matrix} x_n \\ x_{n-1} \\ \vdots \\ x_{n-m} \end{matrix} \right\}, \quad \tilde{w}_n := \left\{ \begin{matrix} w_n \\ v_n \\ v_{n-1} \\ \vdots \\ v_{n-m} \end{matrix} \right\}, \tag{3.22}
$$

where m is the number of delays present for the control feedback term. Then

$$
\begin{aligned}
\tilde{x}_{n+1} &= \tilde{A}\tilde{x}_n + \tilde{B}\tilde{w}_n \\
z_n &= \tilde{C}\tilde{x}_n + \tilde{D}\tilde{w}_n
\end{aligned} \tag{3.23}
$$

where

$$\tilde{A} := \begin{bmatrix} A - B_u K_0 C_y & -B_u K_1 C_y & \dots & -B_u K_{m-1} C_y & -B_u K_m C_y \\ 1 & 0 & \dots & 0 & 0 \\ 0 & 1 & \dots & 0 & 0 \\ \vdots & \vdots & \ddots & \vdots & \vdots \\ 0 & 0 & \dots & 1 & 0 \end{bmatrix},$$

$$\tilde{B} := \begin{bmatrix} B_w & -B_u K_0 D_{yv} & -B_u K_1 D_{yv} & \dots & -B_u K_m D_{yv} \\ 0 & 0 & 0 & \dots & 0 \\ \vdots & \vdots & \vdots & \ddots & \vdots \\ 0 & 0 & 0 & \dots & 0 \end{bmatrix},$$

$$\tilde{C} := \begin{bmatrix} C_z - D_{zu} K_0 C_y & -D_{zu} K_1 C_y & \dots & -D_{zu} K_m C_y \end{bmatrix}, \quad \text{and}$$

$$\tilde{D} := \begin{bmatrix} 0 & -D_{zu} K_0 D_{yv} & -D_{zu} K_1 D_{yv} & \dots & -D_{zu} K_m D_{yv} \end{bmatrix}.$$

The input covariance matrix for this system is

$$\tilde{W}_n := E[\tilde{w}_n \tilde{w}_n'] = \begin{bmatrix} W_n & 0 & \dots & 0 \\ 0 & V_n & \dots & 0 \\ \vdots & \vdots & \ddots & \vdots \\ 0 & 0 & \dots & V_{n-m} \end{bmatrix}.$$

In general, to simplify the notation, the system matrices can be redefined, e.g., $A := \tilde{A}$ (or A_0), etc. So the following general form of the equations of motion for the closed-loop linear system can be used,

$$\begin{aligned} x_{n+1} &= Ax_n + Bw_n \\ z_n &= Cx_n + Dw_n. \end{aligned} \tag{3.24}$$

3.5.3 Performance specification

Define

$$\|z_n\|_\infty = \max_{n\in\{0,N\}} |z_n|, \tag{3.25}$$

where $|z_n|$ denotes the ∞-norm of the vector z_n. Then the performance criterion for the system is

$$\|z_n\|_\infty \leq 1, \tag{3.26}$$

which states that the performance variables in (3.24), which have been scaled appropriately by C and D, must be less than one for the entire time interval of interest in order for the system to achieve satisfactory performance.

The reliability of the system is the probability that the performance criterion will be satisfied,

$$P_{safe}(N) := \mathcal{P}\{\|z_n\|_\infty \leq 1|\mathcal{M}\}, \tag{3.27}$$

where the model class $\mathcal{M}$ is used to represent the assumptions for the system described above (i.e., the probability is conditional on the models used to describe the system and its input). Often, the reliability is quite close to one, so for numerical reasons, the failure probability is preferred, which is related to the reliability by

$$P_{fail}(N) := 1 - P_{safe}(N) = \mathcal{P}\{\|z_n\|_\infty > 1|\mathcal{M}\}. \tag{3.28}$$

The remainder of this section describes how this quantity can be calculated, and also several computationally efficient techniques are developed that can bound P_{fail}. Then, in Section 3.6, the discrete-time failure probability is used to design a controller (with memory) for the 2DOF example problem.

3.5.4 Response probability density function

The reliability of the system evaluated at time step N is the probability that the system has not failed at any of the time steps up to and including N,

$$P_{safe}(N) = \mathcal{P}\left\{ \bigcap_{\substack{n\in\{0,\dots N\} \\ i\in\{0,\dots,n_z\}}} |z_{n_i}| \leq 1 \right\}, \tag{3.29}$$

where z_{n_i} denotes the i^{th} component of z_n, and the conditioning on the model class $\mathcal{M}$ is assumed to be understood. In order to calculate this probability, the joint probability density function for the response variables $\{z_0, z_1, \dots, z_N\}$ (henceforth abbreviated using $\{z_n\}$ to represent the set of z_n's from $n = 0$ to N) is needed, which can then be integrated to determine $P_{safe}(N)$.

Since the system is linear and its inputs and initial state have zero-mean and are Gaussian distributed, the joint PDFs of $\{x_n\}$ and $\{z_n\}$ are also zero-mean Gaussian processes. So, if the covariance matrices can be found for $\{x_n\}$ and $\{z_n\}$, their PDFs are known. At a particular time step n, the covariance matrices that define the distributions require solution of the Lyapunov equation solution associated with the system in (3.24),

$$R_{n+1,n+1} = AR_{n,n}A' + BW_nB', \tag{3.30}$$

where $R_{n,n} := E[x_n x_n']$. This equation can be solved iteratively for $R_{n,n}$ given $R_0 := R_{0,0} = E[x_0 x_0']$ (as in (3.20)). If the system is stable and the stationary response is desired, the time-invariant discrete Lyapunov equation solution can be used, i.e.,

$$R = ARA' + BWB'. \tag{3.31}$$

Now, note that $R_{m,n}$ can be solved iteratively for general n and m using the following

identities,

$$\begin{aligned} R_{n+1,n} &= E\left[x_{n+1}x_n'\right] \\ &= E\left[(Ax_n + Bw_n)x_n'\right] = AR_{n,n}, \end{aligned} \tag{3.32}$$

$$\begin{aligned} R_{n,n+1} &= E\left[x_n x_{n+1}'\right] \\ &= E\left[x_n(Ax_n + Bw_n)'\right] = R_{n,n}A'. \end{aligned} \tag{3.33}$$

Let

$$Q_{n,n} := E\left[z_n z_n'\right] = CR_{n,n}C' + DW_nD'. \tag{3.34}$$

Also necessary for the joint probability density function of the response variables are the cross-correlation terms, given for $m > n$ by

$$\begin{aligned} Q_{m,n} &:= E\left[z_m z_n'\right] \\ &= CA^{(m-n)}R_{n,n}C' + CA^{m-n-1}BW_nD', \end{aligned} \tag{3.35}$$

which can be found using repeated application of (3.32) and (3.33). For $m < n$,

$$Q_{m,n} = Q_{n,m}' = CR_{m,m}A'^{(n-m)}C' + DW_mB'A'^{(n-m-1)}C'. \tag{3.36}$$

Now let $\mathcal{Q}_N$ represent the correlation matrix for $\{z_n\}$,

$$\mathcal{Q}_N = \begin{bmatrix} Q_{1,1} & Q_{1,2} & \cdots & Q_{1,N} \\ Q_{1,2}' & Q_{2,2} & \cdots & Q_{2,N} \\ \vdots & \vdots & \ddots & \vdots \\ Q_{1,N}' & Q_{2,N}' & \cdots & Q_{N,N} \end{bmatrix}. \tag{3.37}$$

Hence, the PDF is found using the standard expression for the Gaussian PDF,

$$p(z_0, z_1, \ldots, z_N) =$$

$$(3.38) \qquad \frac{1}{(2\pi)^{N*n_z/2}|\mathcal{Q}_N|^{1/2}} \exp\left[-\frac{1}{2}\left\{ z_0' \quad z_1' \quad \cdots \quad z_N' \right\} \mathcal{Q}_N^{-1} \left\{ \begin{array}{c} z_0 \\ z_1 \\ \vdots \\ z_N \end{array} \right\}\right],$$

where $|\cdot|$ denotes "determinant" when the argument is a matrix.

3.5.5 Reliability calculation

The reliability calculation requires a multi-dimensional integration of the joint PDF for the performance variables $\{z_n\}$ from -1 to 1 (recall that $|z_n| \leq 1$ implies safety at time n),

$$(3.39) \qquad P_{safe}(N) = \int_{-1}^{1} \cdots \int_{-1}^{1} p(z_0, z_1, \ldots, z_N) dz_{0_1} \ldots dz_{0_{n_z}} dz_{1_1} \ldots dz_{N_{n_z}}.$$

This is a difficult integration to perform, as the dimension of the integral may be quite high ($N \times n_z$ dimensions). Hence, an efficient and accurate approximation is desirable. Several bounding techniques and approximate methods for solving (3.39) are investigated in the remainder of this section. In general, the failure probability is the quantity that should be computed, which is the complement of (3.39).

These solution methods are illustrated using a single-degree-of-freedom (SDOF) oscillator excited by white noise, whose continuous-time state equations are given by

$$(3.40) \qquad \begin{aligned} \dot{x} &= Ax + Bw \\ z &= Cx, \end{aligned}$$

where

$$A = \begin{bmatrix} 0 & 1 \\ -\omega_0^2 & -2\zeta\omega_0 \end{bmatrix}, \quad B = \begin{bmatrix} 0 \\ 1 \end{bmatrix},$$

and

$$C = \begin{bmatrix} 1 & 0 \end{bmatrix}.$$

The input is assumed to be stationary Gaussian white noise, so its variance is given by $E[w(t)w(t+\tau_s)'] = W\delta(\tau_s)$. Following the example in Soong and Grigoriu (1993), the natural frequency ω_0 is chosen to be 2 rad/sec, and the damping ratio ζ is 0.02. Failure is defined to occur whenever the measured output (in this case, oscillator displacement) exceeds 3σ, where σ is defined to be the stationary variance of the response of the continuous system to white noise, $\sigma^2 = \pi W/(4\zeta\omega_0^3)$. For the transformation to discrete time, using a zero-order hold with time-step size τ_s, $A_d = \exp[A\tau_s]$, $B_d = \exp[A\tau_s]\,B\tau_s$, $C_d = C$, and

$$\begin{aligned} x_{n+1} &= A_d x_n + B_d w_n \\ z_n &= C_d x_n. \end{aligned} \tag{3.41}$$

Note that $E[w_n w_m'] = (W/\tau_s)\delta_{nm}$. The variance of the response is computed assuming the system response is stationary, so $E[z_0^2] = E[z_n^2]$, which is constant with respect to n.

3.5.6 Bounds on failure probability

First-order bounds

The failure probability of the discrete-time system can be found by considering the failure probability of a series system (Madsen et al. 1986), since a failure at any one time step indicates failure of the entire system. Let P_F be the overall failure probability for the system (i.e., $P_F = 1 - \mathcal{P}\left\{\bigcap_{\substack{n\in\{0,\ldots,N\} \\ i\in\{0,\ldots,n_z\}}} |z_{n_i}| \le 1\right\} =$

$\mathcal{P}\left\{\bigcup_{\substack{n\in\{0,\ldots,N\}\\ i\in\{0,\ldots,n_z\}}} |z_{n_i}| > 1\right\}$), and let $P_{n_i} = 1 - \mathcal{P}\{|z_{n_i}| \leq 1\}$. Then, as shown by Madsen et al. (1986), to first order[2] the bounds are

$$\max_{\substack{n\in\{0,\ldots,N\}\\ i\in\{0,\ldots,n_z\}}} P_{n_i} \leq P_F \leq \sum_{n=0}^{N}\sum_{i=1}^{n_z} P_{n_i}. \tag{3.42}$$

Since the failure boundaries of this problem are symmetric about zero, the failure probability at the n^{th} time step for the i^{th} performance variable is

$$\begin{aligned} P_{n_i} = \mathcal{P}\{|z_{n_i}| > 1\} &= \Phi(-1, Q_{n_i,n_i}) + (1 - \Phi(1, Q_{n_i,n_i})) \\ &= 2\Phi(-1, Q_{n_i,n_i}), \end{aligned} \tag{3.43}$$

where $\Phi(\beta, \rho)$ represents the Gaussian cumulative distribution function (CDF) evaluated at level β for a variance of ρ. Here, Q_{n_i,n_i} is the $(i,i)^{th}$ entry in the covariance matrix for z_n, given by (3.34), and is used to scale the distance to the failure surface. Under the assumption of stationary response, Q_{n_i,n_i} and P_{n_i} are independent of n (but not of i).

Second-order bounds

Tighter second-order bounds on the failure probability can be formed by considering the joint failure probabilities. To simplify the notation, let $p = i + n \cdot n_z$, $q = j + m \cdot n_z$, so z_p indicates the i^{th} component of z_n and z_q indicates the j^{th} component of z_m, such that $i, j \in \{1, \ldots, (N+1) \cdot n_z\}$. The second-order bounds consider the joint probability of failure between z_p and z_q. See Madsen et al. (1986) for a derivation of the following:

$$P_1 + \sum_{p=2}^{N\cdot n_z} \max\left\{P_p - \sum_{q=1}^{p-1} P_{pq}, 0\right\} \leq P_F \leq \sum_{p=1}^{N\cdot n_z} P_p - \sum_{p=2}^{N\cdot n_z} \max_{q<p} P_{pq}, \tag{3.44}$$

[2] "First order" implies ignoring the joint probabilities.

where the P_p's are arranged such that $P_1 \geq P_2 \geq \ldots \geq P_{N \cdot n_z}$, and P_{pq} is the joint probability

$$P_{pq} := \mathcal{P}\left\{|z_p| > 1 \text{ and } |z_q| > 1\right\}, \tag{3.45}$$

which can be calculated numerically, or it may also be approximated by bounds. Note that for the single performance variable case (i.e., $z_n \in \mathbb{R}^1$) and stationary response, the P_q's are all equal.

The exact joint failure probability for a single-sided failure mode and a two-variable random process can be expressed by the following integral (Madsen et al. 1986),

$$P_{pq} = \Phi(-\beta_p)\Phi(-\beta_q) + \int_0^{\rho_{pq}} \phi(-\beta_p, -\beta_q; z)dz, \tag{3.46}$$

where ρ_{pq} is the correlation coefficient and β_p, β_q represent distances to failure boundaries p and q in a unit-variant standard normal space, and

$$\phi(x, y; \rho) = \frac{1}{2\pi\sqrt{1-\rho^2}} \exp\left[-\frac{1}{2}\frac{x^2 + y^2 - 2\rho xy}{1-\rho^2}\right].$$

For the double-sided failure modes of the SDOF example, the P_p term is identical to the first order case, and the joint probability terms are given by

$$\begin{aligned} P_{pq} = {} & \mathcal{P}\left\{z_p > 1, z_q > 1\right\} + \mathcal{P}\left\{z_p < -1, z_q > 1\right\} + \\ & \mathcal{P}\left\{z_p < -1, z_q < -1\right\} + \mathcal{P}\left\{z_p > 1, z_q < -1\right\} \end{aligned} \tag{3.47}$$

where the "," is used to denote the logical "and." This two-sided failure surface is shown in Figure 3.7. In terms of Gaussian CDFs,

$$\begin{aligned} P_{pq} = {} & 2\left(\Phi(-\beta_p)\Phi(-\beta_q) + \int_0^{\rho_{pq}} \phi(-\beta_p, -\beta_q; z)dz\right) + \\ & 2\left(\Phi(-\beta_p)\Phi(-\beta_q) - \int_{-\rho_{pq}}^{0} \phi(-\beta_p, -\beta_q; z)dz\right). \end{aligned} \tag{3.48}$$

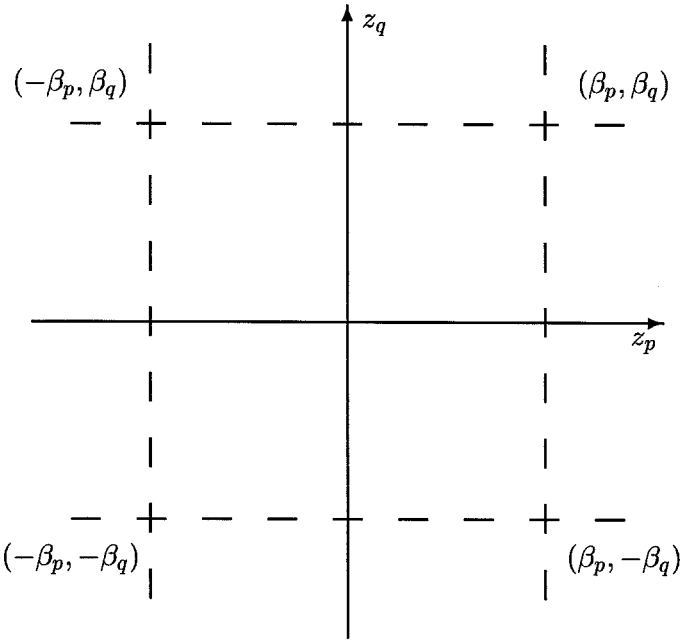

Figure 3.7 Safe region in two dimensions of performance-variable space.

As an alternative to numerically evaluating this integral, for a single-sided failure surface, bounds can be computed for P_{pq} such that, for $\rho_{pq} > 0$,

$$\begin{aligned} &\max\left\{\Phi(-\beta_p)\Phi(-\beta_{q|p}), \Phi(-\beta_q)\Phi(-\beta_{p|q})\right\} \leq P_{pq} \\ &\leq \Phi(-\beta_p)\Phi(-\beta_{q|p}) + \Phi(-\beta_q)\Phi(-\beta_{p|q}). \end{aligned} \tag{3.49}$$

For $\rho_{pq} < 0$, the bounds are

$$0 \leq P_{pq} \leq \min\left\{\Phi(-\beta_p)\Phi(-\beta_{q|p}), \Phi(-\beta_q)\Phi(-\beta_{p|q})\right\}. \tag{3.50}$$

The distances $\beta_{p|q}$ and $\beta_{q|p}$ are given in Madsen et al. (1986) as

$$\beta_{p|q} = \frac{\beta_p - \rho_{pq}\beta_q}{\sqrt{1-\rho_{pq}^2}} \tag{3.51a}$$

$$\beta_{q|p} = \frac{\beta_q - \rho_{pq}\beta_p}{\sqrt{1-\rho_{pq}^2}}. \tag{3.51b}$$

Since, in (3.44), the contribution of P_{pq} is negative to the lower bound of P_F, the upper bound on P_{pq} must be used in this case. Since P_{pq}'s contribution is negative to P_F's upper bound, the lower bound on P_{pq} must be used. For the symmetric double failure surfaces at each time step (as in Figure 3.7), these bounds should be multiplied by 4.

Note that for the stationary single output case (i.e., $n_z = 1$), (3.51a) and (3.51b) are equal, so

$$\beta_{p|q} = \beta_{q|p} = \beta_p \sqrt{\frac{1-\rho_{pq}}{1+\rho_{pq}}}. \tag{3.52}$$

Results for 1^{st}- and 2^{nd}-order bounds

The resulting bounds for the approximations given by (3.42) and (3.44) are calculated as a function of the duration of the time interval of interest and the sampling rate and are displayed in Figures 3.8–3.10. The sampling rates chosen for these figures are $\tau_s = 0.1$ sec, $\tau_s = 0.05$ sec, and $\tau_s = 0.02$ sec, and the number of points is determined by $N = \tau_f/\tau_s$. The first-order bounds are given by the dashed lines and the second-order bounds by the solid lines. The dotted line in the figure is the continuous-time out-crossing rate approximation (Lin 1976), and the dash-dot line shows the result of a Monte Carlo integration of the failure probability (see Section 3.5.7). Note that the lower bounds for both the first-order and second-order approximations are coincident, as $\left\{P_n - \sum_{m=1}^{n-1} P_{nm}\right\}$ from (3.44) is less than zero for this example. In these figures, the upper bounds grow larger as the sampling rate increases, which makes sense, since there are more sampling points and the gap

between the bound and the true value of the failure probability gets added for each sampling point.

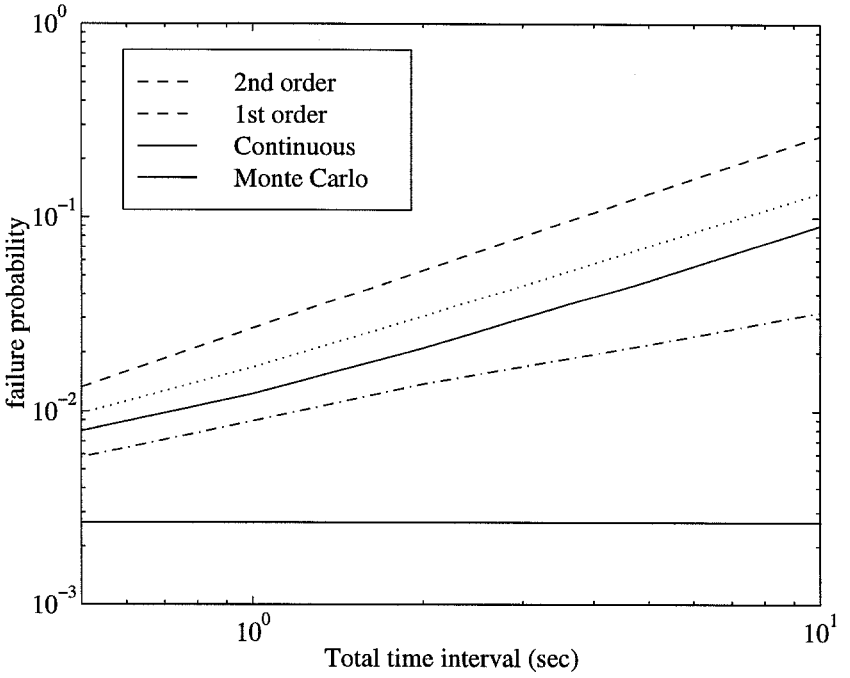

Figure 3.8 Bounds on failure probability, $\tau_s = 0.1$ sec.

3.5.7 Monte Carlo approximation to failure probability integral

Monte Carlo integration is an effective alternative method to approximate (3.39). The method is simple, as random points are generated using the PDF that is the integrand of (3.39), and the reliability is approximated as the number of points that are found to lie within the failure region divided by the total number of points. In practice a transformation to standard normal deviates will be required, since independent unit-variant random variables can easily be generated with a random number generator (such as MATLAB's built-in randn() function, or the routine described by Press et al. 1992). So, let v_n represent the standard normal variables and z_n, $n \in \{1, N\}$, the random variables of interest that appear in (3.39). As before,

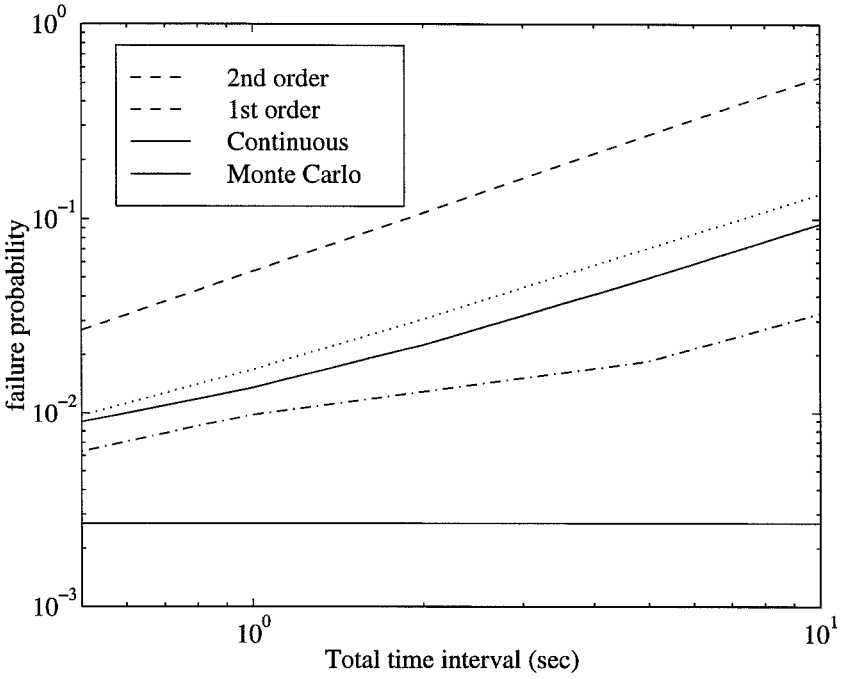

Figure 3.9 Bounds on failure probability, $\tau_s = 0.05$ sec.

let $E[\{z_n\}\{z_n\}'] = \mathcal{Q}_N$, $E[\{v_n\}\{v_n\}'] = I$, then $z_n = \mathcal{Q}_N^{1/2} v_n$, and let

$$q_n = \begin{cases} 1 & \text{if } |z_n| \leq 1 \\ 0 & \text{if } |z_n| > 1. \end{cases} \tag{3.53}$$

Then

$$P_{safe} \simeq \frac{1}{N} \sum_{n=1}^{N} q_n. \tag{3.54}$$

The Monte Carlo integration of (3.39) is given by the dash-dot lines in Figures 3.8–3.10. The results are obtained using 10,000 samples in the Monte Carlo simulation. Note that the Monte Carlo results have no perceptible trend with the time-step size, as would be expected, since the "true" reliability does not depend on the discretization of the system (provided the probability that the system ex-

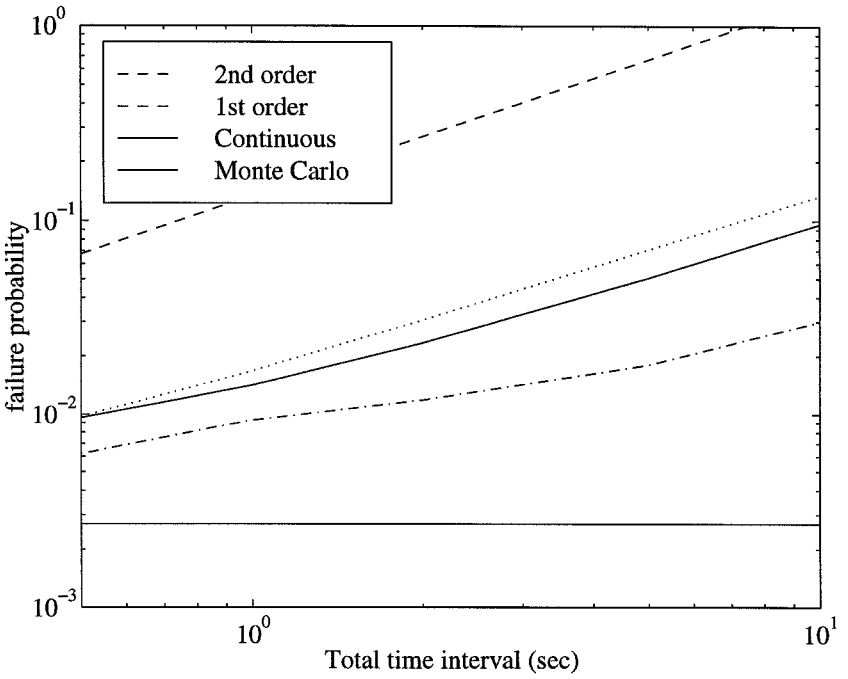

Figure 3.10 Bounds on failure probability, $\tau_s = 0.02$ sec.

its and re-enters the safe region *during* a time-step is negligible). As can be seen in the figures, the discrete-time Monte Carlo failure probabilities do differ significantly (approximately a factor of four) from the continuous-time outcrossing-rate approximation results. This discrepancy may be due to the continuous-time approximation providing an upper bound on the failure probability by adding the failure probabilities for each failure mode, while the discrete-time Monte Carlo approach approximates the desired integral and not this upper bound. Future research could investigate the similarities and differences between the two methods more fully.

3.6 Example using discrete time controller design

This section presents the results of a controller that is designed for the discretized version of the 2DOF example. The control design seeks to minimize the second-

order upper bound to the discrete-time failure probability that is given by (3.44) in Section 3.5.6. The continuous-time representation of the 2DOF example is converted to discrete time using a zero-order hold, based on the sample time τ_s, so

$$\left[\begin{array}{c|c} A & B \\ \hline C & D \end{array}\right] \mapsto \left[\begin{array}{c|c} A_d & B_d \\ \hline C_d & D_d \end{array}\right] := \left[\begin{array}{c|c} e^{A\tau_s} & e^{A\tau_s}B\tau_s \\ \hline C & D \end{array}\right]. \tag{3.55}$$

The outputs from the 2DOF system are the inter-story drifts of each floor and the controller force, and the performance goals are again to minimize the probability that the inter-story drifts exceed their 2% limit and the probability that the control force exceeds its limit of 5% of the structure's seismically-effective weight. In this section, the controller design is performed only for the nominal most-probable model of the system. The extension to the failure probability calculations for the uncertain model follows closely the continuous case using the total probability of failure, (2.21), but it is not presented here.

Using direct velocity-feedback control measured from the 2^{nd} mass, the failure probability of the system can be calculated both in discrete-time using the 2^{nd}-order bounds, (3.44), and in continuous-time using the out-crossing rate approximation, (2.7). This is shown in Figure 3.11, where the solid line represents the discrete-time failure probability approximation using the discrete-time representation of the system, and the dashed line is the out-crossing rate approximation using the continuous-time system. The two curves differ by roughly a factor of two, which, as discussed previously, is partially attributed to the out-crossing rate approximation providing an upper bound on the composite failure probability for the system by adding together the probabilities for each failure mode. Note that the shape of the performance curves is quite similar between the two methods, and the optimum values for k are close, as would be expected.

In addition, controller dynamics can be introduced as in (3.16) by gains multiplying delayed versions of the measured output. The controller parameters and closed-loop system performance as a function of the number of feedback delays m are calculated and presented in Table 3.7, based on a sampling time τ_s of 0.05 sec and a

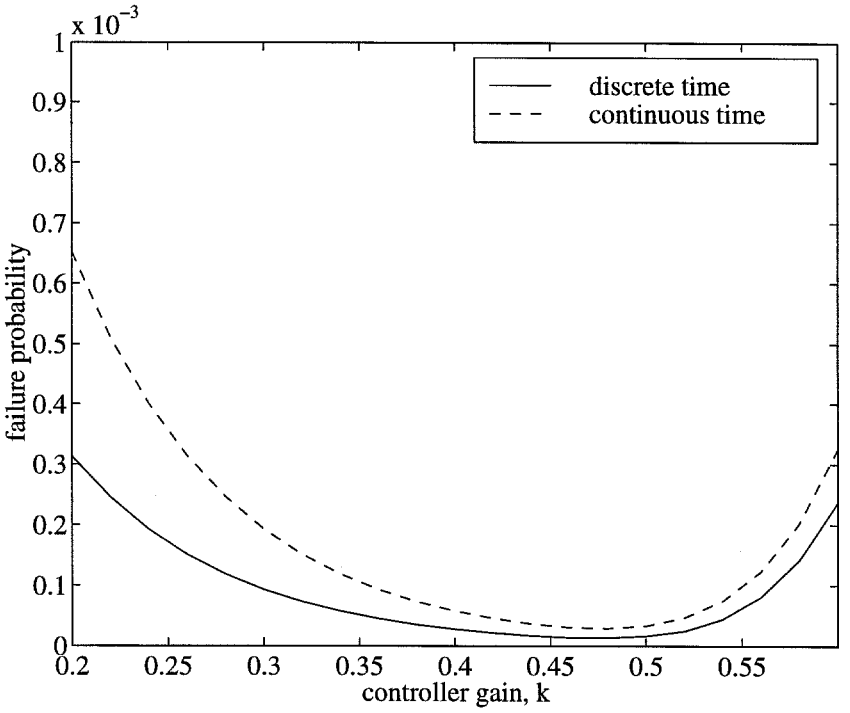

Figure 3.11 Failure probability in continuous and discrete time vs. the output-feedback controller gain.

total time interval of $T_f = 1$ sec. This T_f was chosen due to memory limitations encountered when computing the 2nd-order upper bound on the discrete-time failure probability. In addition, for small failure probabilities and under the assumption of stationarity, the failure probability is roughly proportional to T_f, so the actual value for T_f is not as important as the relative sizes of the calculated failure probabilities for the various controllers that are considered.

For illustrative purposes, the failure probability is plotted as a function of the number of delays (up to five delays) in Figure 3.12. One interesting item to note in Table 3.7 is that only small variations are seen in the lower-delay terms after several delays have been added, and after four delays, very little change is observed at all in k_1, k_2, k_3, and k_4. This is attributed to two reasons, that an effective damping is reducing the importance of the feedback terms multiplying the longer delays, and also that the four delays would correspond to the state-feedback case for the four-state discrete-time system. This second point can be easily demonstrated using the Cayley-Hamilton theorem.

Table 3.7 Discrete-time controller parameters and performance for various numbers of delays of the measured output, $\tau_s = 0.05$ sec, $T_f = 1$ sec.

	Number of measured-output delays					
	0	1	2	3	4	5
K_0	0.4712	0.6238	0.6096	0.5844	0.5950	0.5945
K_1	0	−0.2002	−0.1746	−0.3085	−0.3245	−0.3249
K_2	0	0	−0.0171	0.2632	0.2834	0.2833
K_3	0	0	0	−0.2019	−0.2219	−0.2218
K_4	0	0	0	0	0.0136	0.0142
K_5	0	0	0	0	0	−0.0014
discrete P_f (%), $\times 10^{-3}$	1.32	1.20	1.20	1.13	1.13	1.13

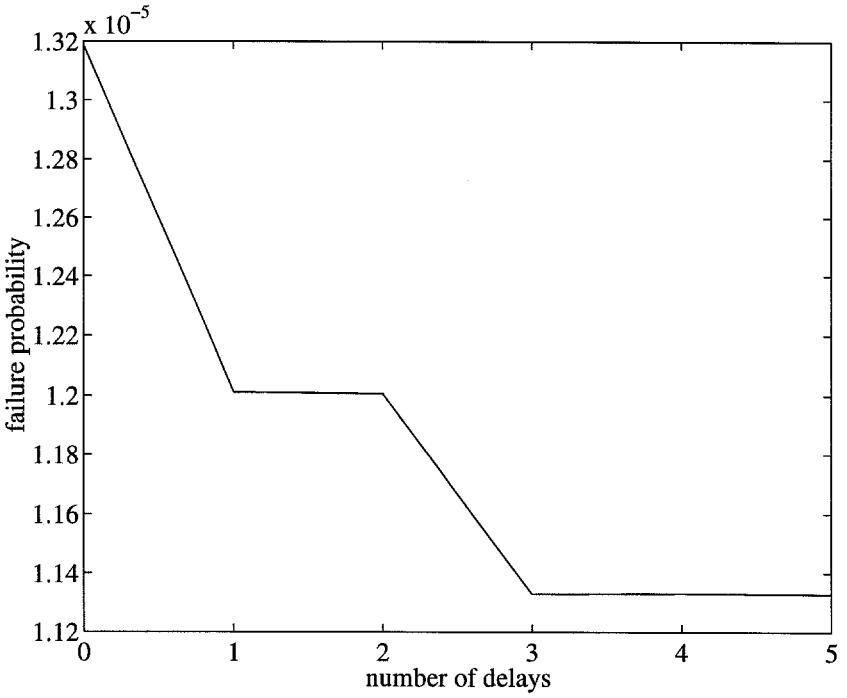

Figure 3.12 Failure probability vs. number of delays used by discrete-time controller, $\tau_s = 0.05$ sec, $T_f = 1$ sec.

Chapter 4

Application to Benchmark structural model

4.1 Benchmark structural control problem

The "benchmark" structural control model is a high-fidelity computer model of the laboratory structure located in the Earthquake Engineering/Structural Dynamics and Control Laboratory at the University of Notre Dame. A detailed description of the laboratory system can be found in Spencer et al. (1997a), Dyke et al. (1994), Dyke et al. (1996), and Dyke et al. (1995). A high-fidelity computer model of this structure has been proposed (Spencer et al. 1997a) as a test-bed for structural control algorithms so that comparisons can be made between the various methodologies. This model is available from the World Wide Web at http://www.nd.edu/~quake. The benchmark structural model is provided as a SIMULINK (1994b) block diagram that includes a linear model of the structure and actuator and incorporates many of the features of the laboratory system, such as the actuator saturation and analog to digital conversion.

In this chapter, the probabilistic robust control methodology that is developed in Chapters 2 and 3 is applied to the design of controllers for the benchmark model.

4.2 Benchmark system description

4.2.1 Laboratory system

A schematic of the Notre Dame laboratory structure that is the basis for the benchmark computer model is shown in Figure 4.1. The laboratory system, which is a model of a three-story braced-steel-frame building, is mounted on a single-axis shaking table. An active mass driver (AMD) hydraulic actuator is mounted on the top level of the structure to impart inertial forces to the structure for control purposes. The benchmark structure is mounted on a single axis shaking table that can provide inputs in the frequency range from 0–50 Hz. Accelerometers are mounted at each floor in the structure, as well as on the base and on the AMD actuator. Furthermore, a LVDT (linear variable differential transformer) is mounted between the actuator and its roof support to measure the relative displacement between the actuator and the roof. This LVDT is provided to stabilize the hydraulic control actuator as well as to provide displacement measurements for output.

The laboratory structure is 158 cm tall with a total mass of 227 kg that is evenly distributed among the three floors. The natural frequencies of the structure are 5.81 Hz, 17.68 Hz, and 28.53 Hz for the first three modes of vibration, with corresponding damping ratios of 0.33%, 0.23%, and 0.30%, respectively.

The Notre Dame laboratory structure is intended to be a scale model of the SUNY Buffalo prototype structural control experiment that is described in Chung et al. (1989) and Chung et al. (1988). The ratio of natural frequencies between the Notre Dame structure and the SUNY Buffalo prototype is approximately 5:1, so the time scaling factor for the benchmark structure is 5, and earthquake input time histories are scaled in the time domain by that amount. Furthermore, to provide appropriate amplitude scaling, the earthquake input magnitudes are scaled by a factor of 4.

The AMD actuator for the Notre Dame structure consists of a hydraulic actuator rod with masses attached to its ends, and the moving mass of the AMD is 5.2 kg. The total mass of the structure and AMD actuator is 309 kg, so the AMD represents

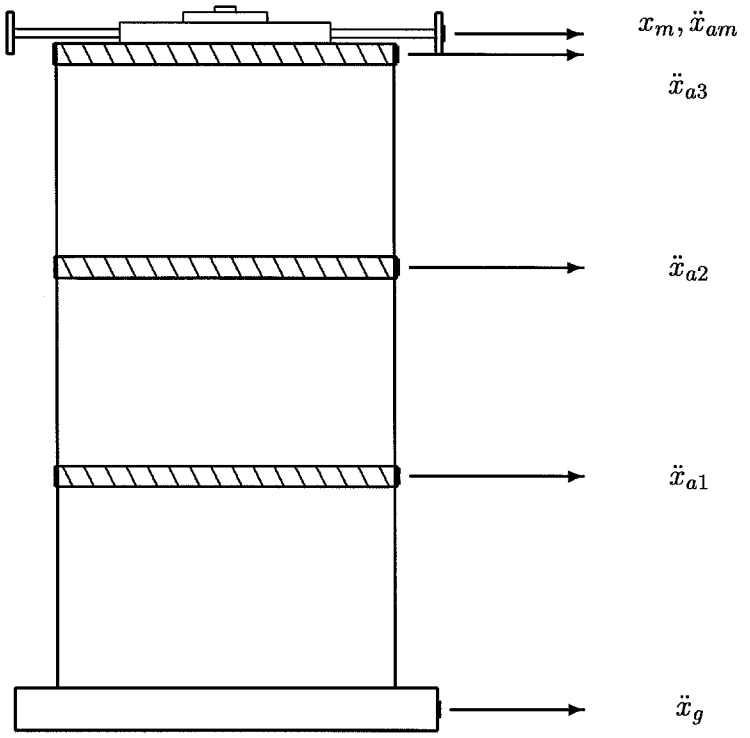

Figure 4.1 Schematic of Notre Dame "Benchmark" structure.

1.7% of the total mass.

The data acquisition hardware for the benchmark structure is sufficient to maintain a sampling and control rate of 1 kHz for each input and output channel. A computation delay of 200 μsec is required for the calculation of the control action and the A/D and D/A conversions. The A/D and D/A converters have 12 bit precision, with a span of ± 3 V. The root-mean-square (rms) noise level on the data channels is approximately 0.01 V, which is 0.15% of the span of the A/D converters.

4.2.2 Benchmark SIMULINK model

The benchmark system is a SIMULINK (The MathWorks, Inc. 1994b) model of the Notre Dame laboratory system. The SIMULINK model is created by inter-connecting the controller with the high-fidelity "evaluation model" of the structure described in Section 4.2.3. The SIMULINK model, which is pictured in Figure 4.2, incorporates several of the nonlinear features of the laboratory system, such as actuator and

sensor saturation, sensor noise, time delays, and discretization of time signals. The system response is modeled through numerical integration of the equations of motion represented in the SIMULINK model. To reduce integration errors, the integration is performed at a time-step of 0.0001 sec using a 4^{th} order Runge Kutta integration scheme (The MathWorks, Inc. 1994b; Press et al. 1992). The system inputs and the controller are updated every 0.001 sec. The closed-loop system response is simulated and the performance is calculated for a variety of performance measures that were defined in Spencer et al. (1997a), so the controller designs can be compared with controllers synthesized for the same system using other methods.

Some of the practical limitations on the controller that exist in the laboratory system and are implemented in the SIMULINK model pictured in Figure 4.2 are listed below:

- The controller is digitally implemented with a sampling time of $T_s = 0.001$ sec.
- A computational delay of 200 μsec exists in the controller implementation (implemented as the block named Unit Delay).
- The A/D and D/A converters for the digital controller have a 12-bit precision and a span of ± 3 V (implemented as the blocks named Quantizer and Saturation).
- Due to limited computational resources on the physical system, the controller (represented in the block labelled Discrete Controller) has a maximum of 12 states.
- Sensor noise with an rms level of 0.01 V is implemented in each channel as a Gaussian rectangular pulse process with zero mean, variance of 0.01 V, and width of 0.001 sec (implemented in the block named Sensor Noises). Actually, this "sensor noise" should be thought of as a combination of noise on the measurement sensors and modeling error between the SIMULINK benchmark model and the laboratory structure.

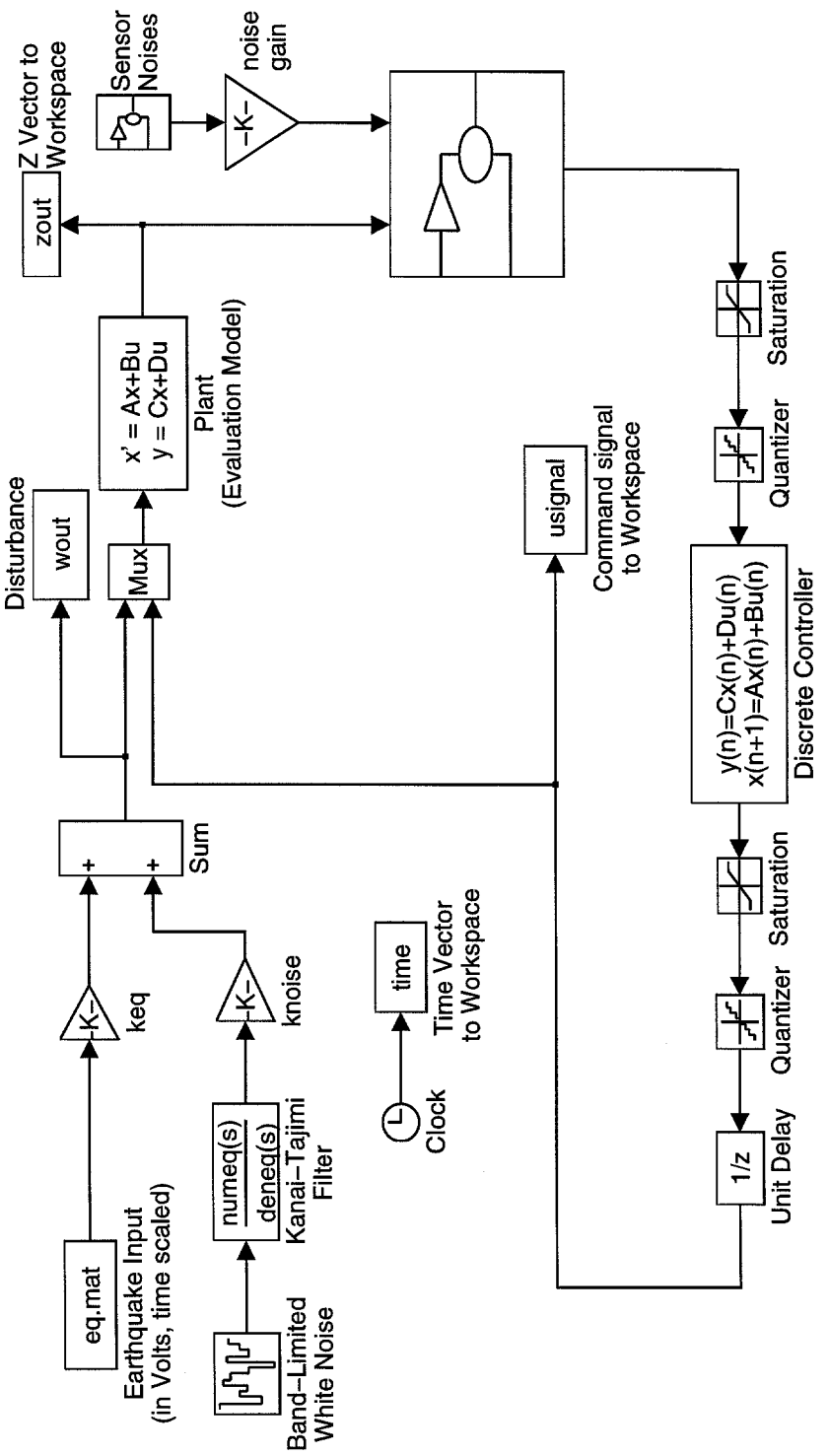

Figure 4.2 SIMULINK block diagram of benchmark system.

- The performance is evaluated using the 28-state "evaluation" model described in Section 4.2.3 (this model is represented by the Evaluation Model block).
- An integration step size of 0.0001 seconds is used for the 4^{th}-order Runge-Kutta integration to reduce integration errors.

4.2.3 Actuator-structure linear model

A high-fidelity linear model of the system that includes the vibrational modes of the structure as well as the dynamics of the actuator is provided with the benchmark system model. This "evaluation" model, used to evaluate the performance of the system, was developed using frequency-domain system identification techniques, which are described in Dyke et al. (1994), Dyke et al. (1995), and Dyke et al. (1996). The system identification method involved fitting parameterized curves in the frequency-domain to the transfer functions that were obtained experimentally. In this manner, a 28-state linear model was obtained for the system that accurately models its behavior in the frequency range from 0–100 Hz (Spencer et al. 1997a). This model is available from the benchmark problem web site (http://www.nd.edu/~quake).

The high-fidelity linear actuator-structure model can be represented with the following state equations (Spencer et al. 1997a),

$$\dot{x} = Ax + \begin{bmatrix} B & E & 0 \end{bmatrix} \begin{Bmatrix} u \\ \ddot{x}_g \\ v \end{Bmatrix}$$

$$\begin{Bmatrix} y \\ z \end{Bmatrix} = \begin{bmatrix} C_y \\ C_z \end{bmatrix} x + \begin{bmatrix} D_y & F_y & v_{rms} I_y \\ D_z & F_z & 0 \end{bmatrix} \begin{Bmatrix} u \\ \ddot{x}_g \\ v \end{Bmatrix}. \tag{4.1}$$

In (4.1), x is the state vector, $\ddot{x}_g$ is the ground acceleration, u is the single control input,

$$y = \begin{Bmatrix} x_m & \ddot{x}_{a1} & \ddot{x}_{a2} & \ddot{x}_{a3} & \ddot{x}_{am} & \ddot{x}_g \end{Bmatrix}' \tag{4.2}$$

is the measured-output vector,

$$z = \left\{ \begin{array}{cccccccccccc} x_1 & x_2 & x_3 & x_m & \dot{x}_1 & \dot{x}_2 & \dot{x}_3 & \dot{x}_m & \ddot{x}_{a1} & \ddot{x}_{a2} & \ddot{x}_{a3} & \ddot{x}_{am} \end{array} \right\}' \tag{4.3}$$

is the vector of response quantities that can be regulated, and v is the vector of "measurement" noise, which in practice is a combination of sensor noise and modeling error. In (4.2) and (4.3), the quantities x_1, x_2, x_3, and x_m represent the displacement of the structure at floors 1, 2, and 3, and the actuator displacement, respectively, $\dot{x}_1$, $\dot{x}_2$, $\dot{x}_3$, and $\dot{x}_m$ are the velocities at these locations, $\ddot{x}_{a1}$, $\ddot{x}_{a2}$, $\ddot{x}_{a3}$, and $\ddot{x}_{am}$ are the absolute accelerations, and $\ddot{x}_g$ is the ground acceleration. The accelerometers on the structure allow direct measurement of the accelerations $\ddot{x}_{a1}$, $\ddot{x}_{a2}$, $\ddot{x}_{a3}$, and $\ddot{x}_{am}$, and the relative position of the actuator, x_m, is measured directly by the LVDT mounted between the top floor and the actuator piston rod. The system matrices A, B, E, C_y, C_z, D_y, D_z, F_y, and F_z are available from http://www.nd.edu/~quake.

Note that z in (4.1) represents the response of the linear actuator-structure model, while the actual performance is simulated using the benchmark system. The discrepancy between these quantities, due to modeling error, which could also be described probabilistically, is assumed to be sufficiently small in the benchmark study that it can be safely neglected.

4.2.4 Reduced-order model for controller design

Standard model reduction techniques can be used to create a reduced-order "design" model that is more tractable for controller design purposes than the high order "evaluation" one. A 10-state reduced-order design model was also provided with the SIMULINK benchmark model. This reduced-order design model corresponds closely to the full-order one in the frequency range from 0 to 30 Hz, as can be seen in Figure 4.3. This frequency range includes the three fundamental structural modes that are the primary contributors to the inter-story drifts. In this figure, the frequency-response function from the ground input, $\ddot{x}_g$, to the first story drift, d_1, is

plotted using a solid line for the full-order model and a dashed line for the 10-state reduced-order model.

Alternative model reduction methods are also considered herein, such as model reduction through truncation of a balanced realization for the system, or by Hankel norm minimization (Zhou et al. 1996). The other model reduction methods are studied to verify the accuracy of the reduced-order model designed by Spencer et al. (1997a), because the model reduction method they used is is not described in their paper. The 10-state reduced-order models obtained through these methods are compared with the 10-state design model[1] and the full-order one in Figure 4.4. The transfer functions from $\ddot{x}_g$ to the third floor displacement ($T_{\ddot{x}_g \to x_3}$) and the third floor acceleration ($T_{\ddot{x}_g \to \ddot{x}_{a3}}$) are shown. The balanced-truncation and Hankel-norm minimization methods appear to yield quite similar models. These models resemble the full-order model more closely than the "design" model for the transfer function $T_{\ddot{x}_g \to x_3}$, but not as well for the transfer function $T_{\ddot{x}_g \to \ddot{x}_{a3}}$. The 10-state "design" model that was distributed with the benchmark model data appears to be as accurate as the reduced-order models from the other model reduction schemes, and it will be used throughout this chapter as the basis for controller design. The simulations to measure the system's performance are always performed using the 28-state evaluation model and the SIMULINK block diagram.

The system matrices A_r, B_r, E_r, C_{yr}, C_{zr}, D_{yr}, D_{zr}, F_{yr}, and F_{zr} associated with the reduced order "design" system are also provided with the SIMULINK benchmark model. The equations of motion for the reduced order system, which are similar to

[1] "Design model" will be used exclusively to refer to the reduced-order model that was distributed with the benchmark problem description.

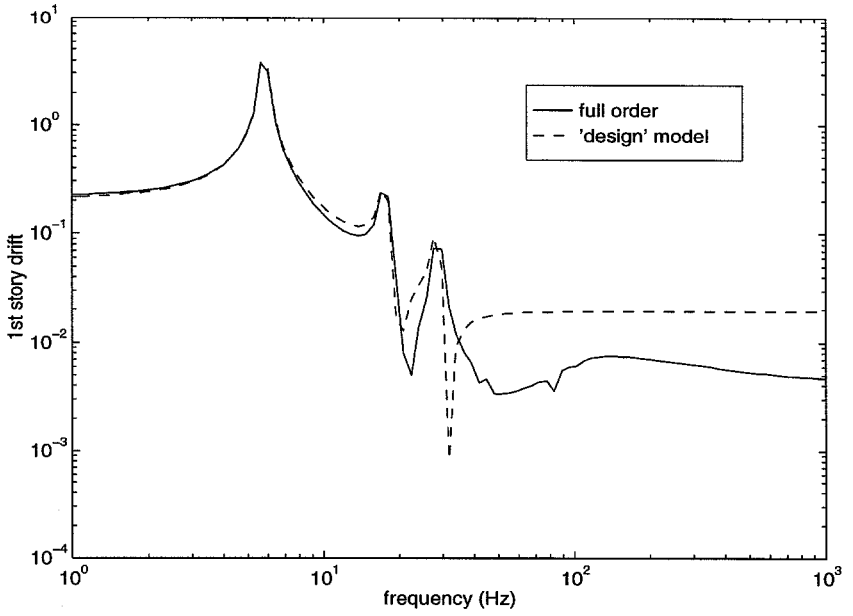

Figure 4.3 Transfer functions from $\ddot{x}_g$ to d_1 for full and reduced order models.

(4.1), are given by

$$\begin{aligned} \dot{x} &= A_r x + \begin{bmatrix} B_r & E_r & 0 \end{bmatrix} \begin{Bmatrix} u \\ \ddot{x}_g \\ v \end{Bmatrix} \\ \begin{Bmatrix} y \\ z \end{Bmatrix} &= \begin{bmatrix} C_{yr} \\ C_{zr} \end{bmatrix} x + \begin{bmatrix} D_{yr} & F_{yr} & \sigma_r I_y \\ D_{zr} & F_{zr} & 0 \end{bmatrix} \begin{Bmatrix} u \\ \ddot{x}_g \\ v_r \end{Bmatrix}. \end{aligned} \tag{4.4}$$

Note that v_r represents the sensor noise and modeling error for the reduced-order linear model of the benchmark system. This term has a different modeling error component than the sensor noise/modeling error v for the full order model, (4.1). In general, $\sigma_r \geq v_{rms}$, as the reduced-order model has more modeling error than the full-order one. The standard deviations v_{rms} and σ_r, for v and v_r, respectively, can be obtained by comparing the response of the benchmark system with the simulated response using the evaluation and design linear models, in turn. In this manner,

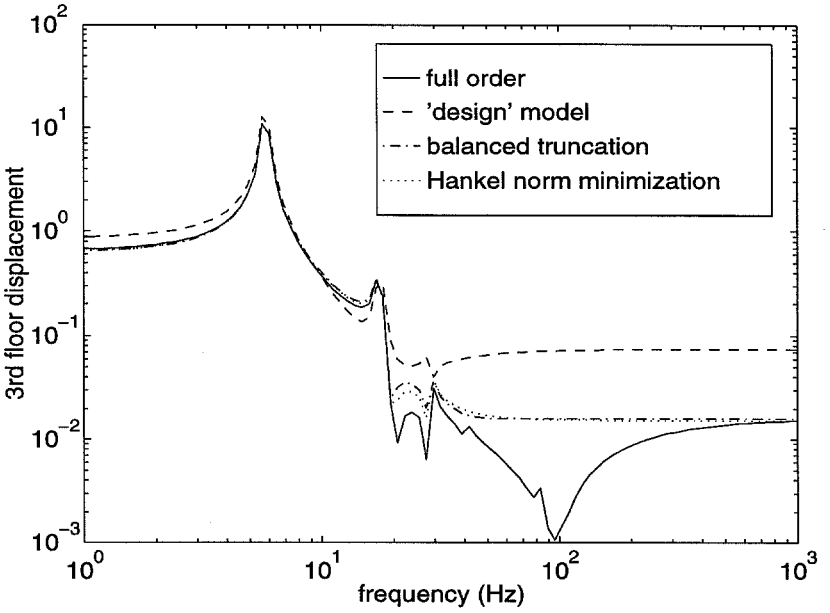

(a) $T : \ddot{x}_g \rightarrow x_3$

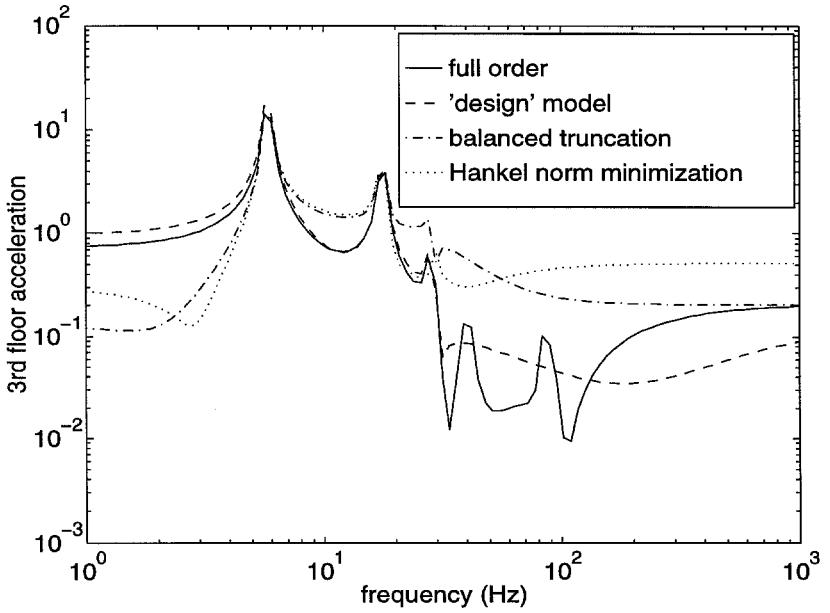

(b) $T : \ddot{x}_g \rightarrow \ddot{x}_{a3}$

Figure 4.4 Full versus reduced order model transfer functions for several model reduction methods.

the non-parametric modeling error is modeled as a Gaussian process, and can be included in the performance analysis for the system.

4.3 Performance calculation for design

The performance variables included in the design objective are the inter-story drifts and drift velocities, as well as the relative position and absolute acceleration of the actuator. The variables needed to compute the failure probabilities for these performance variables are denoted by

$$z_p := \left\{ d_1 \quad d_2 \quad d_3 \quad x_m \quad \dot{d}_1 \quad \dot{d}_2 \quad \dot{d}_3 \quad \dot{x}_m \quad \ddot{x}_{am} \quad \widetilde{\ddot{x}}_{am} \right\}', \tag{4.5}$$

where $d_i := (x_i - x_{i-1})$ is the interstory drift for story i, $\dot{d}_i$ is its velocity, and x_m, $\dot{x}_m$, and $\ddot{x}_{am}$ are the position, velocity, and acceleration of the actuator mass, respectively. The quantity $\widetilde{\ddot{x}}_{am}$ is an estimate of the derivative of the actuator's acceleration, which is required for the failure probability calculation in (2.8) and (2.12), and is obtained using a filter that mimics a differentiator at frequencies below 30 Hz. The differentiator's transfer function is given by

$$H_{\widetilde{\ddot{x}}_{am}\ddot{x}_{am}} = \frac{\omega_{df}^2}{s^2 + 2\zeta_{df}\omega_{df}s + \omega_{df}^2}, \tag{4.6}$$

with $\omega_{df} = 60\pi \simeq 188.5$ rad/sec and $\zeta_{df} = 1/\sqrt{2}$. Let the system G_z denote the relationship between z and z_p such that $z_p := G_z z$.

In addition, the control law is constructed using the acceleration feedback from the accelerometers mounted on each floor, which is a subset of the entire output vector y. Hence, $y_c = L_y y$, where $y_c = \left\{ \ddot{x}_{a1} \quad \ddot{x}_{a2} \quad \ddot{x}_{a3} \right\}'$.

The controller objective is evaluated on the basis of the theoretical stationary system response to a filtered white-noise excitation, where the filter is the well-known Kanai-Tajimi filter (Clough and Penzien 1975), such that the spectrum of the filter output mimics that of the stationary portion of a "typical" earthquake.

The power spectral density function for this filter is

$$S_{\ddot{x}_g\ddot{x}_g}(\omega) = \frac{S_0(4\zeta_g^2\omega_g^2\omega^2 + \omega_g^4)}{(\omega^2 - \omega_g^2)^2 + 4\zeta_g^2\omega_g^2\omega^2}, \tag{4.7}$$

which can be represented in the time domain with the following state equations

$$\begin{aligned} \dot{x}_f &= A_f x_f + B_f w \\ \ddot{x}_g &= C_f x_f \end{aligned} \tag{4.8}$$

where w is zero-mean Gaussian white noise with unit variance,

$$A_f := \begin{bmatrix} 0 & 1 \\ -\omega_g^2 & -2\zeta_g\omega_g \end{bmatrix}, \quad B_f := \begin{bmatrix} 0 \\ 1 \end{bmatrix}, \tag{4.9}$$

and

$$C_f := \sqrt{S_0 2\pi}\begin{bmatrix} \omega_g^2 & 2\zeta_g\omega_g \end{bmatrix}. \tag{4.10}$$

Also, S_0 is specified by Spencer et al. (1997a) such that the input variance is uniform for all ω_g and ζ_g, so

$$S_0 := \sigma_w^2 \frac{0.03\zeta_g}{\pi\omega_g(4\zeta_g^2 + 1)} \text{ g}^2 \cdot \text{sec}. \tag{4.11}$$

The constant σ_w is used to scale the input variance for different levels of excitation, and $\sigma_w = 1$ implies $\sigma_{\ddot{x}_g} = 0.12$ g. The factor of 0.03 arises from $0.03 \simeq 2 * 0.012^2$, which is found by solving for the spectral intensity of the filter (4.7) given input filter with spectral intensity of unity.

As before, let G represent the linear system given by the state-space equations of motion $\dot{x} = Ax + Bw$, $y = Cx + Dw$. Using this notation, let G_{des} represent the state equations for the linear "design" model, G_f the Kanai-Tajimi filter of (4.8), and G_c the state equations for the controller, which is described in Section 4.6. A block diagram of the system interconnection for the design model is shown in

Figure 4.5.

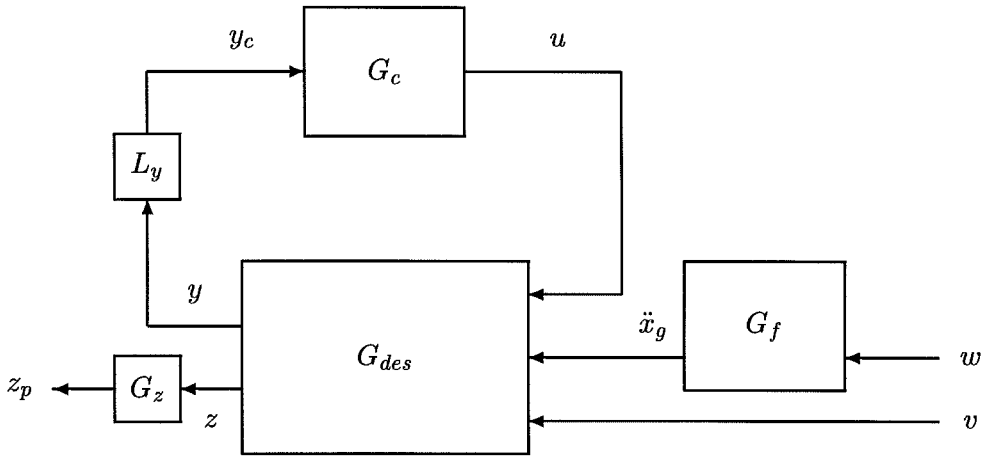

Figure 4.5 Closed-loop interconnection for controller design.

4.4 Model uncertainty

Uncertainty exists in the model parameters for the Kanai-Tajimi filter (4.7), where ω_g denotes the natural frequency of the input filter, ζ_g the damping ratio. The input variance for the filter is given by σ_w, which scales S_0 in (4.11). The parameters describing the system model are assumed to be accurate, and hence "certain," for evaluating the system performance in the frequency range from 0–30 Hz. The non-parametric modeling error, along with the measurement noise, is modeled as a Gaussian process with standard deviation $v_{rms} = 0.01$ V for the evaluation model, and by $\sigma_r \simeq 0.04$ V for the reduced-order design model. This value for the reduced-order design model was obtained by comparing the simulated displacement response of the uncontrolled, linear, reduced-order model to the response of the SIMULINK system. The probability density functions (PDFs) chosen to model the uncertain input parameters are shown in Figure 4.6, and are described as follows:

- ω_g is log-normally distributed with mean 50 rad/sec and $\sigma_{\log \omega_g} = 0.2$,
- ζ_g is log-normally distributed with mean 0.5 and $\sigma_{\log \zeta_g} = 0.2$, and
- σ_w is log-normally distributed with mean 1.0 and $\sigma_{\log \sigma_w} = 0.2$.

The log-normal PDFs are chosen for these parameters because, by applying the principle of maximum entropy to uncertain, strictly positive parameters, the log-normal distribution maximizes the uncertainty in these parameters (Jaynes 1978). The total failure probability does not, however, depend strongly on the form of the probability models, because the value of the integral in (2.21) is determined largely by the integrand's behavior at its peak. So, provided the choices for the probability models have the same most-probable values and similar shapes to their distributions about that point, little variation occurs in the calculated total failure probability. Although other probability models could be considered for the parametric uncertainty, such as the normal distribution or the χ^2 distribution, their PDFs would appear similar in the region of greatest contribution to (2.21), and hence would yield nearly identical probabilistic performance levels.

Spencer et al. (1997a) specify a range of uncertainty for ω_g and ζ_g, given by 20 rad/sec $\leq \omega_g \leq$ 120 rad/sec and $0.30 \leq \zeta_g \leq 0.75$. The probability distributions that are used to describe these parameters are selected such that the specified parameter ranges correspond (approximately) to the 5% and 95% probabilities for the cumulative distribution functions for the parameter uncertainties. In addition, σ_w is allowed to vary to represent the uncertainty in the earthquake intensity. For example, for the two earthquake records provided, σ_w is 1.4 for the El Centro record and 1.2 for the Hachinohe record, where the variance is calculated using the entire duration of the records. In practice, with a careful study of soil conditions of a site, proximity to major faults, and other factors, the PDFs for these ground-motion parameters could be refined to reflect the local site conditions. The log-normal distributions are chosen to represent the parameter uncertainty because this distribution corresponds to the maximum entropy distribution for these parameters with single-sided uncertainty. The calculated performance of the system appears to be

very sensitive to the shape of these distributions for the reliability-based performance measure, so further investigation into the selection of the probability distributions that model the uncertainty is a good topic for further research. The variables are assumed to be stochastically independent, so the joint PDF is the product of these PDFs.

4.5 Performance measures

The performance measure used for the control design procedure is the reliability as estimated by the out-crossing rate approximation from (2.7) in Chapter 2. For the "nominal" controller design, this performance is calculated for the system that uses the most-probable parameter values for the uncertain parameters defined in Section 4.4. For the "robust" control design, parameter uncertainty is considered, and the total system reliability is calculated according to (2.21).

To calculate the reliability of the system, failure is defined to occur when any of the following occur:

- the drift in any story exceeds 1.5 cm (approximately 3% of the story height),
- the actuator stroke exceeds its limit of 9 cm, or
- the actuator acceleration exceeds 6 g.

As discussed previously in Chapter 3, choosing these actuator limits forces the controller to behave strictly linearly and could lead to overly conservative controller designs. For this example, however, the controllers that are designed appear to be effective while still avoiding saturation.

While the probabilistic controller is designed to minimize the closed-loop system's failure probability, in order to compare this design with other control methodologies, its "performance" is assessed using the ten evaluation criteria J_1–J_{10} proposed by Spencer et al. (1997a), which represent measures of a variety of response quantities. Evaluation criteria J_1 through J_5 represent root-mean-square

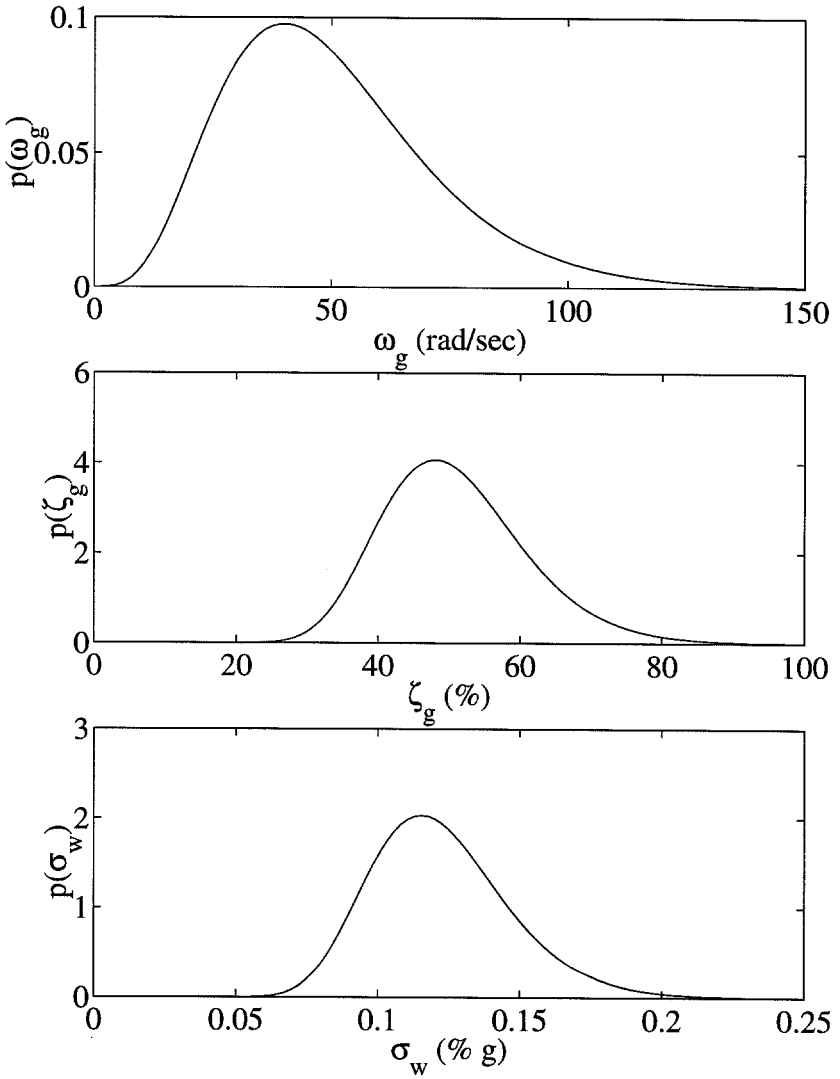

Figure 4.6 Probability density functions for the uncertain variables ω_g, ζ_g, and σ_w.

(rms) response quantities for the controlled system, normalized by the rms response of the uncontrolled system, for the "worst-case" Kanai-Tajimi filter parameters $\omega_g = 36.4$ rad/sec and $\zeta_g = 0.3$, with $\sigma_w = 1$. These response ratios are the interstory drift (J_1), absolute acceleration (J_2), actuator displacement relative to the third story (J_3), relative actuator velocity (J_4), and absolute actuator acceleration (J_5). The quantities J_1 and J_3 are normalized by the rms relative displacement of the third floor with respect to the base for the uncontrolled system with $\omega_g = 37.3$ rad/sec, $\zeta_g = 0.3$, $\sigma_w = 1$, where the rms displacement is $\sigma_{x_{3o}} = 1.31$ cm. Criterion J_4 is normalized by the third floor rms relative velocity, $\sigma_{\dot{x}_{3o}} = 47.9$ cm/sec, and J_2 and J_5 are normalized by the rms absolute acceleration of the third floor, $\sigma_{\ddot{x}_{a3o}} = 1.79$ g. Due to nonlinear components of the SIMULINK model, the rms response quantities for the controlled system are obtained by averaging the response to computer-generated random noise for 200 seconds.

Evaluation criteria J_6 through J_{10} represent the peak values of the same response quantities for the deterministic response of the closed-loop system to two scaled earthquake inputs, the north-south component of the 1940 El Centro Earthquake, and the north-south component of the 1968 Hachinohe Earthquake. These criteria are normalized by the peak response quantities of the uncontrolled system for each earthquake. For the El Centro response, J_6 and J_8 are normalized by $x_{3o} = 3.37$ cm, J_9 by $\dot{x}_{3o} = 131$ cm/sec, and J_7 and J_{10} by $\ddot{x}_{a3o} = 5.05$ g. For the Hachinohe response, J_6 and J_8 are normalized by $x_{3o} = 1.66$ cm, J_9 by $\dot{x}_{3o} = 58.3$ cm/sec, and J_7 and J_{10} by $\ddot{x}_{a3o} = 2.58$ g.

4.6 Controller design

4.6.1 Failure probability calculation

The controller design seeks to minimize the failure probability of the system. As shown in (2.12), the out-crossing rate of a scalar stochastic process is simply a function of the variance of the response and its derivative. The variances of the response quantities are obtained by solving the Lyapunov Equation associated with

the closed-loop system pictured in Figure 4.5. These are substituted into (2.12), then the approximate failure probability for each model is obtained from (2.8). For the "uncertain-model" controller, the total failure probability given by (2.21) is then evaluated using an asymptotic expression (Papadimitriou et al. 1997).

Let G_{clp}, with inputs w and v and output z_p, be the system formed by the closed-loop inter-connection of Figure 4.5, so G_{clp} has the following form, where the system matrices can be derived from (4.1), (4.8), and (4.17),

$$\dot{x}_{clp} = A_{clp}x_{clp} + B_{clp}\begin{Bmatrix} w \\ v \end{Bmatrix} \tag{4.12}$$

$$z_p = C_{clp}x_{clp}.$$

Let $x_{clp} = \begin{Bmatrix} x_c' & x_r' & x_f' \end{Bmatrix}'$ represent the state of the closed-loop system, and recall that z_p is its output. The covariance matrix of the performance variables is

$$E[z_p z_p'] = C_{clp}RC_{clp}', \tag{4.13}$$

where "E" denotes expected value, and

$$R := E\left[x_{clp}x_{clp}'\right] \tag{4.14}$$

is the solution to the standard Lyapunov Equation

$$A_{clp}R + RA_{clp}' + B_{clp}B_{clp}' = 0, \tag{4.15}$$

where w and v from (4.12) are independent zero-mean Gaussian white-noise processes with unit variance.

The failure possibilities considered for this example include the interstory drifts, and "failure" occurs when the drift in any one story exceeds the drift limit β, where the limit is chosen to be 1.5 cm, or approximately 3% of the story height. In practice, assuming the purpose of the structural control system is to reduce the earthquake

damage to the structure, the limiting value for the inter-story drift should correspond to the displacement level that would cause structural damage. Attaining a drift ratio of 3% during an earthquake would indicate that some damage has likely occurred in a moment-resisting steel frame (similar to the laboratory structure). Note, however, that this simplified approach ignores the nonlinear response of the system and the ductility of the steel frame structure. Additional failure possibilities for the AMD benchmark model are that the actuator exceeds the limits of its stroke and its maximum allowable acceleration. Hence, for the AMD actuator, failure is defined to occur when the required actuator displacement, x_m, exceeds its stroke of $\pm\xi_1 =$ 9 cm, or when the required actuator acceleration, $\ddot{x}_{am}$, exceeds $\pm\xi_2 = 6$ g.

Other failure possibilities could be considered for the control design for the structure, such as exceeding the maximum allowable base shear force, exceeding comfortable acceleration levels in the structure, or for the actuator, exceeding the actuator power or force limits. The control objective can easily be re-defined to represent a different combination of these possible failures.

An illustration of a three-dimensional projection of the failure surface is shown in Figure 4.7 (note that the true failure surface is five-dimensional for this problem). The three dimensions pictured are the drifts for the first two stories (d_1 and d_2), and the actuator displacement (x_m). The complete "safe" region is defined by

$$\mathcal{S} := \left\{ \begin{array}{c} \max(|d_1(t)|, |d_2(t)|, |d_3(t)|) \le \beta, \\ |x_m(t)| \le \xi_1, |\ddot{x}_{am}| \le \xi_2 \end{array} \quad \text{for } t \in (0, T] \right\}, \tag{4.16}$$

where $T = 10$ sec. The failure surface boundary, $\partial\mathcal{S}$, is defined by $\beta = 1.5$ cm, $\xi_1 = 9$ cm, and $\xi_2 = 6$ g.

4.6.2 Controller class

The following state equations are used to describe the linear control system G_c,

$$\begin{aligned} \dot{x}_c &= A_c x_c + B_c y_c \\ u &= C_c x_c \end{aligned} \tag{4.17}$$

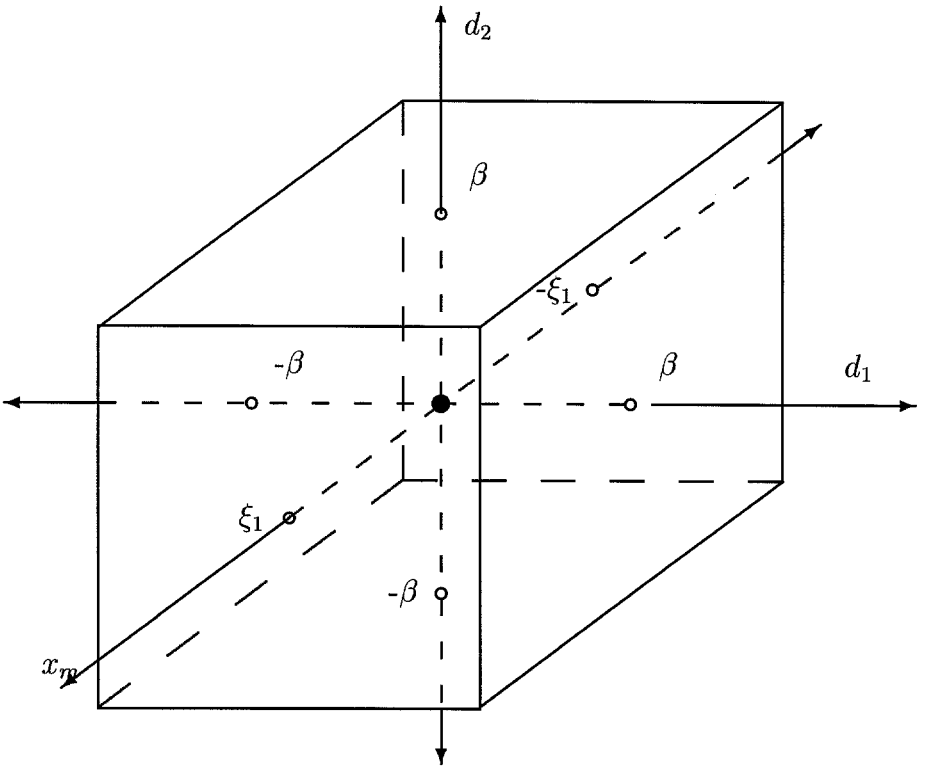

Figure 4.7 Safe region in response-variable space.

where x_c represents the states of the controller, which are the states of the frequency-weighting low-pass filter, and B_c represents the output-feedback gains.

Output-feedback controllers are considered for the control design optimization, where the measured absolute acceleration of each floor of the model is fed back to the controller. Since the primary contribution to the inter-story drift for earthquake excitations is expected to come from the flexible modes of the structure, which all occur below 30 Hz for the uncontrolled system, a frequency-dependent weighting function is included in the controller that seeks to minimize the structural response in this lower frequency range and to reduce the control effort in the range of the higher frequency noise and modeling error. The roll-off frequency for the low-pass weighting function, when specified *a priori* rather than included in the controller

design, is $\omega_b = 60\pi = 188.5$ rad/sec, and the low-pass filter is a second-order Butterworth filter. Therefore, the controller has a state of dimension 2, and easily satisfies the controller dimension limit of 12 specified for the benchmark problem (Spencer et al. 1997a). The controller parameters that are free to vary for the optimization are the three proportional-feedback gains, $K = \begin{Bmatrix} k_1 & k_2 & k_3 \end{Bmatrix}$, that multiply the accelerations from the sensors at floors 1, 2, and 3 of the structure, respectively, and ω_b, when this is considered as a design parameter.

In this section, the results of four controllers that are designed for the AMD benchmark model are presented. The first two, termed the "nominal-model controllers," are designed using the reduced-order "design" model to minimize the failure probability for a particular Kanai-Tajimi excitation model. This model uses the parameter values $\omega_g = 50.0$ rad/sec, $\zeta_g = 0.5$, and $\sigma_w = 1$, which correspond to the mean values of the parameters (and are close to the most probable ones) for the PDFs given in Figure 4.6. The second two controllers, termed the "uncertain-model controllers," are again designed using the reduced-order design model to minimize the total failure probability. These controllers explicitly incorporate the uncertainty of the excitation model parameters ω_g, ζ_g, and σ_w. The initial guess during the optimization for the uncertain-model control-feedback gains is taken from the result from the nominal-model controller optimization. For each case (nominal model and uncertain model), one controller is designed for the three output-feedback gains using a roll-off frequency of $\omega_b = 20\pi$ rad/sec for the low-pass filter. The other controllers include this roll-off frequency as a design parameter for the controller optimization.

Direct output-feedback without the use of a dynamic compensator is also considered (see Section 4.8). However, satisfactory performance is not attainable in this case because the actuator acceleration is too large due to the higher-frequency sensor noise and modeling error. A study of the affect of the roll-off frequency for the low-pass filter on the performance of the nominal-model controller is conducted in Section 4.8, and lower roll-off frequencies are observed to reduce the acceleration requirements for the AMD actuator that constrain the probabilistic performance.

Concurrently, the AMD displacements increase, but they do not begin to constrain the performance until the required AMD acceleration and displacement levels are comparable.

4.7 Results

4.7.1 Controller design for most probable model

For Controller 1, the nominal-model controller designed using $\omega_b = 188.5$ rad/sec for the roll-off frequency of the controller low-pass filter, and ground-motion parameters $\omega_g = 50$ rad/sec, $\zeta_g = 0.50$, has the optimal acceleration-feedback gains $K_1 = \begin{Bmatrix} 0.0339 & 0.0538 & 0.0958 \end{Bmatrix}$ (see Table 4.3 for a summary of the various controller designs considered in this section). The ten performance criteria J_1–J_{10} are listed for this model in Table 4.1. The criteria J_1–J_5 are evaluated by simulating the response of the closed-loop system in SIMULINK to a stationary computer-generated "white" signal with variance $\sigma_{\ddot{x}_g} = 0.12$ g for 200 seconds duration, then computing the variances of the relevant response variables. The simulated response of the system controlled using Controller 1 is shown in Figure 4.8 for the north-south (NS) component of the 1940 El Centro Earthquake input and in Figure 4.10 for the NS component of the 1968 Hachinohe Earthquake input. For comparison, the El Centro Record, as well as the response of the uncontrolled system to that input, are shown in Figure 4.12.

For Controller 2, ω_b is allowed to vary as a controller design parameter, and the gains $K_2 = \begin{Bmatrix} 0.354 & 0.320 & 0.237 \end{Bmatrix}$ are found along with $\omega_b = 33.4$ rad/sec. Note from Table 4.1 that this controller has significantly better performance than Controller 1, particularly for the failure probability performance measure. Recall that the failure probability is a nonlinear (exponential) function of the mean-square response quantities, so this large quantitative difference is not surprising for much smaller relative differences in the mean square response quantities (i.e., performance criteria J_1 through J_5). The improved performance when ω_b is taken as a controller design parameter can be understood by examining the effect of the low-pass fil-

ter when ω_b is less than the frequency of the first structural mode. When this occurs, the low-pass filter actually serves as an integrator, so now rather than acceleration-feedback control, (pseudo-) velocity feedback control is being used. Through velocity-feedback control, the effective damping of the structure can be directly increased, reducing the level of structural response significantly, and hence the better performance for this controller.

The simulated response to the NS El Centro Earthquake record for the system controlled by Controller 2 is displayed in Figure 4.9. Its response to the NS component of the 1968 Hachinohe Earthquake is shown in Figure 4.11. The Fourier amplitude spectra of the first-story drift response of the controlled system with Controller 2 and the uncontrolled system to the El Centro input are shown in Figure 4.13, where the attenuation of the first two modes of vibration by the controller action is apparent.

These nominal-model controllers are both successful in reducing the inter-story drifts, and hence the failure probabilities. For Controller 2, which achieved the lowest response levels and failure probabilities, the maximum drift calculated for the controlled system during the El Centro earthquake is 1.17 cm (compared to 2.09 cm for the uncontrolled system), and only 0.631 cm of drift is achieved during the Hachinohe earthquake (versus 0.958 cm for the uncontrolled system). The maximum actuator displacements that are found for these inputs are 4.46 cm and 2.69 cm, and the maximum accelerations are 4.22 g and 2.39 g. For the earthquake inputs, the maximum response ratios J_6–J_{10} given in Table 4.1 occur during the Hachinohe earthquake. The maximum actuator displacements, accelerations, and input voltages, as well as the rms values of these quantities, all satisfy the constraints for the AMD benchmark actuator (Spencer et al. 1997a) for Controller 2 (note that the maximum actuator acceleration of 6 g is exceeded for Controller 1).

4.7.2 Robust controller design for uncertain model

In contrast to the nominal model controllers in the previous section, Controllers 3 and 4 are designed for the uncertain model in order to explicitly provide robustness

Table 4.1 Controller performance for various evaluation criteria (normalized by uncontrolled response).

		Controller Number			
		Nominal		Robust	
	Performance Measure	1 Fixed ω_b	2 Optimal ω_b	3 Fixed ω_b	4 Optimal ω_b
Mean Square Response	J_1 (σ_d)	0.322	0.208	0.299	0.207
	J_2 ($\sigma_{\ddot{x}}$)	0.525	0.348	0.487	0.348
	J_3 (σ_{x_m})	0.606	0.836	0.675	0.846
	J_4 ($\sigma_{\dot{x}_m}$)	0.602	0.817	0.668	0.826
	J_5 ($\sigma_{\ddot{x}_m}$)	0.995	0.666	1.027	0.673
	$\|x_m(t)\|_2$ (cm)	0.79	1.10	0.88	1.11
	$\|\ddot{x}_{am}(t)\|_2$ (g)	1.78	1.19	1.84	1.21
	$\|u(t)\|_2$ (V)	0.16	0.29	0.18	0.30
Maximum El Centro Response	J_6 ($\|d\|_\infty$)	0.423	0.347	0.401	0.345
	J_7 ($\|\ddot{x}\|_\infty$)	0.687	0.536	0.671	0.535
	J_8 ($\|x_m\|_\infty$)	0.659	1.324	0.772	1.341
	J_9 ($\|\dot{x}_m\|_\infty$)	0.634	1.186	0.722	1.200
	J_{10} ($\|\ddot{x}_m\|_\infty$)	1.239	0.836	1.298	0.859
	$\|x_m(t)\|_\infty$ (cm)	2.22	4.46	2.60	4.52
	$\|\ddot{x}_{am}(t)\|_\infty$ (g)	6.26	4.22	6.56	4.34
	$\|u(t)\|_\infty$ (V)	0.51	1.25	0.62	1.26
Maximum Hachi-nohe Response	J_6 ($\|d\|_\infty$)	0.483	0.380	0.467	0.380
	J_7 ($\|\ddot{x}\|_\infty$)	0.785	0.687	0.733	0.684
	J_8 ($\|x_m\|_\infty$)	0.729	1.618	0.858	1.644
	J_9 ($\|\dot{x}_m\|_\infty$)	0.755	1.524	0.895	1.558
	J_{10} ($\|\ddot{x}_m\|_\infty$)	1.225	0.928	1.308	0.936
	$\|x_m(t)\|_\infty$ (cm)	1.21	2.69	1.42	2.73
	$\|\ddot{x}_{am}(t)\|_\infty$ (g)	3.16	2.39	3.37	2.41
	$\|u(t)\|_\infty$ (V)	0.31	0.75	0.36	0.76
	Robust P_f (%)	17.9	0.067	16.5	0.067
	Nominal P_f (%)	1.81	2.18×10^{-9}	2.15	2.18×10^{-9}

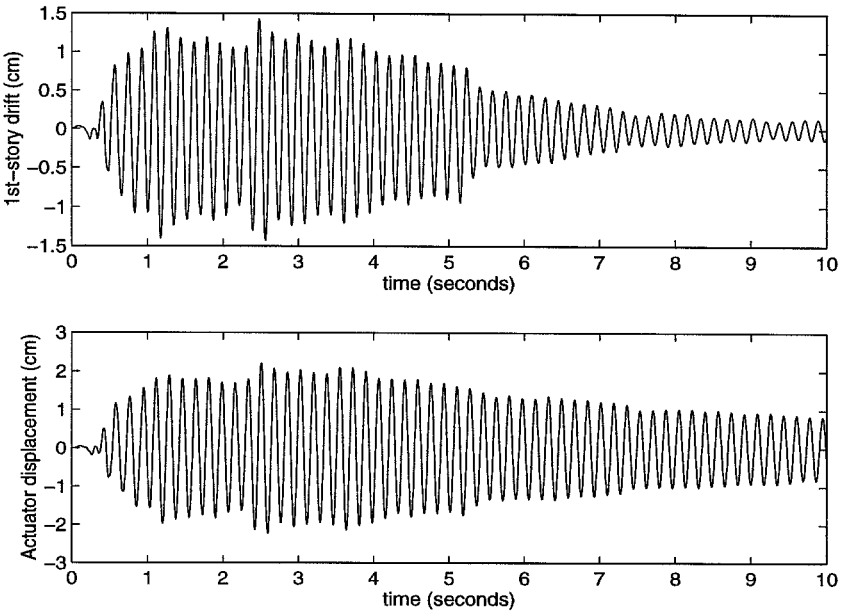

Figure 4.8 Response to scaled NS component of the 1940 El Centro Earthquake, Controller 1.

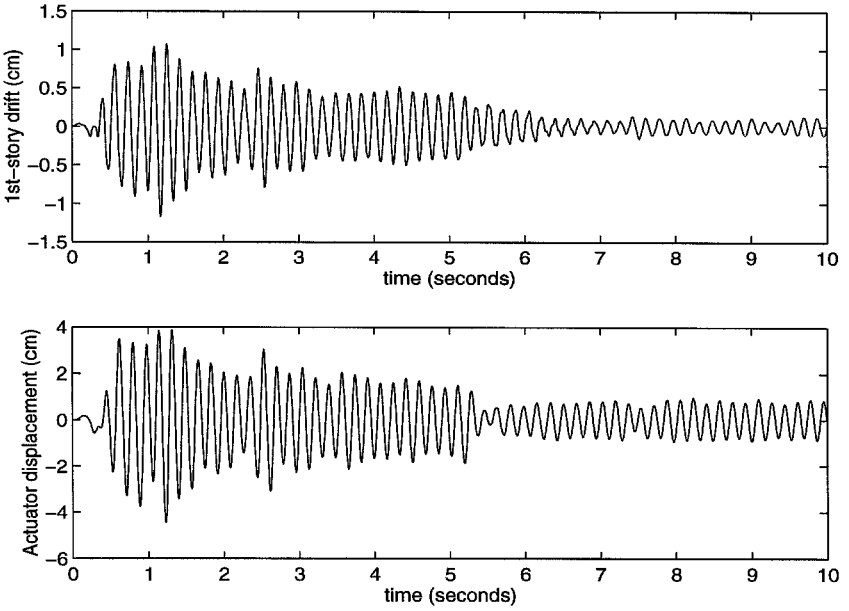

Figure 4.9 Response to scaled NS component of the 1940 El Centro Earthquake, Controller 2.

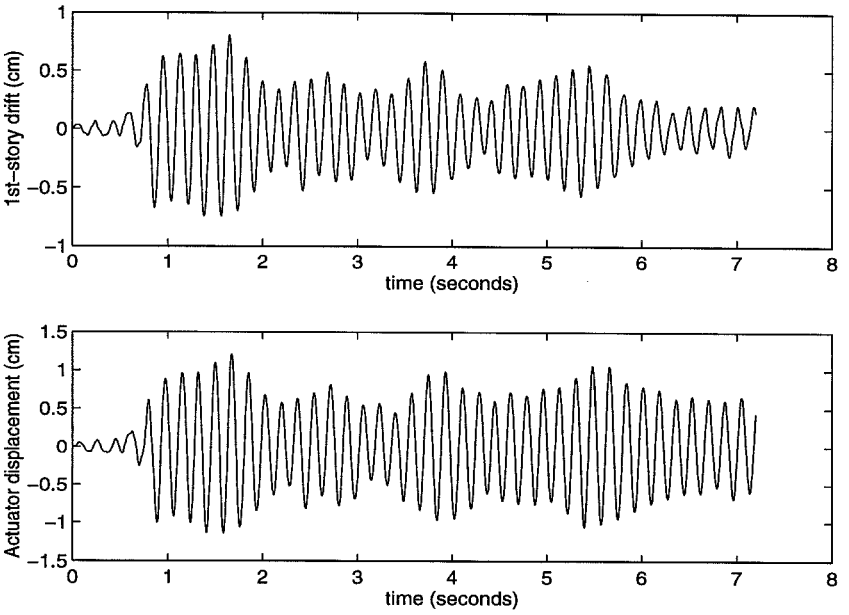

Figure 4.10 Response to scaled NS component of the 1968 Hachinohe Earthquake, Controller 1.

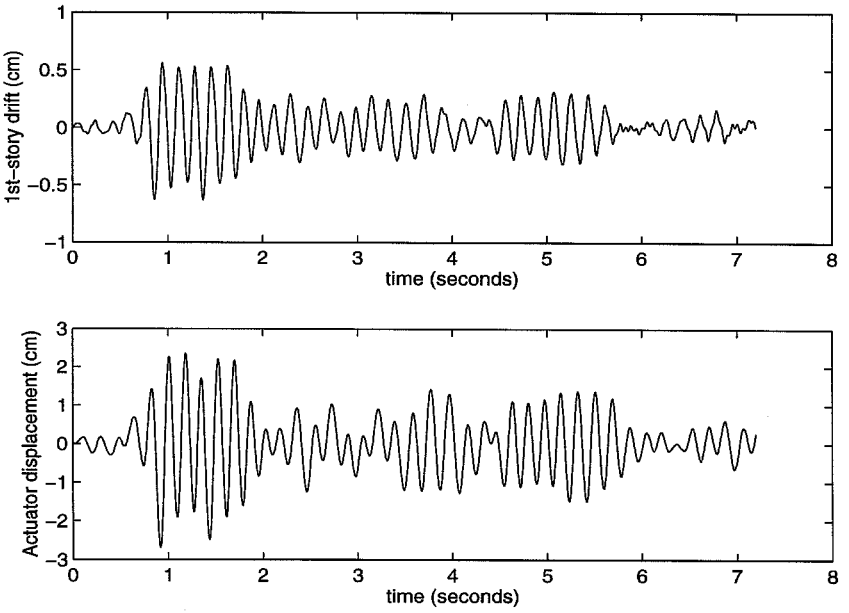

Figure 4.11 Response to scaled NS component of the 1968 Hachinohe Earthquake, Controller 2.

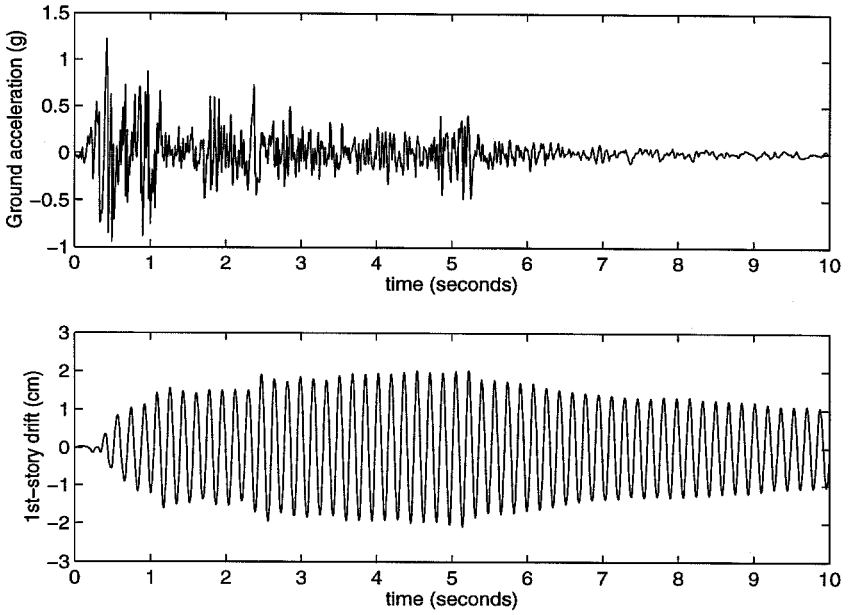

Figure 4.12 Response of the uncontrolled AMD model; scaled El Centro Earthquake excitation.

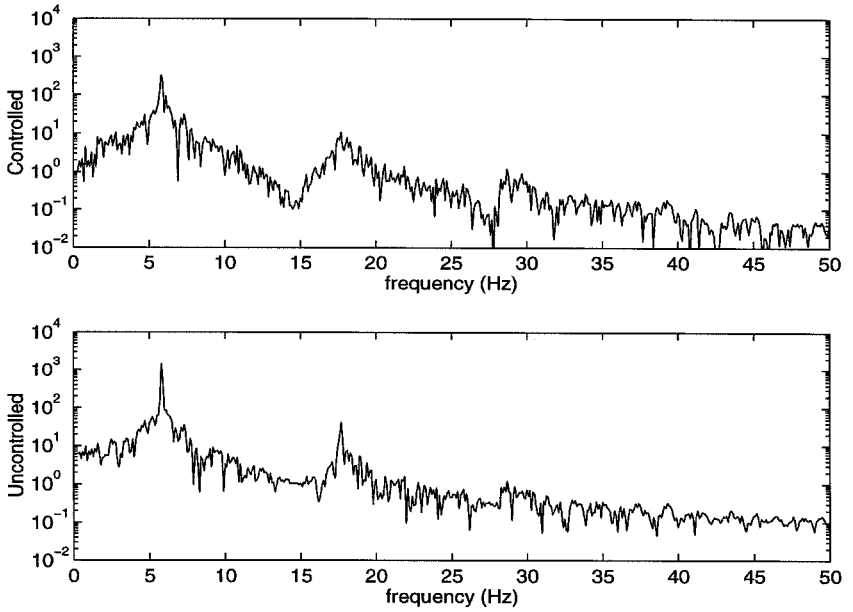

Figure 4.13 Fourier amplitude spectrum of the first-story drift, controlled (Controller 2) and uncontrolled systems, El Centro Earthquake input.

with respect to parameter variations in the excitation model, where the PDFs for the uncertain variables are shown in Figure 4.6. Given a particular controller, the total failure probability is obtained through an asymptotic approximation to (2.21). This result is minimized over the space of acceleration output-feedback controller parameters, with $\omega_b = 188.5$ rad/sec for Controller 3 and ω_b free to vary for Controller 4.

The feedback gains for Controller 3 are $K_3 = \begin{Bmatrix} 0.0454 & 0.0576 & 0.126 \end{Bmatrix}$ and for Controller 4, with $\omega_b = 33.1$, $K_4 = \begin{Bmatrix} 0.431 & 0.291 & 0.235 \end{Bmatrix}$. The ten performance criteria J_1–J_{10} are again shown in Table 4.1. The response of the closed-loop system for Controller 3, whose response appears quite similar to that shown for Controller 1 in Figures 4.8 and 4.10, is shown in Figure 4.14 for the response to the El Centro Earthquake and in Figure 4.16 for response to the Hachinohe Earthquake. Controller 4's response appears quite similar to that shown for Controller 2 in Figures 4.9 and 4.11, and is shown in Figure 4.15 for the response to the El Centro Earthquake and in Figure 4.17 for response to the Hachinohe Earthquake. Again, the maximum actuator displacements, accelerations, and input voltages, as well as the rms values of these quantities, all satisfy the constraints for the AMD benchmark actuator (Spencer et al. 1997a) for Controller 4, but the maximum actuator acceleration is exceeded for Controller 3 under the El Centro earthquake.

The total failure probabilities, (2.21), can be calculated for the uncertain model controllers and the nominal model controllers using the PDFs for the parametric uncertainty shown in Figure 4.6. The total failure probabilities are listed at the bottom of Table 4.1 as the "robust P_f," and the failure probabilities for the nominal system are included as "nominal P_f." The duration of the time interval for the failure probability calculation is taken to be 10 seconds, yielding a failure probability of $P_{f_1} = 17.9\%$ for Controller 1, $P_{f_2} = 0.067\%$ for Controller 2, $P_{f_3} = 16.5\%$ for Controller 3, and $P_{f_4} = 0.067\%$ for Controller 4. For comparison, the total failure probability for the uncontrolled system is found to be nearly 100% for this example. Recall from Section 2.2.3 that these are likely to be over-estimates of the "true" failure probabilities, as they are upper bounds given by the sum of the failure

probabilities for each failure possibility.

The optimal gains for Controllers 2 and 4 are nearly identical, indicating that, for the input-model uncertainty considered for this system, the control gains that minimize the nominal failure probability also minimize the total failure probability.

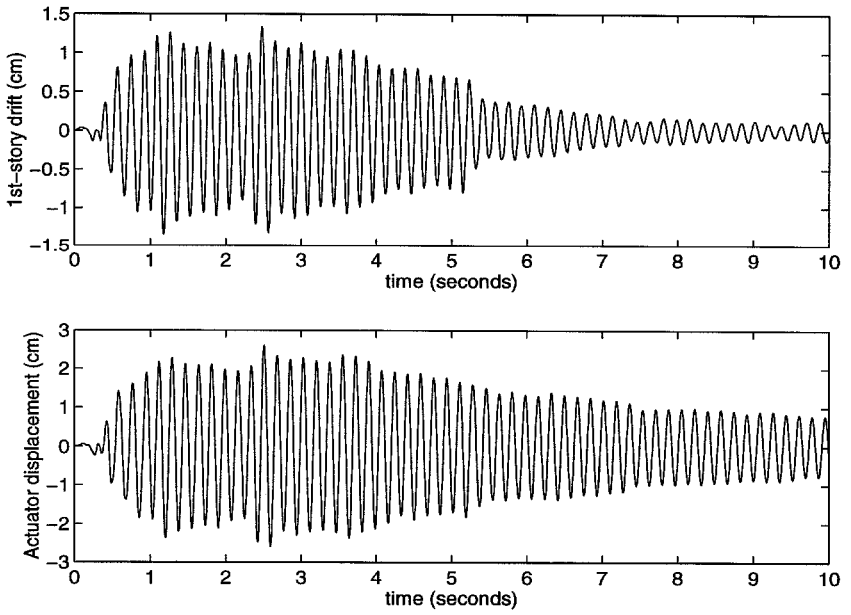

Figure 4.14 Response to scaled NS component of the 1940 El Centro Earthquake, Controller 3.

In Table 4.2, the performance of the second controller (Controller 2) is compared with the performance of other controllers that were designed for the benchmark system. Descriptions of these controllers and their design methods can be found in the Proceedings of the 1997 Structures Congress (Kempner and Brown 1997). All of the controllers that are listed in Table 4.2 have a state dimension of twelve, except for the probabilistic robust controller ("PRC"), which, as mentioned previously, has a state dimension of two. As is apparent from the table, the performance of the PRC controller is comparable or even better than most of the other controller designs listed in the table, validating its use for this application. Presumably, using a higher-order dynamic controller, the PRC controller performance would be improved even further. This could be investigated in future research.

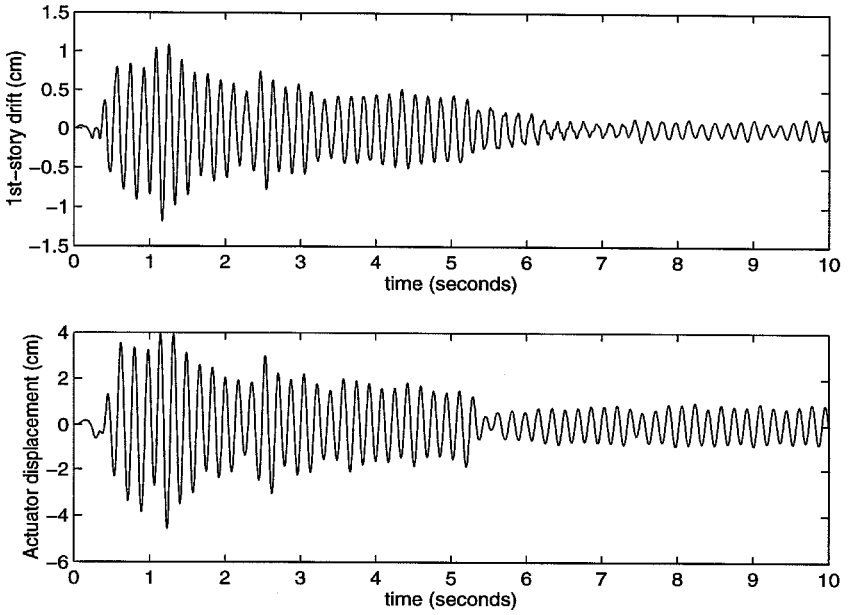

Figure 4.15 Response to scaled NS component of the 1940 El Centro Earthquake, Controller 4.

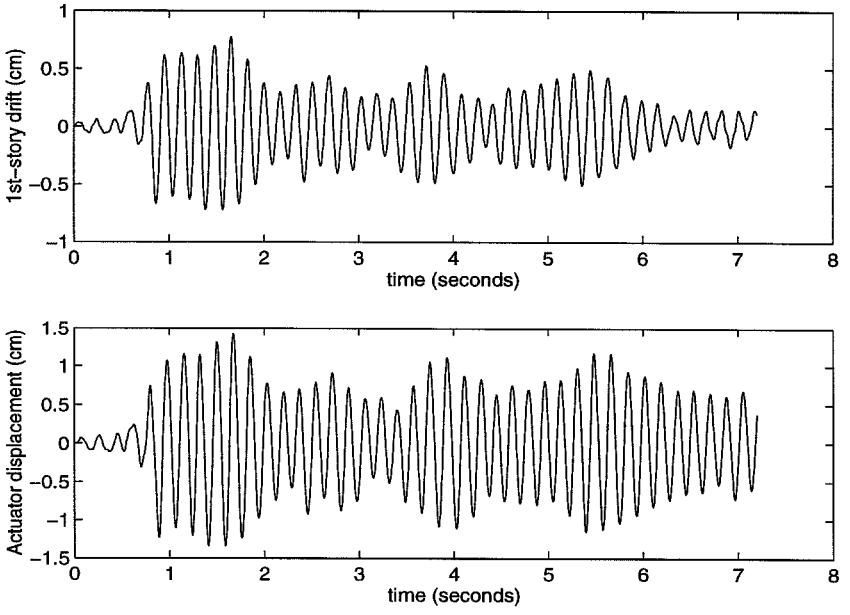

Figure 4.16 Response to scaled NS component of the 1968 Hachinohe Earthquake, Controller 3.

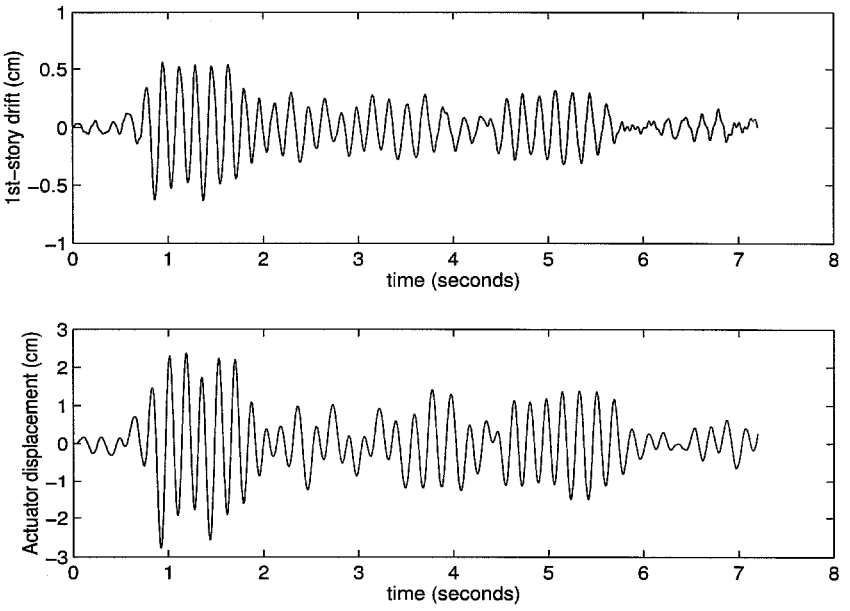

Figure 4.17 Response to scaled NS component of the 1968 Hachinohe Earthquake, Controller 4.

Table 4.2 Performance comparison for several controllers designed for the benchmark control problem.

	Mean square response				
	J_1	J_2	J_3	J_4	J_5
	σ_d	$\sigma_{\ddot{x}}$	σ_{x_m}	$\sigma_{\dot{x}_m}$	$\sigma_{\ddot{x}_m}$
PRC (May and Beck 1997)	0.207	0.348	0.846	0.826	0.673
$\mathcal{H}_2$ (Spencer et al. 1997a)	0.283	0.440	0.510	0.513	0.628
Covariance (Lu and Skelton 1997)	0.209	0.316	0.376	0.380	0.521
μ (Balas 1997)	0.146	0.223	0.617	0.623	0.600
$\mathcal{H}_\infty$ (Smith et al. 1997)	0.256	0.403	0.554	0.554	0.637
	Maximum response				
	J_6	J_7	J_8	J_9	J_{10}
	$\|d\|_\infty$	$\|\ddot{x}\|_\infty$	$\|x_m\|_\infty$	$\|\dot{x}_m\|_\infty$	$\|\ddot{x}_m\|_\infty$
PRC (May and Beck 1997)	0.380	0.684	1.644	1.558	0.936
$\mathcal{H}_2$(Spencer et al. 1997a)	0.456	0.711	0.670	0.775	1.340
Covariance (Lu and Skelton 1997)	0.442	0.658	0.723	0.891	1.277
μ (Balas 1997)	0.378	0.679	1.429	1.537	1.237
$\mathcal{H}_\infty$ (Smith et al. 1997)	0.406	0.749	0.835	0.878	0.967

4.7.3 Simulated performance of specific controllers

This section describes the results for simulations of the closed-loop system for the four controller designs discussed in the previous section. The design of these controllers are summarized here.

- Controller 1: nominal-model controller with fixed Butterworth filter roll-off frequency, $\omega_b = 60\pi$ rad/sec, and $\omega_g = 50.0$ rad/sec, $\zeta_g = 0.50$, $\omega_{df} = 60\pi$ rad/sec.

- Controller 2: nominal-model controller with Butterworth filter roll-off frequency as a control design parameter, and $\omega_g = 50.0$ rad/sec, $\zeta_g = 0.50$, $\omega_{df} = 60\pi$ rad/sec.

- Controller 3: uncertain-model controller with fixed Butterworth filter roll-off frequency, $\omega_b = 60\pi$ rad/sec, and $\omega_g^0 = 50.0$ rad/sec, $\zeta_g^0 = 0.50$, and $\omega_{df} = 60\pi$ rad/sec.

- Controller 4: uncertain-model controller with Butterworth filter roll-off frequency as a control design parameter, and $\omega_g^0 = 50.0$ rad/sec, $\zeta_g^0 = 0.50$, $\sigma_{\ddot{x}_g}^0 = 1.0$, and $\omega_{df} = 60\pi$ rad/sec.

The gains for these controllers are summarized in Table 4.3. The performance levels of the four controllers are calculated using the response of the SIMULINK benchmark system (Spencer et al. 1997a), and are listed in Table 4.1, along with their "robust" failure probability performance levels.

Table 4.3 Controller parameters used for performance evaluations.

Name	ω_b (rad/sec)	k_1	k_2	k_2
Controller 1	188.5	0.0339	0.0538	0.0958
Controller 2	33.4	0.354	0.320	0.237
Controller 3	188.5	0.0454	0.0576	0.126
Controller 4	33.1	0.431	0.291	0.235

4.8 Nominal-model controller design sensitivity

4.8.1 Overview of probabilistic controller design process

One question that might be asked about the controllers that have been found to minimize the failure probability of the nominal model is how the controller design differs if certain of the modeling parameters vary. This section analyzes the sensitivity of the controller design and performance measures to variations in the model and controller design parameters. In this first subsection, the calculated probability of failure, P_f, corresponds to the "nominal" case described in the previous section. In addition to the system parameters described by Spencer et al. (1997a), a number of additional parameters are used in the controller design to describe filters, limit states, and other variables specific to the probabilistic control design for this application. The nominal-model controller design makes use of the following linear systems:

- a reduced-order linear model of the benchmark system that is distributed on the Notre Dame Benchmark Structure Internet home page along with a higher-order linear model that accurately represents the dynamic response of the laboratory system in the frequency range 0–100 Hz,
- a second-order filter (i.e., linear oscillator) to model the ground input, and
- a differentiating filter to approximate the derivatives of the actuator acceleration performance variable.

The sensitivity of the controller design and the system performance to the parameters describing these systems is the subject of this section (and the next one, which discusses the *robust* or uncertain-model controller design). In addition, for some of the control design schemes, the following are used:

- a low-pass Butterworth filter as a frequency weight for the design,
- an integrating filter to estimate the velocities from the feedback accelerations.

To review, the first three natural frequencies for the uncontrolled model (corresponding to the three structural modes for the physical model) are 5.81 Hz (36.5 rad/sec), 17.68 Hz (111 rad/sec), and 28.53 Hz (179 rad/sec). The damping ratios associated with these modes are 0.33%, 0.23%, and 0.30%–clearly the structure's performance would benefit from an increase in the damping. For reference, a bode plot of the 10-state reduced-order "design" model for the uncontrolled system is shown in Figure 4.18.

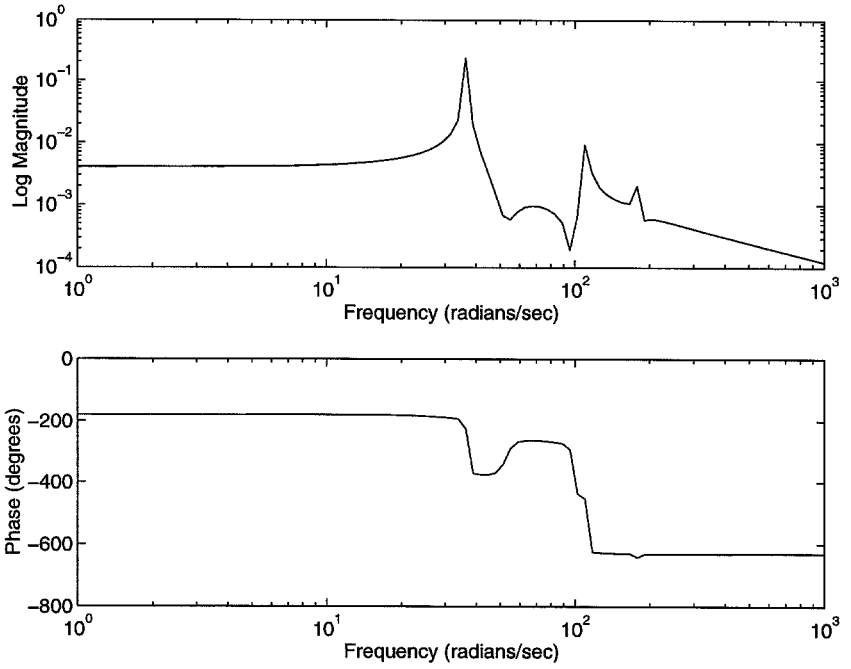

Figure 4.18 Bode plot for 3rd-story drift for uncontrolled system.

4.8.2 Acceleration output feedback with Butterworth filter

Initial design

For this design, a Butterworth filter is included in the controller to reduce the response of the controller to higher frequency disturbances that are more likely to be due to sensor noise than building motion and hence control should be avoided in

this region. This filter helps to reduce the peak acceleration level of the actuator, and hence lower the probability that the actuator exceeds its maximum allowable acceleration. The second-order Butterworth filter roll-off frequency is chosen to be $\omega_b = 10$ Hz. The Kanai-Tajimi model parameters used to estimate the performance for this design are the worst-case input-filter parameters for the uncontrolled system, i.e., $\omega_g = 37.3$ rad/sec, $\zeta_g = 0.3$. The failure modes that are considered are the three inter-story drifts (d_1, d_2, and d_3), the actuator displacement (x_m), and the actuator acceleration ($\ddot{x}_{am}$). The failure levels for these quantities are displayed in Table 4.4. Recall that the derivatives of these quantities are also necessary in order to use the out-crossing rate approximation for the failure probability. While the inter-story drift velocities and the actuator velocity are available directly as outputs from the design model, the derivative of the actuator acceleration is needed to compute the actuator acceleration failure probability. This filter is given by (4.6), re-written here as the transfer function

$$G_{\dot{z}z}(s) = \frac{\omega_{df}^2 s}{s^2 + 2\zeta_{df}\omega_{df} s + \omega_{df}^2}, \tag{4.18}$$

where $\omega_{df} = 10$ Hz is the roll-off frequency and $\zeta_{df} = 1/\sqrt{2}$. The Bode plot for this differentiator is shown in Figure 4.19.

Table 4.4 Failure levels for performance variables.

Max. Inter-story Drift (in.)	Max. Actuator Displ. (in.)	Max. Actuator Accel. (g)
1.50	9.00	6.00

The optimal acceleration-feedback controller gains and the performance (i.e., failure probability approximation) of the controlled system are shown in Table 4.5. For comparison, the performance function for the uncontrolled system using the same Kanai-Tajimi parameters is approximately $P_f \simeq 1$. Note that the out-crossing rate approximation may not be very good for large out-crossing rates; however, regardless of the accuracy of the estimate, the uncontrolled system appears to have a large failure probability, and the system's reliability improves greatly with the

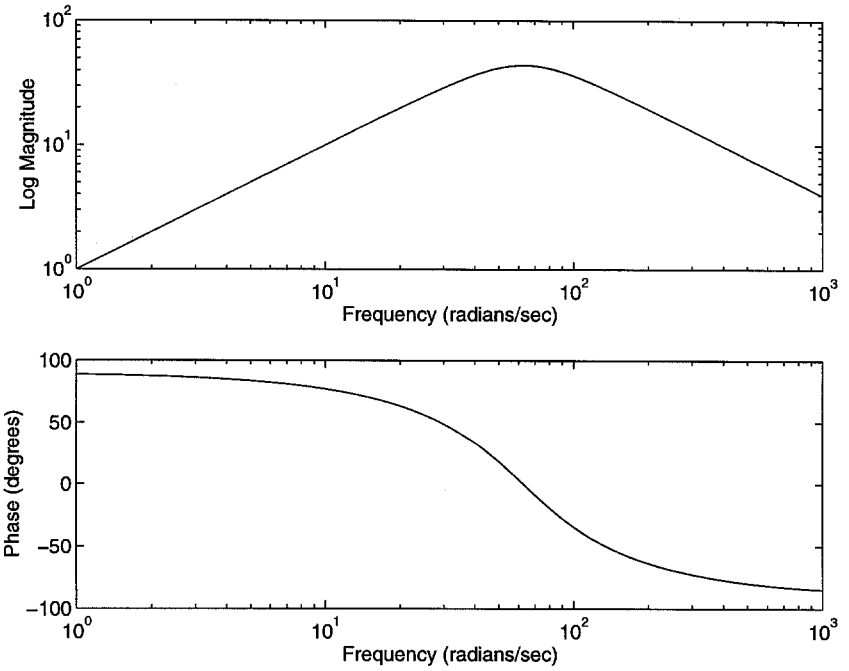

Figure 4.19 Bode plot for derivative filter, (4.18).

implementation of a controller.

Table 4.5 Original controller design.

	Model parameters			Controller parameters		
P_f	ω_g (rad/sec)	ζ_g	ω_b (rad/sec)	k_1	k_2	k_3
1.01×10^{-5}	37.3	0.30	62.8	0.0195	0.222	0.0895

Sensitivity to variations in the Kanai-Tajimi input model

This section explores differences in the design of the nominal-model controller due to variations in the parameters describing the Kanai-Tajimi input filter. These results are summarized in Table 4.6 for the Butterworth filter roll-off frequency $\omega_b = 20\pi$ rad/sec and in Table 4.7 for $\omega_b = 60\pi$ rad/sec. As seen from these tables, the values of the acceleration feedback gains are not particularly sensitive to the

damping coefficient ζ_g of the Kanai-Tajimi filter, but they do demonstrate some variation with ω_g. Also, note the large changes in the performance objective P_f for the different choices of input filter parameters. The wide range in the failure probabilities is primarily due to the filter parameters rather than the controller parameters.

Table 4.6 Nominal controller design for variations in Kanai-Tajimi filter parameters, $\omega_b = 20\pi$ rad/sec.

	Model parameters			Controller parameters		
P_f	ω_g (rad/sec)	ζ_g	ω_b (rad/sec)	k_1	k_2	k_3
3.33×10^{-16}	20.0	0.30	62.8	0.0200	0.143	0.104
4.08×10^{-12}	20.0	0.40	62.8	0.0465	0.141	0.0918
5.56×10^{-10}	20.0	0.50	62.8	0.0471	0.148	0.0914
3.97×10^{-2}	37.3	0.30	62.8	0.0195	0.222	0.0895
3.48×10^{-3}	37.3	0.40	62.8	0.0325	0.196	0.0901
3.20×10^{-4}	37.3	0.50	62.8	0.0413	0.178	0.0918
1.33×10^{-4}	50.0	0.30	62.8	0.0528	0.162	0.0952
4.25×10^{-5}	50.0	0.40	62.8	0.0523	0.160	0.0957
6.89×10^{-6}	50.0	0.50	62.8	0.0545	0.155	0.0966
8.60×10^{-13}	80.0	0.30	62.8	0.0695	0.133	0.110
7.94×10^{-12}	80.0	0.40	62.8	0.0711	0.133	0.110
7.30×10^{-12}	80.0	0.50	62.8	0.0719	0.133	0.110

The set of possible Kanai-Tajimi filter parameters is specified in Spencer et al. (1997a). The range of possible ω_g is 20 rad/sec to 120 rad/sec, and the range of possible damping ratios ζ_g runs from 0.3 to 0.75. The following values for the natural frequency of the input filter are the ones most often used in the analyses in this chapter:

- $\omega_g = 37.3$ rad/sec, which causes the maximum mean-square response among the performance variables for the uncontrolled system, and
- $\omega_g = 50.0$ rad/sec, which is the most probable value for ω_g in the probability distributions that describe the Kanai-Tajimi filter frequency and are considered in the uncertain-system controller design.

Table 4.7 Nominal controller design for variations in Kanai-Tajimi filter parameters, $\omega_b = 60\pi$ rad/sec.

	Model parameters			Controller parameters		
P_f	ω_g (rad/sec)	ζ_g	ω_b (rad/sec)	k_1	k_2	k_3
5.36×10^{-8}	20.0	0.30	188.5	0.0234	0.0468	0.0670
1.01×10^{-5}	20.0	0.40	188.5	0.0250	0.0503	0.0741
1.41×10^{-4}	20.0	0.50	188.5	0.0273	0.0516	0.0796
9.39×10^{-1}	37.3	0.30	188.5	0.0827	0.103	0.165
4.43×10^{-1}	37.3	0.40	188.5	0.0448	0.0742	0.111
1.46×10^{-1}	37.3	0.50	188.5	0.0380	0.0638	0.102
9.28×10^{-2}	50.0	0.30	188.5	0.0380	0.0632	0.0981
5.03×10^{-2}	50.0	0.40	188.5	0.0359	0.0588	0.0976
1.81×10^{-2}	50.0	0.50	188.5	0.0339	0.0538	0.0958
4.81×10^{-7}	80.0	0.30	188.5	0.0215	0.0369	0.0789
1.62×10^{-6}	80.0	0.40	188.5	0.0233	0.0361	0.0816
1.44×10^{-6}	80.0	0.50	188.5	0.0243	0.0347	0.0824

For the damping ratios of the input filter:

- $\zeta = 0.30$ yields the maximum response, and
- $\zeta = 0.50$ is selected as the most probable in the uncertainty models.

Comparison between static and dynamic controller

This section explores the impact of the roll-off filter on the performance of the system, and substantiates its usefulness. This is best demonstrated using frequency-response plots and the $\mathcal{H}_2$ norm of the controlled systems from specific inputs to specific outputs.

The controller design for the comparisons in this section use the following model parameters:

- $\omega_g = 50$ rad/sec, $\zeta_g = 0.50$ are the Kanai-Tajimi filter parameters,
- both $\omega_b = 60\pi$ rad/sec and $\omega_b = 20\pi$ rad/sec are considered for the Butterworth filter roll-off frequency,

- $\omega_{df} = 60\pi$ rad/sec is the differentiating filter roll-off frequency used to estimate $\widetilde{\ddot{x}}_{am}$.

Five controllers are used to study the impact of the Butterworth filter on the controller response, a static-output feedback controller, two dynamic controllers that include the Butterworth filter, and two static controllers that use the same output-feedback gains as the dynamic ones, but without the dynamic filter. The static acceleration-output feedback controller minimizes the failure probability of the closed loop system without a controller filter, yielding

$$K_s = \begin{Bmatrix} 0.00815 & 0.0158 & 0.0232 \end{Bmatrix}. \tag{4.19}$$

The dynamic controllers include the Butterworth roll-off filter with the two different frequencies that are considered, and minimizes the failure probability of the closed loop system including the filter. For $\omega_b = 20\pi$ rad/sec,

$$K_{d1} = \begin{Bmatrix} 0.0565 & 0.151 & 0.0976 \end{Bmatrix}, \tag{4.20}$$

and for $\omega_b = 60\pi$ rad/sec,

$$K_{d2} = \begin{Bmatrix} 0.0324 & 0.0491 & 0.0917 \end{Bmatrix}. \tag{4.21}$$

Displayed in Tables 4.8 and 4.9 are the failure probabilities and $\mathcal{H}_2$-norms, denoted by $\|T_{p\to q}\|_2$ for the $\mathcal{H}_2$-norm from input p to output q, from various inputs to various outputs of the controlled systems. In this table, v_3 is used to represent the third component of the sensor noise. To further illustrate the static versus dynamic compensator comparison, the magnitude plots of the transfer functions are shown in Figures 4.20 and 4.21. In the figures, the controllers with the Butterworth filter are shown by the solid lines, the static-feedback controller with gain K_s is shown by the dashed lines, and the static feedback controllers using the feedback gains K_{d1} and K_{d2} are shown by the dotted lines. Clearly, the static-feedback con-

trol cases exhibit significant sensitivity to higher-frequency noise[2], particularly for the actuator acceleration term. Hence, rolling off the sensitivity of the controller to this high-frequency noise is desirable, largely to reduce the required actuator acceleration.

Table 4.8 Comparison between static and dynamic controllers, $\omega_b = 20\pi$.

Measure	Dynamic K_{d1}	Static K_s	Static K_{d1}
overall P_f [a]	4.29×10^{-2}	1.0	1.0
P_f, $\ddot{x}_g \to d_1$	3.24×10^{-6}	4.44×10^{-1}	1.62×10^{-4}
P_f, $\ddot{x}_g \to \ddot{x}_{am}$	8.87×10^{-3}	2.62×10^{-1}	1.53×10^{-1}
P_f, $v_3 \to \ddot{x}_{am}$	0 [b]	3.72×10^{-14}	1.00
$\|T_{\ddot{x}_g \to d_1}\|_2$	0.309	0.461	0.344
$\|T_{\ddot{x}_g \to x_m}\|_2$	0.512	0.421	0.607
$\|T_{\ddot{x}_g \to \ddot{x}_{am}}\|_2$	1.41	1.73	1.65
$\|T_{v_3 \to x_m}\|_2$	6.35×10^{-3}	∞ [c]	∞
$\|T_{v_3 \to \ddot{x}_{am}}\|_2$	0.241	∞	∞

[a] Recall the total failure probability is approximated (and over-estimated) by adding the failure probability for each mode, and large values of P_f are usually poorer approximations.

[b] Value of 0 due to the finite precision of the computer.

[c] The $\mathcal{H}_2$ norm is unbounded due to direct feed-through of noise.

Sensitivity to Butterworth filter roll-off frequency.

Another parameter to study is the roll-off (or "corner") frequency of the Butterworth filter selected for the controller. Note that this is included as a controller parameter in Section 4.7, and the controller optimization could attempt to determine its optimal value (in addition to the optimal acceleration-feedback gains). However, in this section, the roll-off frequency ω_b is specified *a priori*, and the three acceleration-feedback gains are determined from the optimization. The results of variations in the controller design and performance for two choices of the input parameters are displayed in Table 4.10.

[2] Recall that the noise is represented by Gaussian white noise with variance given by $v_{rms} = 0.01$ Volts.

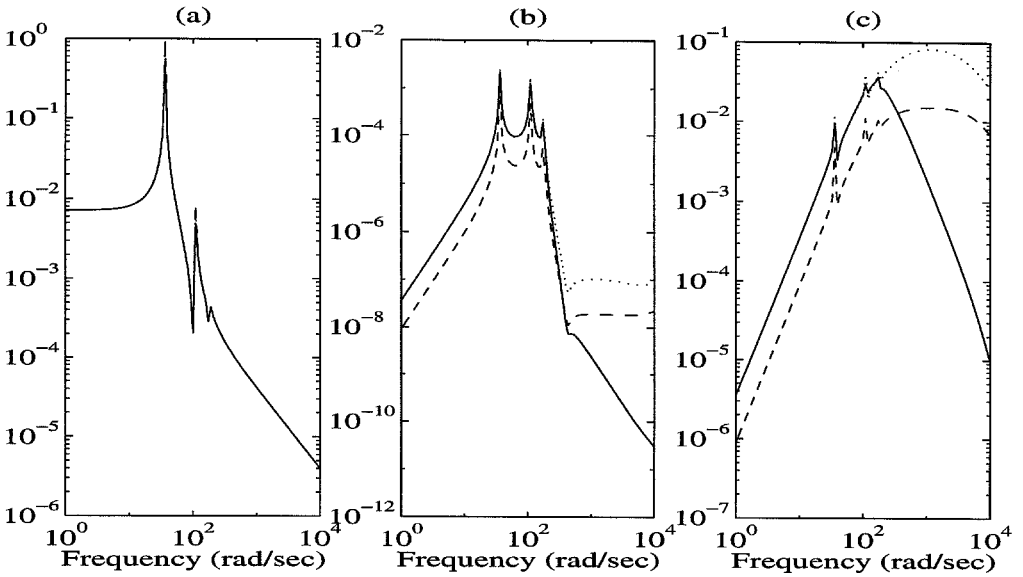

Figure 4.20 Transfer function magnitudes for (a) $T_{\ddot{x}_g \to d_1}$, (b) $T_{\ddot{x}_g \to \ddot{x}_{am}}$, and (c) $T_{v_3 \to \ddot{x}_{am}}$, respectively. Solid line: controller with Butterworth filter, $\omega_b = 30$ Hz, dashed line: gain K_s, dotted line: gain K_{d1}.

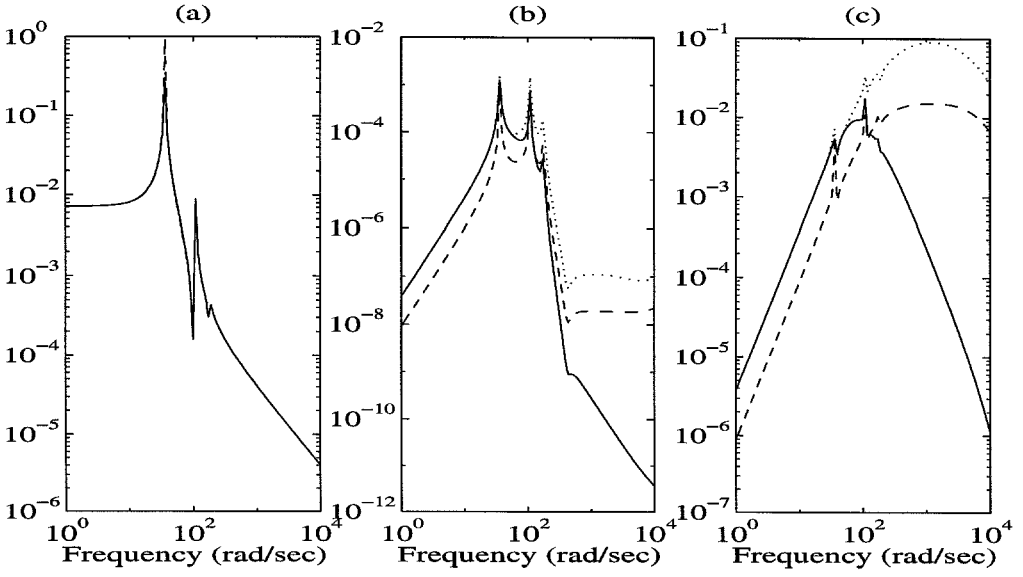

Figure 4.21 Transfer function magnitudes for (a) $T_{\ddot{x}_g \to d_1}$, (b) $T_{\ddot{x}_g \to \ddot{x}_{am}}$, and (c) $T_{v_3 \to \ddot{x}_{am}}$, respectively. See Figure 4.20 for line-type key, here solid line is for the dynamic compensator, $\omega_b = 10$ Hz, and the dotted line represents K_{Scd2}.

Table 4.9 Comparison between static and dynamic controllers, $\omega_b = 60\pi$.

Measure	Dynamic K_{d2}	Static K_s	Static K_{d2}
overall P_f [a]	8.77×10^{-8}	1.00	1.00
P_f, $\ddot{x}_g \to d_1$	7.62×10^{-8}	4.44×10^{-1}	1.62×10^{-4}
P_f, $\ddot{x}_g \to \ddot{x}_{am}$	7.04×10^{-6}	$.62\times10^{-1}$	1.53×10^{-1}
P_f, $v_3 \to \ddot{x}_{am}$	0 [b]	3.72×10^{-14}	1.00
$\|T_{\ddot{x}_g \to d_1}\|_2$	0.231	0.461	∞ [c]
$\|T_{\ddot{x}_g \to x_m}\|_2$	0.421	0.478	∞
$\|T_{\ddot{x}_g \to \ddot{x}_{am}}\|_2$	1.04	1.73	∞
$\|T_{v_3 \to x_m}\|_2$	1.52×10^{-2}	∞ [d]	∞
$\|T_{v_3 \to \ddot{x}_{am}}\|_2$	5.69×10^{-2}	∞	∞

[a] Recall the total failure is approximated (and over-estimated) by adding the failure probability for each mode.

[b] Value of 0 due to the finite precision of the computer.

[c] This system proved to be unstable.

[d] The $\mathcal{H}_2$ norm is unbounded due to direct feed-through of noise.

Sensitivity to differentiating filter parameters

A differentiator is necessary in order to obtain the derivative of the actuator acceleration, which is used in the out-crossing rate approximation to determine the probability that the actuator acceleration will exceed its maximum level of 6 g. The transfer function for this system is given by (4.18). For the study of this section, the roll-off frequency for the filter, ω_{df}, is allowed to vary, while ζ_{df} is held fixed at $1/\sqrt{2}$.

When designing the filter, ω_{df} should be larger than the maximum frequency of interest to provide a good estimate of the derivatives of the variables of interest. Each of the controller designs in Table 4.11 incorporated a second-order Butterworth filter into the controller with a roll-off frequency at 20π rad/sec.

4.8.3 Velocity output feedback with fixed Butterworth filter

The output-feedback controller can be designed on the basis of velocity feedback, too, assuming an integrating filter is used to estimate the velocities at the measurement locations from their acceleration values. The transfer function for the filter

Table 4.10 Nominal controller design for variations in corner frequency of Butterworth filter.

	Model parameters			Controller parameters		
P_f	ω_g (rad/sec)	ζ_g	ω_b (rad/sec)	k_1	k_2	k_3
1.27×10^{-4}	37.3	0.30	30.0	0.776	0.282	0.232
2.91×10^{-4}	37.3	0.30	40.0	0.111	0.356	0.137
4.51×10^{-3}	37.3	0.30	50.0	0.0182	0.304	0.0814
4.30×10^{-2}	37.3	0.30	62.8	0.0195	0.222	0.0895
1.35×10^{-1}	37.3	0.30	75.0	0.0256	0.171	0.109
4.07×10^{-1}	37.3	0.30	100.0	0.0141	0.133	0.131
6.68×10^{-1}	37.3	0.30	125.0	0.0347	0.118	0.130
5.88×10^{-11}	50.0	0.50	30.0	0.562	0.319	0.314
2.07×10^{-10}	50.0	0.50	40.0	0.156	0.300	0.137
6.80×10^{-8}	50.0	0.50	50.0	0.0678	0.226	0.0866
8.51×10^{-6}	50.0	0.50	62.8	0.0545	0.155	0.0966
9.61×10^{-5}	50.0	0.50	75.0	0.0550	0.106	0.120
8.07×10^{-4}	50.0	0.50	100.0	0.0221	0.0848	0.124
3.63×10^{-3}	50.0	0.50	125.0	0.0259	0.0765	0.109

Table 4.11 Nominal controller design for variations in the differentiating filter.

	Model parameters			Controller parameters		
P_f	ω_g (rad/sec)	ζ_g	ω_{df} (rad/sec)	k_1	k_2	k_3
2.77×10^{-2}	37.3	0.30	30.0	0.00965	0.241	0.0864
3.47×10^{-2}	37.3	0.30	50.0	0.00944	0.236	0.0832
3.70×10^{-2}	37.3	0.30	62.8	0.0114	0.233	0.0839
3.85×10^{-2}	37.3	0.30	75.0	0.0137	0.229	0.0852
4.04×10^{-2}	37.3	0.30	100.0	0.0192	0.221	0.0882
4.73×10^{-6}	50.0	0.50	30.0	0.0529	0.158	0.0962
6.14×10^{-6}	50.0	0.50	50.0	0.0527	0.157	0.0955
6.69×10^{-6}	50.0	0.50	62.8	0.0531	0.157	0.0957
7.07×10^{-6}	50.0	0.50	75.0	0.0535	0.156	0.0959
7.61×10^{-6}	50.0	0.50	100.0	0.0543	0.154	0.0964

that is used is

$$G_{\dddot{x}\ddot{x}}(s) = \frac{s}{s^2 + 2\zeta_{vf}\omega_{vf}s + \omega_{vf}^2}, \tag{4.22}$$

which is the filter that was given in Spencer et al. (1997a) with $\omega_{vf} = (2\pi)^{-1}$ rad/sec and $\zeta_{vf} = (\sqrt{2})^{-1}$. The bode plot for this transfer function can be seen in Figure 4.22. The results for different velocity feedback controller designs are given in Table 4.12. As seen in Table 4.12, the nominal failure probability is lower using velocity feedback than the acceleration feedback case when ω_b is large, but much worse when ω_b is small. This is due to the roll-off filter behaving like a differentiator at frequencies above the roll-off frequency. When this roll-off frequency frequency falls below the frequency range of interest, the feedback approximates the measured displacements, and as was seen in Chapter 3, position-feedback control is not always very effective. The other effect the roll-off filter has is that it distorts the phase, which is the cause of the performance degradation that is seen in the table.

Table 4.12 Controller design for (pseudo)-velocity feedback.

	Model parameters			Controller parameters		
P_f	ω_g (rad/sec)	ζ_g	ω_b (rad/sec)	k_1	k_2	k_3
1.0	37.3	0.30	62.8	7.01	−2.52	9.77
3.45×10^{-1}	50.0	0.50	62.8	13.1	−7.47	12.9
6.08×10^{-3}	37.3	0.30	188.5	−0.510	11.36	5.22
3.08×10^{-3}	50.0	0.50	188.5	0.241	9.11	4.39

4.8.4 Acceleration output feedback with addition of Butterworth filter roll-off frequency as a controller parameter

In this section, the Butterworth filter that has been included in the controller design previously as a frequency-dependent weighting function is now included as a design parameter in the optimization. The controller class for the optimization now includes the three acceleration-feedback gains k_1, k_2, and k_3 and the roll-off frequency

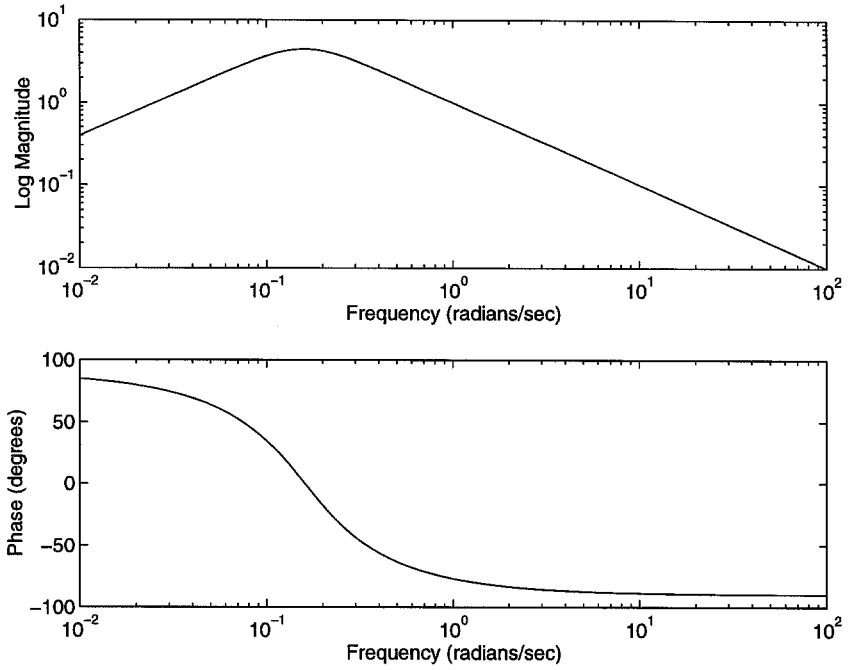

Figure 4.22 Bode plot for velocity-estimate filter $G_{\dot{x}\ddot{x}}$.

ω_b for the Butterworth filter that is incorporated into the controller to reduce its sensitivity to high-frequency noise. A Bode plot of the transfer function of a typical second-order Butterworth filter is shown in Figure 4.23. The value roll-off frequency ω_{df} for the differentiating-filter (4.18) is 60π rad/sec for the results in this section. The controllers that are designed are displayed in Table 4.13 for two cases of the ground motion parameters: $\omega_g = 37.3$ rad/sec, $\zeta_g = 0.30$, and $\omega_g = 50.0$ rad/sec, $\zeta_g = 0.50$. The latter case corresponds to Controller 2 in Section 4.7.1.

Table 4.13 Acceleration feedback control design with additional Butterworth filter roll-off frequency parameter.

	Model parameters		Controller parameters			
P_f	ω_g (rad/sec)	ζ_g	ω_b (rad/sec)	k_1	k_2	k_3
9.03×10^{-5}	37.3	0.30	33.0	0.447	0.274	0.257
2.38×10^{-11}	50.0	0.50	33.4	0.354	0.320	0.237

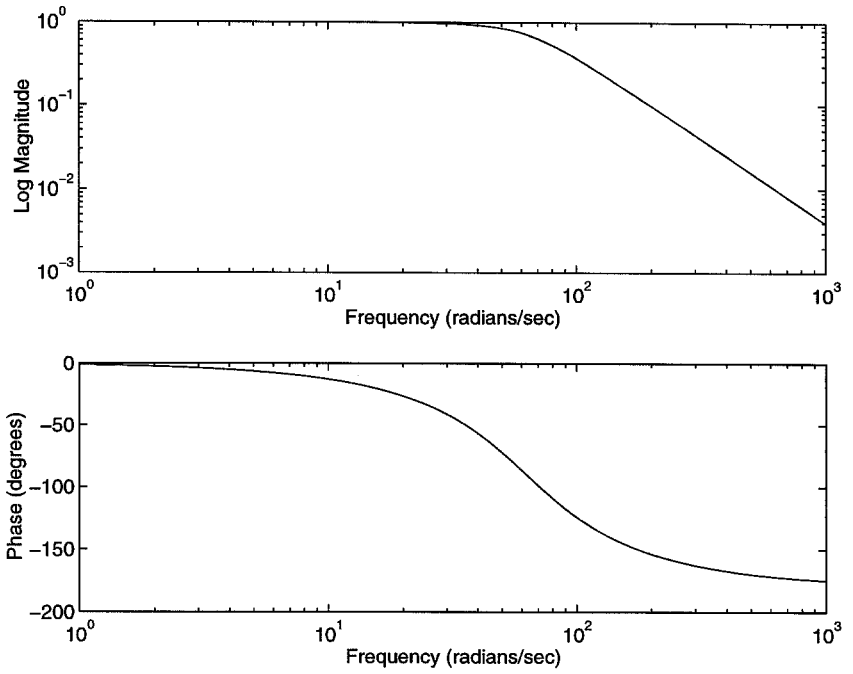

Figure 4.23 Bode plot for Butterworth frequency-weighting filter.

4.9 Studies of robust-model controller design

4.9.1 Overview

The robust-controller design developed in Chapter 3 explicitly considers the uncertainty in the models of the benchmark system in the selection of the "optimal" controller. The probability models for the parametric uncertainty of the input filter are used to compute the probable robust performance that serves as the controller objective function. Often, the calculated performance is not very sensitive to the particular form of the probability distributions for the uncertain parameters, provided the distributions exhibit the same general behavior, i.e., provided the most probable values and the local shape of the distribution about that peak are similar among the distributions under consideration. However, the performance does depend on the most probable value of the parameter and its variance. The sensitivity of the controller design to the probability models and their parameters is the subject

of Section 4.9.2.

4.9.2 Robust controller design for acceleration feedback

Sensitivity to peak values for uncertain-variable probability density functions.

The variations in the optimal uncertain-model control design with the value for the most-probable parameters are explored in this section. The probability models for the uncertain parameters are chosen to be log-normal distributions for the Kanai-Tajimi filter frequency, damping ratio, and input magnitude, as discussed previously in Section 4.4. A standard log-normal distribution (Benjamin and Cornell 1970) is scaled by the most-probable values of each parameter, and this standard distribution is described by

$$p(\theta) = \frac{1}{\theta \sigma_{\log\theta}\sqrt{2\pi}} \exp\left[-\frac{1}{2}\left(\frac{\log\theta - \mu_{\log\theta}}{\sigma_{\log\theta}}\right)^2\right], \tag{4.23}$$

where $\mu_{\log\theta}$ represents the mean of the natural logarithm of θ and $\sigma_{\log\theta}$ is the log of the variance of θ, termed the "log-variance." Throughout this section, each of the parameter probability distributions has a log-variance of 0.2.

The variations in the optimal controller gains with respect to the most probable values for the uncertain parameters are summarized in Table 4.14 (using $\omega_b = 30\pi$ rad/sec). In this table, the most-probable parameter values are indicated with a "0" superscript, while the parameter values that serve as the design points for the asymptotic approximation to (2.21) (see Section 2.5.4) are indicated with an "$*$." The set of values for ω_g^0 is, in rad/sec, $\{37.3, 50.0, 75.0, 100.0\}$, ζ_g is chosen from $\{0.30, 0.50, 0.60\}$, and $\sigma_{\ddot{x}_g}$ is kept constant at 0.12 g. For each pair of rows in the table, the first row displays the most-probable parameter values, while the second row contains the parameter values found as the "design points," that is, the parameters that maximize the integrand of (2.21).

The robust performance is also calculated for the uncontrolled system for the various most-probable parameter values described above. The results of this study

are shown in Table 4.15. For the robust performance calculations in Table 4.15, recall that failure probability performance measure is an *approximation* to the failure probability of the system, and is obtained by summing the failure probabilities for each failure possibility.

One comment on the robust controller optimization is that the failure probability performance for the robust example is often quite flat with respect to the controller parameters. This sometimes leads to difficulties in the optimization, requiring a large number of iterations for convergence. This behavior is also seen in the figures in Chapter 3, which plot the failure probability as a function of a single controller gain. The flatness in the objective function with respect to the controller gains is a consequence of the nonlinear failure-probability-based objective function. Since most of the controllers in this range achieve nearly equal performance, any one that provides satisfactory performance could be used.

Sensitivity to form of probability models

Alternative probability models could be considered for the parameter uncertainty besides log-normally distributed uncertainty. Other popular models would include the χ^2-distribution or a normal (or truncated normal) one. For each PDF considered, the probability distribution parameters can be selected so the different distributions exhibit very similar behavior around their most probable values. For example, in Figure 4.24 the PDFs and CDFs of a normal (solid line), log-normal (dashed line), and χ^2 (dotted line) distribution appear quite similar when the distribution parameters are chosen appropriately. Hence, since the asymptotic approximation depends largely on the shape of the probability density function at its maximum point (as this peak typically determines the maximum of the integrand from the total probable performance), the effects at the tails from the different distributions are assumed to be negligible, at least compared within the accuracy of the asymptotic approximation to evaluate the performance.

Table 4.14 Performance, "design" point for asymptotic integration, and controller parameters for uncertain-model controller, $\omega_b = 20\pi$ rad/sec and $\omega_{df} = 60\pi$ rad/sec.

		Model parameters			Controller parameters		
CPU time (sec)	robust P_f	ω_g^0, ω_g^* (rad/sec)	ζ_g^0, ζ_g^*	$\sigma_{\ddot{x}_g}^0$, $\sigma_{\ddot{x}_g}^*$ (g)	k_1	k_2	k_3
1.68×10^3	1.17×10^{-1}	37.3	0.300	0.120	0.110	0.225	0.103
		36.7	0.261	0.145			
1.67×10^3	2.56×10^{-2}	37.3	0.500	0.120	0.0914	0.144	0.134
		36.5	0.409	0.166			
1.97×10^3	1.30×10^{-2}	37.3	0.600	0.120	0.0924	0.144	0.134
		36.2	0.480	0.174			
1.10×10^3	5.47×10^{-2}	50.0	0.300	0.120	0.103	0.210	0.103
		39.7	0.260	0.149			
2.07×10^3	1.29×10^{-2}	50.0	0.500	0.120	0.0826	0.155	0.127
		40.8	0.408	0.168			
1.95×10^3	6.54×10^{-3}	50.0	0.600	0.120	0.0809	0.149	0.130
		41.1	0.479	0.176			
1.83×10^3	1.79×10^{-3}	75.0	0.300	0.120	0.107	0.156	0.110
		45.0	0.271	0.163			
1.80×10^3	8.76×10^{-4}	75.0	0.500	0.120	0.0857	0.145	0.125
		49.4	0.429	0.183			
2.43×10^3	5.21×10^{-4}	75.0	0.600	0.120	0.0774	0.147	0.120
		50.8	0.500	0.191			
2.65×10^3	6.28×10^{-5}	100.0	0.300	0.120	0.0669	0.157	0.115
		53.4	0.292	0.186			
2.37×10^3	7.77×10^{-5}	100.0	0.500	0.120	0.0849	0.134	0.125
		63.7	0.462	0.209			
1.74×10^3	5.77×10^{-5}	100.0	0.600	0.120	0.0895	0.130	0.127
		66.9	0.534	0.215			

Table 4.15 Robust performance and "design" point for asymptotic integration for uncontrolled system.

	Model parameters		
"P_f"	ω_g^0, ω_g^* (rad/sec)	ζ_g^0, ζ_g^*	$\sigma_{\ddot{x}_g}^0$, $\sigma_{\ddot{x}_g}^*$ (g)
8.98×10^{-1}	37.3	0.300	0.120
	36.5	0.278	0.124
1.0	37.3	0.500	0.120
	35.9	0.477	0.117
7.95×10^{-1}	37.3	0.600	0.120
	35.8	0.572	0.117
7.60×10^{-1}	50.0	0.300	0.120
	42.8	0.280	0.127
6.96×10^{-1}	50.0	0.500	0.120
	47.3	0.477	0.118
5.58×10^{-1}	50.0	0.600	0.120
	46.8	0.565	0.120
2.15×10^{-1}	75.0	0.300	0.120
	61.6	0.293	0.131
2.24×10^{-1}	75.0	0.500	0.120
	63.1	0.471	0.133
1.95×10^{-1}	75.0	0.600	0.120
	63.0	0.554	0.136
5.53×10^{-2}	100.0	0.300	0.120
	75.0	0.302	0.149
6.67×10^{-2}	100.0	0.500	0.120
	77.8	0.474	0.149
5.76×10^{-2}	100.0	0.600	0.120
	77.8	0.554	0.151

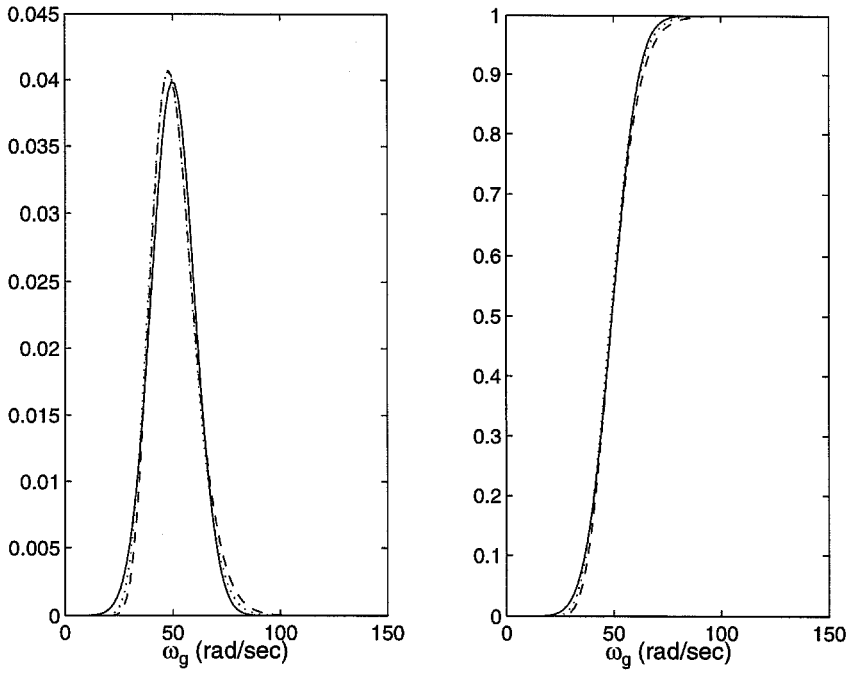

Figure 4.24 Normal, log-normal, and χ^2 probability density functions and cumulative distribution functions for ω_g.

4.9.3 Robust control design including roll-off frequency as a controller parameter

Similarly to the nominal-model controller design approach, the roll-off frequency of the frequency-weighting filter is included as a controller parameter. The results of the controller optimization including this parameter are shown in Table 4.16.

4.10 Comments on the Benchmark application

The controllers that are designed for the AMD benchmark model achieve reductions of almost two orders of magnitude in the failure probability of the controlled systems relative to the uncontrolled one, where the failure probability is found from the inter-story drifts and the AMD actuator stroke and acceleration for this example. Controllers 2 and 4 achieve similar performance levels (as do Controllers 1 and 3),

Table 4.16 Acceleration-feedback robust control design with additional roll-off frequency parameter.

	Model parameters			Controller parameters			
Robust P_f	ω_g^0, ω_g^* (rad/sec)	ζ_g^0, ζ_g^*	$\sigma_{\ddot{x}_g}^0$, $\sigma_{\ddot{x}_g}^*$ (g)	ω_b (rad/sec)	k_1	k_2	k_3
6.83×10^{-4}	50.0	0.50	0.12	32.2	0.347	0.315	0.297
	40.2	0.380	0.195				
2.52×10^{-5}	75.0	0.50	0.12	32.3	0.455	0.407	0.163
	45.7	0.396	0.207				

which is due to the limited flexibility of the controller class which is considered and the consideration of uncertainty only in the model of the input. All of the benchmark controller constraints, on actuator command signal, acceleration, and displacement, are satisfied for Controllers 2 and 4, although the maximum actuator acceleration constraint is (slightly) violated under the El Centro input for Controllers 1 and 3. A more complicated controller class, such as one containing a state estimator, would be expected to show a greater difference in performance between the nominal-model and uncertain-model controllers. This is a topic for further research.

As a further comment, during the revisions of the thesis, an error was discovered in the out-crossing rate. Initially, in incorrect value for the numerical coefficient in (2.12) was used, $1/\sqrt{2\pi}$, rather than the correct value of $1/\pi$. This error was identified during the revisions, and the failure probabilities that are presented herein reflect the correct values. The difference is small and only quantitative, the qualitative nature of the results are unchanged. New optimizations were not performed for the controller design, as the previous optima that were found are quite close to what the new ones would be.

Chapter 5

Application to flexible laboratory structure

5.1 Overview

The Caltech Flexible Structure was originally designed to study control design and system identification issues for lightweight space trusses. For this research, however, it will be used as an analog to a civil engineering structure to demonstrate the probabilistic robust control analysis methodology that is developed in Chapters 2 and 3. The Caltech Flexible Structure, pictured in Figure 5.1, is a three-story lightweight aluminum truss with a triangular floor plan. The structure is quite flexible, with a natural frequency for the fundamental (pendulum) mode of the structure of 0.9 Hz, and the natural frequencies for the 9 dominant structural modes range from 0.9 Hz to 6.3 Hz. This frequency range is similar to that typically found in tall (10 to 20 story) steel-frame buildings. In addition, the majority of the energy associated with earthquake excitations is generally contained in this frequency range.

In this chapter, the flexible structure is used primarily to demonstrate the pre-data and post-data analysis method for the probabilistic robust control methodology. In addition, controllers are designed for the nominal models of the structure to attempt to optimize the structure's performance. The pre-data and post-data analysis techniques are applied to uncertain models of the uncontrolled and controlled system. The purpose of this analysis is to show how the probable performance of the system changes when new information is available in the form of vibration response data.

Two models are considered, a pre-data model that is identified from "old" response data from the structure, and a post-data model that uses new response data to update the model description. The pre-data model serves as a "prior" when updating the performance with new data through the application of Bayes's Theorem. The model uncertainty for the two models is described probabilistically. Typically, to account for the modeling error, the probability distributions for pre-data model parameters are more broad than the distributions for the post-data model parameters.

Controllers are designed for the system using standard $\mathcal{H}_2$ control design techniques and using the reliability-based performance objective described in Chapters 2 and 3. Due to constraints on available computation-time, the controller designs are based only on the "nominal" most-probable models of the pre-data and post-data systems. The probable performance of the uncertain systems are analyzed using the methods of Section 2.5.

The Caltech Flexible Structure has been studied previously by Moser (1992) (also in Moser and Caughey 1991), and Balas (1990) for experimental validation of structural control for flexible space structures. The primary analysis and controller design methods that they used were $\mathcal{H}_\infty$ and μ-synthesis techniques. Furthermore, Moser (1992) applied several system identification techniques to identify a modal model for the flexible structure that is pictured in Figure 5.1. In this work, the previous studies were used primarily for reference on the modeling and description of the laboratory system.

5.2 Description of the laboratory system

5.2.1 Light-weight truss

The truss structure pictured in Figure 5.1 is suspended from an aluminum plate bolted to a rigid steel frame (rigid relative to the light-weight aluminum truss), so as a civil engineering model it could be considered as an "upside-down" building with rigid floor diaphragms. This structure is suspended so it can be made very

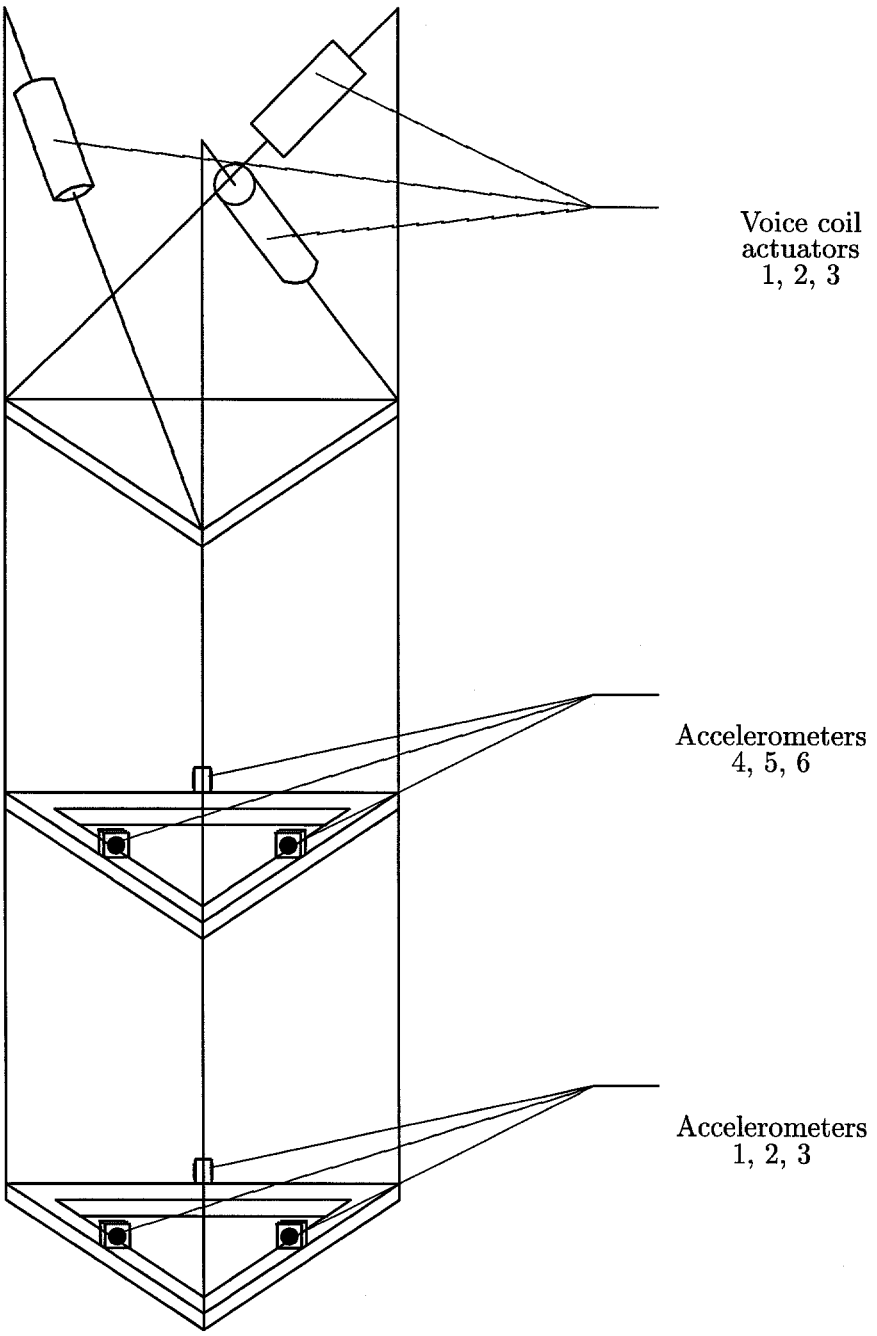

Figure 5.1 Schematic of Caltech flexible structure.

flexible, similar to light-weight space trusses, without concern for the compressive strength of the members or the stability of the structure. The structure has a total height of 2.32 m and an equilateral triangular cross section with each side 0.406 m in length. The vertical members of the structure are thin aluminum rods. Aluminum platforms separate the adjacent stories of the structure and serve as "floors." The upper floor is a solid aluminum plate of 9.53 mm thickness, and the lower two floors have a triangular cut-out, with side length measuring 0.356 m, in the center, and are 6.40 mm thick. The cut-outs in the lower two floors serve to lighten the structure and to bring the natural frequencies of the torsional and bending modes close together, leading to a more challenging control analysis and design problem.

5.2.2 Voice coil actuators

Three voice coil actuators (VCAs, singular is VCA) are connected with diagonal members between the top floor of the structure and the stiff aluminum connecting plate. These actuators are rated at ± 13.5 N at ± 5 V and have a bandwidth of 60 Hz. The VCAs are analogous to active tendons or braces (Spencer et al. 1997b; Soong 1990; Chung et al. 1989), which are a common actuator studied for civil engineering structural control applications.

5.2.3 Proof mass actuators

Three proof mass actuators (PMAs) are also attached to the bottom of the structure. The PMAs are not controlled in this study, but a description of their properties is provided herein for reference.

The PMAs are not in the load path, and hence can only impart inertial forces to the structure. They can provide ± 6.5 N of force given a command signal of ± 5 V (the saturation level of the D/A converter). The PMAs have a bandwidth of 5 Hz, although they are ineffective at low frequencies as large displacements are required in order to provide significant forces. In their present state, these actuators are attached to the structure, but they are not active. To minimize their contribution to the dynamics of the overall structure, the proof masses are held stationary by

foam pads.

5.2.4 Accelerometers

Six accelerometers are installed to monitor the structure. These are uniaxial Sunstrand QA700 accelerometers that are mounted in the center of each of the triangular sides of the lower two platforms. The directional sense of each accelerometer is parallel to the side on which it is mounted. The frequency response of these sensors is flat and has very low noise between 0 and 200 Hz. The output signals are conditioned by a four pole Butterworth filter with a 100 Hz cutoff frequency before being fed into the data acquisition and control system. The scaling factor for these accelerometers is 63 V/g. Three accelerometers are mounted on the bottom level of the structure and three on the second level, as shown in Figure 5.1.

5.2.5 Data acquisition and actuator command

Data is acquired and the actuator command outputs are specified through a 66 MHz PC. The analog input signals are discretized using a CIO-DDA06 analog-to-digital (A/D) computer board (Computer Boards, Inc. 1991), while the command signals are converted from digital-to-analog (D/A) and written to the actuators through a CIO-DAS16/330 computer board (Computer Boards, Inc. 1994). The A/D and D/A conversions have 12 bit precision. The voltage range for the devices is ± 5 V, and hence the discretization interval is (10 V)/(2^{12} divisions) = 2.44×10^{-3} Volts per division. For the feedback control, the necessary state-space computations are performed in discrete time by the PC.

5.2.6 Software

The software that is used to control the flexible structure calls the real-time kernel Sparrow (Murray et al. 1995) to capture data from the accelerometers, load trajectory files, perform on-line calculations of control forces, and specify the outputs to the actuators. A sampling rate of 100 Hz is chosen for this application, which is sufficiently high above the frequency range of interest for the structure (approxi-

mately 0–10 Hz) to avoid aliasing. This sampling rate can be achieved easily by the software running on a 486/66 MHz computer, allowing sufficient time between the time steps for the state-space calculations that are necessary to compute the control force.

5.3 Identification of modal model for the structure

5.3.1 Introduction

System identification is used to develop a mathematical model for the flexible structure that can be used for performance analysis and controller design. The model that is identified on the basis of the response data from the structure should accurately predict its response in the frequency range of interest. With an accurate model, the performance of the physical system can be inferred from the performance of the model. The structure is modeled as a linear system, which simplifies both the system identification and the controller design. This section describes the procedure for obtaining an accurate linear model of the flexible structure.

5.3.2 System identification input

The input that is used for the system identification of the structure is designed to distribute the input energy evenly among the modal frequencies. This input is pictured in both the time domain and frequency domain in Figure 5.2, where the Fourier amplitude spectrum of the input appears completely flat in the frequency range of interest. The "random" phase of the input has been selected such that the amplitude in the time domain remains small, so the actuator does not saturate and the response behaves linearly.

To reduce the impact of the system's transient response, the input excitation shown in Figure 5.2 is repeated four times for the identification. Only the response data from the last loop over the input signal is used for system identification. A separate identification is performed for each VCA.

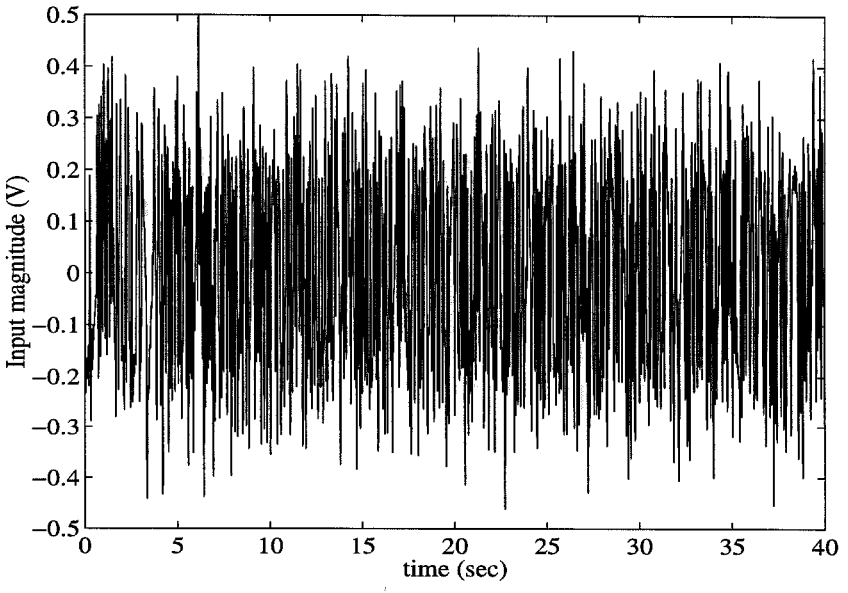

(a) Time domain

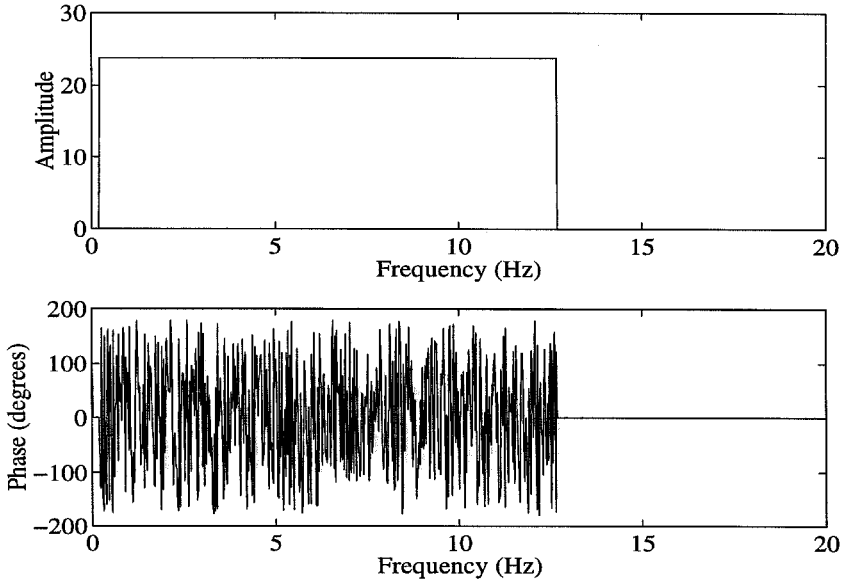

(b) Frequency domain

Figure 5.2 Input with flat Fourier amplitude spectrum, random phase.

5.3.3 Data sets

Modal models are identified for two different sets of response data from the structure. The two data sets are chosen to illustrate the methods of Section 3.4 for updating the performance description of the system using new response data. The first data set was taken from an early vibration test of the structure, and the second was taken over a year later, following the relocation of the structure to a new laboratory. Although the structure was reassembled in the same configuration it had prior to the move, its identified natural frequencies are up to 5% different than those for the pre-move model, and the damping ratios are found to differ by up to 100% from the pre-move modal model. The pre-data and post-data analysis of the flexible structure is discussed in detail in Section 5.4.

The differences between the models are most likely largely due to the following sources:

- changes in the distribution of masses due to minor hardware changes,
- changes in the contributions to damping from loose wires,
- inadvertent inter-changing of some of the structural members (they were not individually labeled for the move),
- different end conditions for the connections between the members and the rigid mounting plate.

5.3.4 Time-domain system identification

A time-domain system identification algorithm is used to construct a modal model for the structure. This algorithm is implemented in the computer program Mode-ID (Beck 1990), developed by Beck (1978).

Mode-ID extracts the natural frequencies, damping ratios, and modeshape components of a linear model with classical normal modes (Caughey and O'Kelly 1965) that best fits the response data in a least squares sense. The algorithm seeks to minimize the square of the 2-norm of the prediction error (normalized by the magnitude

of the measured output), which is defined by

$$J(\boldsymbol{\theta}) := \sum_{i=1}^{n} \|y_i - q_i(f, \boldsymbol{\theta})\|^2 \tag{5.1}$$

where $\boldsymbol{\theta}$ is the vector of modal parameters, $y_i, q_i \in \mathbb{R}^{n_0}$ are the measured and predicted model responses at time i ($i \in \{1, \ldots, n\}$), respectively, n_0 is the number of output channels, f_i is the measured input at time i, n is the number of sampled data points, and $\|\cdot\|$ is the Euclidean norm on $\mathbb{R}^{n_0}$. The model response, $\{q_i\}$, is calculated from the model with modal parameters $\boldsymbol{\theta}$ using the given inputs $\{f_i\}$. In the procedure, J is minimized with respect to $\boldsymbol{\theta}$ using a "modal-sweep" method, which involves a combination of successive relaxation and a modified method of steepest descent. Beck (1989) has shown that within a Bayesian probability framework, the modal parameters that are estimated by Mode-ID can be viewed as the most probable values based on the given data (in addition, see Beck 1996).

Previously, Mode-ID has been applied to modal identification from measured seismic or forced-vibration response of several civil engineering structures, including high-rise buildings (Beck and Jennings 1980; Nisar et al. 1992), a highway overpass (Werner et al. 1987), an off-shore oil platform (Mason et al. 1989), and several other structures. Under ambient excitation conditions, Mode-ID has also been applied to modal identification of a 9-story reinforced-concrete building (Beck et al. 1994) and an 11-story steel-frame building (Beck et al. 1995).

5.3.5 Modal identification of structure

A modal model of the structure is obtained using Mode-ID for the system response to the input to each VCA that is described in Section 5.3.3. From each data set and input, a modal model of the system is identified that includes the 9 structural modes. These modes can be recognized as either flexural modes or torsional modes of the structure. The flexural modes occur in pairs, as their motion corresponds to bending in two (roughly) orthogonal directions. The modes are, in order of increasing frequency, the first flexural modes (both approximately 0.9 Hz), first tor-

sional (about 1.6 Hz), second flexural (both approximately 2.2 Hz), second torsional (about 3.7 Hz), third flexural (both around 3.8 Hz), and third torsional (approximately 6.3 Hz). The identified damping ratios range from 0.4–5%. For the pre-move data sets that are collected from the excitation of the first VCA (VCA 1), the modal frequencies (in Hertz) and damping ratios (percent) identified from the different excitations are summarized in Table 5.1. The results from the excitation of VCA 2 and VCA 3, in turn, are shown in Tables 5.2 and 5.3. The results of the system identification of the modal model for the post-move system are shown in Table 5.4, Table 5.5, and Table 5.6. In Tables 5.1 through 5.6, ω_r and ζ_r denote the natural frequency and damping ratio for mode r ($r \in \{1, \ldots, 9\}$), $\phi_i^{(r)}$ is the modeshape component at accelerometer i ($i \in \{1, 2, 3\}$), and $\psi_j^{(r)}$ is the participation factor of the r^{th} mode due to the j^{th} VCA input.

Due to the symmetry of the structure, the modeshape components for the flexural modes of the structure are more difficult to extract than the frequencies and damping ratios. For these closely-spaced flexural modes, an infinite number of potential modeshape vectors exist. Hence, although "modeshape components" can be found that enable successful prediction of the system response, the modeshape components do vary from test to test, which makes the construction of a comprehensive modal model difficult. This is accomplished in the next section by appending together modal models that are identified for a specific actuator, which increases the number of modes used for the modal model of the system.

5.3.6 Modal model of structure

The final step in the construction of a modal model for the system is to combine the modal identification results from the tests for each actuator into a 3-input/3-output model of the system. This can be accomplished by appending together three modal models, where each of the modal models is identified from the measured response of the structure to a single actuator in turn. Standard model reduction techniques could be used to reduce this system to the 9 structural (i.e., 18 states) of the structure, although the neat arrangement of the modal system matrices as

Table 5.1 "Pre-move" modal property data identified using input VCA 1.

Mode	ω_r (Hz)	ζ_r %	$\phi_1^{(r)}$	$\phi_2^{(r)}$	$\phi_3^{(r)}$	$\psi_1^{(r)}$
FLX 1	0.872	0.878	−0.168	−0.623	0.764	0.041
FLX 1	0.893	1.327	0.778	−0.607	−0.159	−0.137
TOR 1	1.590	0.884	0.573	0.605	0.552	−0.144
FLX 2	2.250	2.845	0.708	−0.683	−0.181	0.303
FLX 2	2.292	3.001	−0.258	0.913	−0.316	0.145
TOR 2	3.858	5.248	−0.299	−0.709	−0.639	0.070
FLX 3	3.598	1.212	0.676	−0.533	−0.508	0.102
FLX 3	3.613	1.800	−0.024	0.733	0.680	0.325
TOR 3	5.993	1.590	0.587	0.588	0.556	−0.078

Table 5.2 "Pre-move" modal property data identified using input VCA 2.

Mode	ω_r (Hz)	ζ_r %	$\phi_1^{(r)}$	$\phi_2^{(r)}$	$\phi_3^{(r)}$	$\psi_2^{(r)}$
FLX 1	0.869	0.669	−0.120	−0.622	0.774	−0.088
FLX 1	0.900	1.193	0.802	−0.531	−0.274	−0.087
TOR 1	1.586	0.780	0.595	0.592	0.544	0.174
FLX 2	2.257	3.148	0.672	−0.731	−0.120	0.303
FLX 2	2.303	2.786	−0.723	0.133	0.678	0.165
TOR 2	3.763	3.924	−0.587	−0.809	0.020	−0.080
FLX 3	3.625	2.252	−0.327	−0.663	−0.674	0.615
FLX 3	3.630	2.313	−0.031	0.750	0.661	0.368
TOR 3	5.977	1.700	0.585	0.565	0.582	0.086

Table 5.3 "Pre-move" modal property data identified using input VCA 3.

Mode	ω_r (Hz)	ζ_r %	$\phi_1^{(r)}$	$\phi_2^{(r)}$	$\phi_3^{(r)}$	$\psi_3^{(r)}$
FLX 1	0.871	0.625	−0.260	−0.842	0.472	0.420
FLX 1	0.871	0.657	0.237	0.925	−0.300	0.334
TOR 1	1.587	0.765	0.593	0.614	0.521	0.145
FLX 2	2.294	2.164	0.755	−0.585	−0.296	0.099
FLX 2	2.302	2.097	0.026	0.695	−0.718	0.209
TOR 2	3.626	2.309	−0.309	−0.688	−0.657	0.642
FLX 3	3.731	2.426	−0.254	−0.009	−0.967	−0.130
FLX 3	3.632	2.458	−0.006	0.751	0.661	0.379
TOR 3	5.990	1.764	0.582	0.656	0.480	0.083

Table 5.4 "Post-move" modal property data identified using input VCA 1.

Mode	ω_r (Hz)	ζ_r %	$\phi_1^{(r)}$	$\phi_2^{(r)}$	$\phi_3^{(r)}$	$\psi_1^{(r)}$
FLX 1	0.877	0.867	−0.926	0.034	0.375	−0.215
FLX 1	0.876	0.753	0.633	0.443	−0.634	−0.233
TOR 1	1.634	0.671	0.576	0.555	0.600	−0.146
FLX 2	2.199	2.785	−0.006	0.758	−0.653	0.199
FLX 2	2.300	2.121	−0.907	0.229	0.354	0.094
TOR 2	3.673	2.646	0.589	0.436	0.681	0.546
FLX 3	3.733	4.232	−0.596	−0.245	−0.765	0.390
FLX 3	3.893	1.885	0.511	−0.604	0.611	0.128
TOR 3	6.334	1.027	0.547	0.572	0.612	−0.077

Table 5.5 "Post-move" modal property data identified using input VCA 2.

Mode	ω_r (Hz)	ζ_r %	$\phi_1^{(r)}$	$\phi_2^{(r)}$	$\phi_3^{(r)}$	$\psi_2^{(r)}$
FLX 1	0.879	0.806	−0.047	−0.679	0.733	0.181
FLX 1	0.884	0.370	−0.583	−0.782	−0.220	0.076
TOR 1	1.633	0.640	0.573	0.568	0.591	0.137
FLX 2	2.204	2.836	0.151	0.681	−0.716	0.212
FLX 2	2.299	2.244	0.877	−0.468	−0.113	0.074
TOR 2	3.661	1.644	0.801	0.586	0.127	−0.372
FLX 3	3.661	1.613	0.787	0.340	−0.515	0.191
FLX 3	3.924	1.570	0.319	0.270	−0.908	−0.072
TOR 3	6.330	1.023	0.542	0.567	0.621	0.080

Table 5.6 "Post-move" modal property data identified using input VCA 3.

Mode	ω_r (Hz)	ζ_r %	$\phi_1^{(r)}$	$\phi_2^{(r)}$	$\phi_3^{(r)}$	$\psi_3^{(r)}$
FLX 1	0.881	0.496	0.792	0.165	0.589	0.052
FLX 1	0.882	0.458	0.549	−0.441	−0.710	0.132
TOR 1	1.632	0.565	0.569	0.564	0.598	0.185
FLX 2	2.278	2.133	0.704	0.469	−0.533	−0.329
FLX 2	2.281	1.968	0.065	0.872	−0.485	0.235
TOR 2	3.659	1.464	0.469	0.366	0.804	−0.373
FLX 3	3.658	1.496	0.247	−0.093	0.965	0.157
FLX 3	3.952	1.355	0.985	−0.022	−0.171	0.082
TOR 3	6.326	1.052	0.553	0.569	0.609	0.079

sub-components of the state matrices is lost in the reduction. For the modal model that is constructed in this section, no model reduction is performed, and the model that is used is created by appending the modal model that predicts the acceleration response to input at VCA 1 to the modal model created using VCA 2 as input, yielding a 36-state system. For the experiments discussed in this chapter, VCA 1 is used exclusively to provide the system excitation, and VCA 2 is used exclusively for control purposes. Note that the simplest method would be to excite all three actuators at once, in order to simultaneously identify the participation factors for each mode. However, this was not performed prior to the relocation of the structure, so this method could not be used (at least for the pre-move model).

The modal equations for the identified model can be used for control design purposes. Consider the modal system excited by the p^{th} input VCA and controlled by the q^{th} VCA,

$$\ddot{x} + \Theta\dot{x} + \Lambda x = \psi_p w_g + \psi_q u \tag{5.2}$$

where $\Lambda = \text{diag}\,(\omega_1, \omega_2, \ldots, \omega_9)$ is the diagonal matrix of modal frequencies, $\Theta = \text{diag}\,(2\zeta_1\omega_1, 2\zeta_2\omega_2, \ldots, 2\zeta_9\omega_9)$ is the linear viscous damping matrix, and ψ_p and ψ_q are the p^{th} and q^{th} columns of the modal participation factor matrix, which has one column for each VCA input. The input ground motion, which is translated into a force from the p^{th} VCA that acts on the structure, is given by $w_g(t) \in \mathbb{R}$, and the feedback control force acting through the q^{th} VCA is given by $u(t) \in \mathbb{R}$. The input ground motion used for the controller design is a Kanai-Tajimi linear filter (Clough and Penzien 1975) with natural frequency of 50 rad/sec and a damping ratio of 50%, similar to the one described in Section 4.3.

The state equation for the uncontrolled modal model based on the r^{th} VCA

input is

$$
\begin{aligned}
\dot{x}_r &= \begin{bmatrix} 0 & I \\ -\Lambda_r & -\Theta_r \end{bmatrix} x_r + \begin{bmatrix} 0 \\ -\psi_p^{(r)} \end{bmatrix} w_g \\
z_r &= \begin{bmatrix} \Phi_r' & 0 \\ 0 & \Phi_r' \end{bmatrix} x_r \\
y_r &= \begin{bmatrix} -\Phi_r'\Lambda_r & -\Phi_r'\Theta_r \end{bmatrix} x_r + \begin{bmatrix} \Phi_r'\psi_p^{(r)} \end{bmatrix} w_g,
\end{aligned}
\tag{5.3}
$$

where $y_r(t) \in \mathbb{R}^3$ represents the measured acceleration outputs and $z_r(t) \in \mathbb{R}^6$ are the performance variables for VCA input r. The matrices Λ, Θ, and Ψ from (5.2) are subscripted with an r as well to indicate the modal model identified using excitation from a particular actuator. The matrix of partial modeshape factors is given by $\Phi_r \in \mathbb{R}^{9\times 3}$. For the experimental studies performed throughout this chapter, the 1^{st} VCA provides the system excitation, and the 2^{nd} VCA is used for feedback control. The 3^{rd} VCA is not used.

The modal models that are identified for the two VCA inputs are used to model the response of the laboratory structure for controller analysis and design. Similar to the benchmark structure application (Chapter 4), a high-fidelity SIMULINK (1994b) model is used to accurately describe the laboratory system. The first ten seconds of the simulated acceleration response of the system to the identification input from Section 5.3.2, which is acting through VCA 1, is shown in Figure 5.3, and the SIMULINK (1994b) block diagram is pictured in Figure 5.4. The fast Fourier transforms (FFTs) of the simulated and measured response are shown in Figure 5.5, where the simulated response (solid line) and measured response (dashed line) nearly coincide for most of the modes of the structure (except for the first flexural mode). For the first flexural mode, the peak of model response is much smaller than the one found from FFT of the response data. This could result from several factors. The first is that the area under this peak is small, so the resulting best-fit model from MODE-ID may not be very sensitive to this first flexural mode peak. In addition, significant ambient vibrations could exist that the structure's response

to this "unmeasured" input is comparable to the forced response in this frequency range, which would cause noise in the modal properties that are identified for this mode.

The final state equations that are used for control design are

$$
\begin{aligned}
\dot{x} &= \begin{bmatrix} 0 & I \\ \begin{bmatrix} -\Lambda_1 & 0 \\ 0 & -\Lambda_2 \end{bmatrix} & \begin{bmatrix} -\Theta_1 & 0 \\ 0 & -\Theta_2 \end{bmatrix} \end{bmatrix} x + \begin{bmatrix} 0 & 0 & 0 \\ -\psi_1 & 0 & 0 \\ 0 & 0 & \psi_2 \end{bmatrix} \begin{Bmatrix} w_g \\ v \\ u \end{Bmatrix} \\
z &= \begin{bmatrix} \begin{bmatrix} \Phi_1' & \Phi_2' \end{bmatrix} & 0 \\ 0 & \begin{bmatrix} \Phi_1' & \Phi_2' \end{bmatrix} \\ 0 & 0 \end{bmatrix} x + \begin{bmatrix} 0 & 0 & 0 \\ 0 & 0 & 0 \\ 0 & 0 & \gamma_u \end{bmatrix} \begin{Bmatrix} w_g \\ v \\ u \end{Bmatrix} \qquad (5.4) \\
y &= \left[\begin{bmatrix} -\Phi_1'\Lambda_1 & -\Phi_2'\Lambda_2 \end{bmatrix} \quad \begin{bmatrix} -\Phi_1'\Theta_1 & -\Phi_2'\Theta_2 \end{bmatrix} \right] x + \begin{bmatrix} 0 & \nu_{rms} I & 0 \end{bmatrix} \begin{Bmatrix} w_g \\ v \\ u \end{Bmatrix},
\end{aligned}
$$

where $y(t) \in \mathbb{R}^3$ represents the *measured* outputs as before, $v(t) \in \mathbb{R}^3$ is the measurement noise and modeling error term, and $z(t) \in \mathbb{R}^7$ the *performance* outputs, which are the relative displacements and velocities at the measured locations as well as the actuator command signal, $u(t) \in \mathbb{R}$. Note that the control effort is weighted by γ_u, and the measurement noise/modeling error $v(t)$ is scaled by ν_{rms}. Furthermore, the *measured* outputs for the controller design have no feed-through of the input or control force, as is standard in controller design.

5.4 Pre-data and post-data analysis

5.4.1 System descriptions

The purpose of re-analyzing a system when new data becomes available is to improve the accuracy of the performance description. This can be accomplished using the method outlined in Section 3.4. In this section, the goal is to assess the performance of the post-move structure. This performance is analyzed using two descriptions of

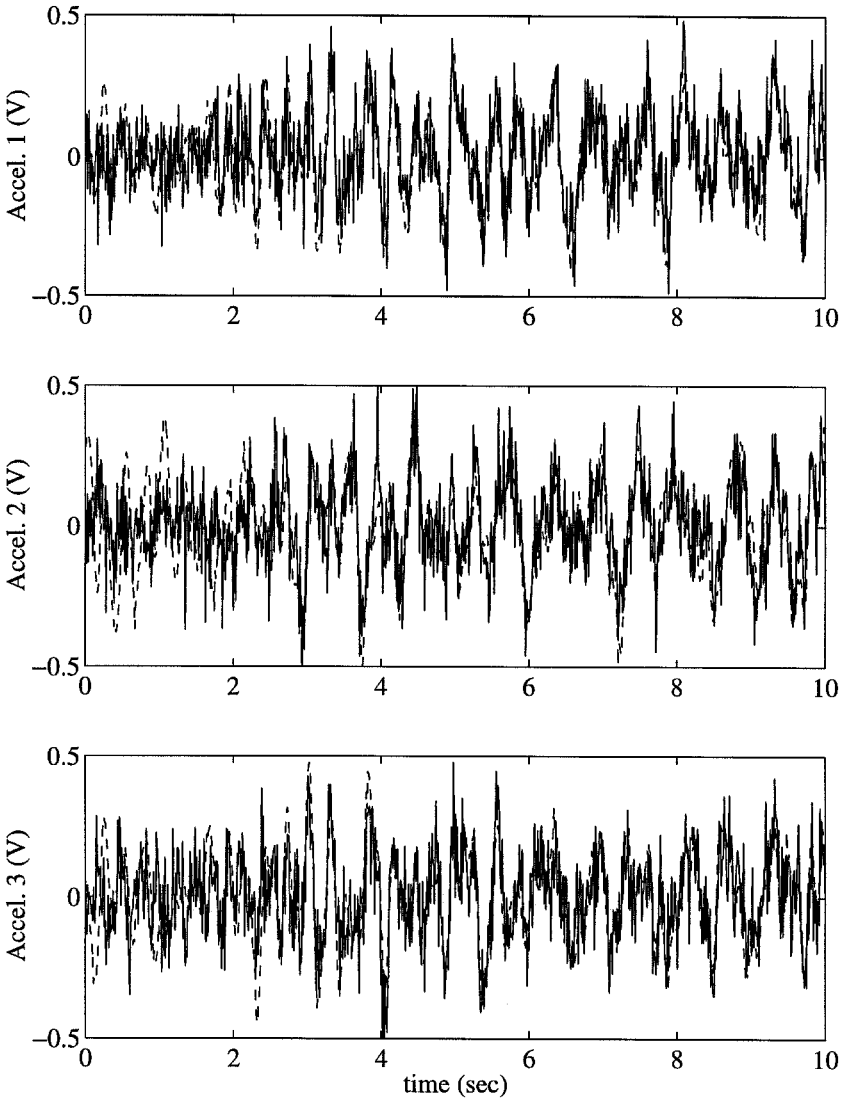

Figure 5.3 Simulated response (solid) using post-move model and measured post-move response (dashed) of structure to flat-spectrum input through VCA 1.

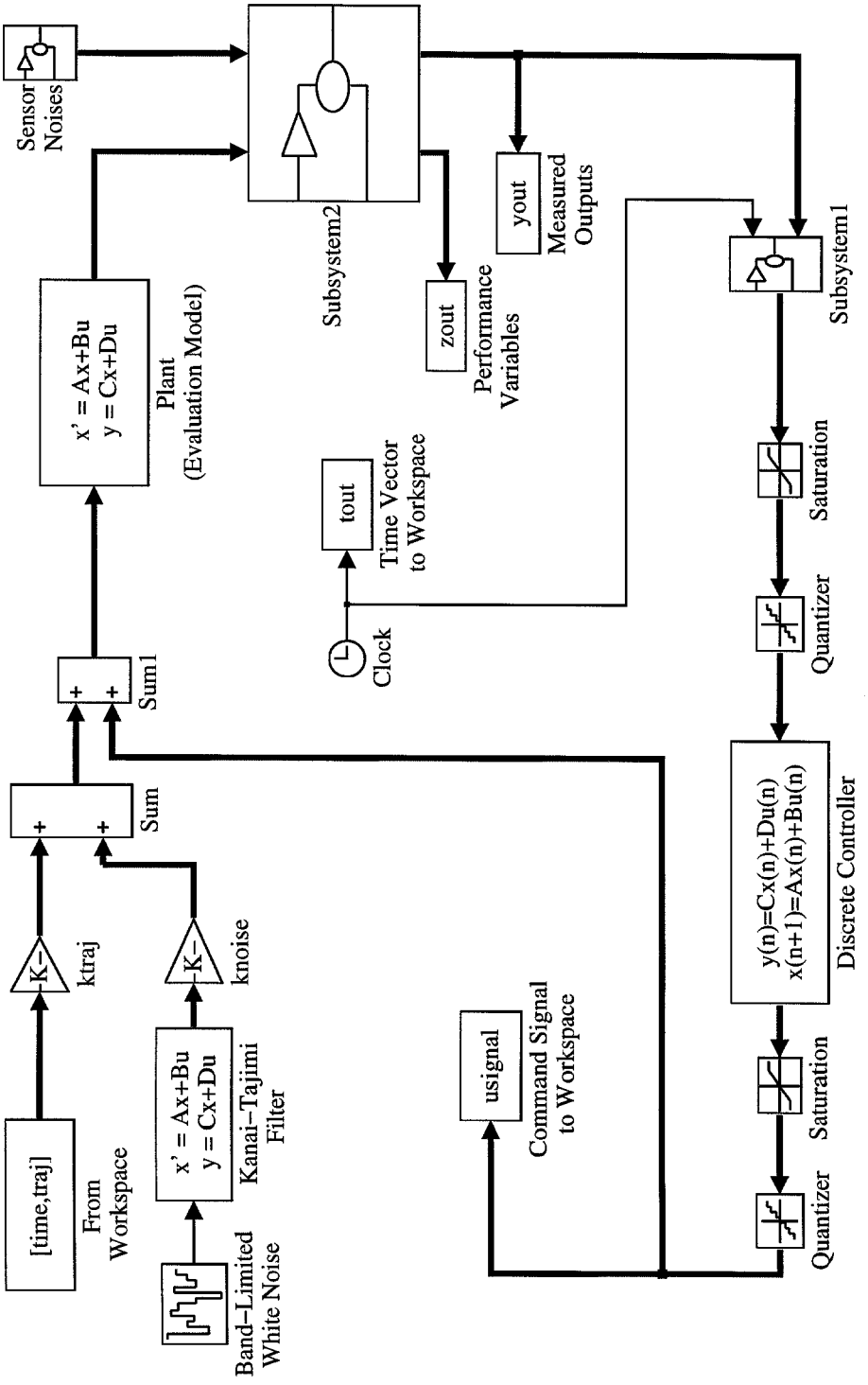

Figure 5.4 SIMULINK (1994b) block diagram for Caltech flexible structure.

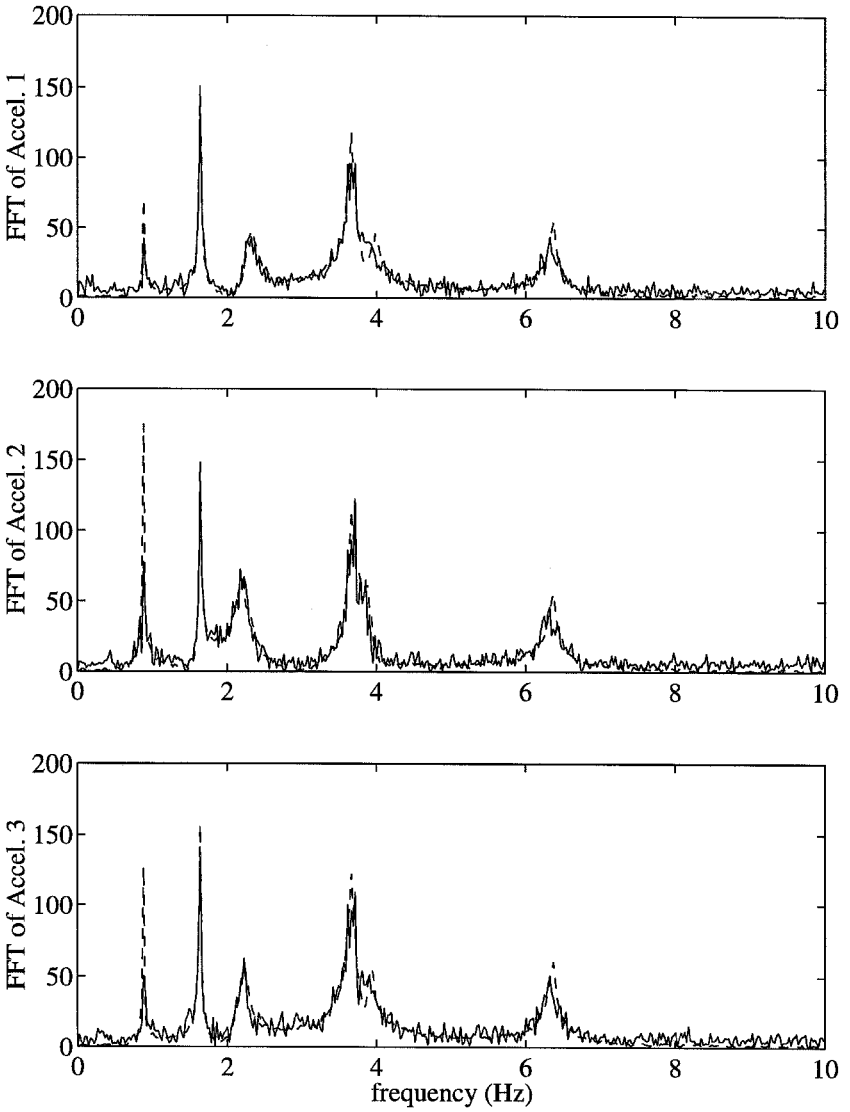

Figure 5.5 FFT of the simulated response of the post-move model (solid) and measured response of the post-move structure (dashed) to the flat-spectrum input through VCA 1.

the system. The first is based on the frequencies and damping ratios identified from the pre-move response data, and is called the "pre-data" model. The second, the "post-data" model, makes use of an updated description of the model uncertainty, and is based on the response data taken after the structure was moved.

The pre-data model contains a combination of the modal properties that are identified from the pre-move and post-move response data sets. The natural frequencies and damping coefficients are taken from the pre-move data set, while the modeshape components and modal participation factors are taken from the post-move response data. Although using the same modeshape components for both the pre-data and post-data models and considering those components to be accurate is not very realistic, consistent identification of the modeshape components is difficult. This simplifying assumption is made, however, in order to illustrate the post-data analysis method. Further exploration of the uncertainty in the modeshape components in future work would be helpful.

The normalized 2-norms of the prediction errors for both models are displayed in Table 5.7, where the prediction errors have been normalized by dividing them by the 2-norm of the measured post-move response. These norms are computed from taking the square root of (5.1), and they compare the post-move response data with the response predicted by the modal models for the system. As expected, the post-data prediction error is smaller for each VCA input than the pre-data error, since the post-data model as identified by Mode-ID is the one that minimizes the 2-norm of the prediction error. The pre-data models described above do not appear to fit the data very well, with errors on the order of the magnitude of the signal. The large modeling error can be explained for the pre-data model by the narrowness of the peaks of the system transfer function, as small variations in frequency can cause the peaks to no longer coincide. In addition, the predicted response is a strong function of the damping ratios, and these vary substantially between the pre-move and post-move tests for certain modes (primarily the flexural modes). For reference, the transfer functions from the input of VCA 1 and VCA 2 to the three accelerometers for the pre-data and post-data models are displayed in Figure 5.6. In

this figure, the peaks of the post-data model are (in general) higher than those for the pre-data model, due to the lower damping ratios that were identified for most of the modes of this model.

Table 5.7 Measures-of-fit for pre-data and post-data models, relative to measured post-data response.

Input	$\|y - q(\boldsymbol{\theta})\|_2 / \|y\|_2$	
	pre-data	post-data
VCA 1	1.05	0.203
VCA 2	1.08	0.187
VCA 3	1.04	0.178

5.4.2 Model uncertainty

As discussed previously in Chapter 2, the modeling error is used to account for the discrepancy between the actual and the predicted response of the system. This modeling error is a combination of parametric model uncertainty and the non-parametric prediction error. The probabilistic robust analysis is able to explicitly consider these uncertainties.

For the probabilistic robust analysis of the flexible structure, probability distributions are assigned to the uncertain pre-data and post-data models. For the pre-data model, the distributions are based largely on engineering judgment. A lognormal distribution is used to model the frequency and damping parameter uncertainty. For the post-data model the parameter covariance matrix, as obtained by analysis of the curvature of the measure-of-fit from (5.1) (Beck 1996; Beck and Katafygiotis 1998), is used to determine the probability distribution for the uncertain parameters. This distribution has been shown to be asymptotically correct as the amount of measured data from the system becomes large (Beck 1996; Beck and Katafygiotis 1998).

The most probable values for the natural frequencies and damping ratios of the pre-data model were identified using Mode-ID (Beck 1990), and these parameter values become the most probable parameters for the pre-data model uncertainty

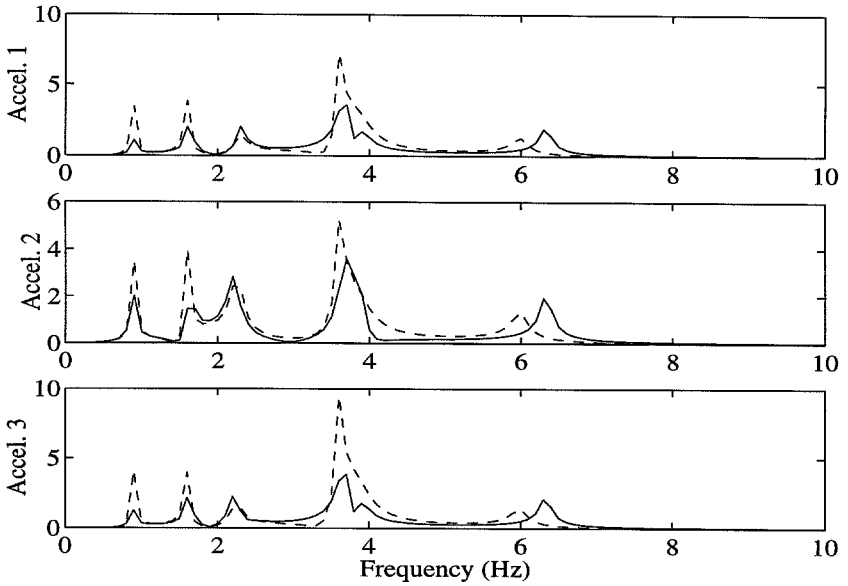

(a) VCA 1 (disturbance actuator)

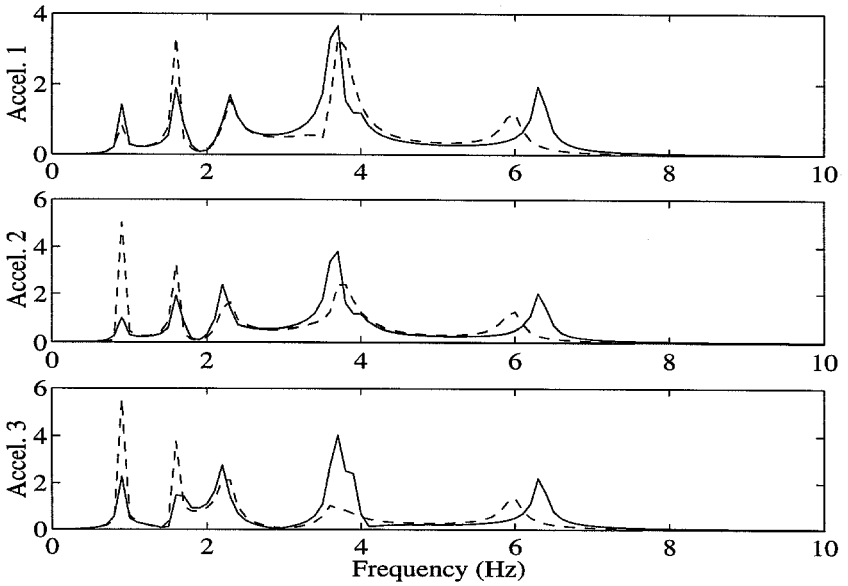

(b) VCA 2 (control actuator)

Figure 5.6 Comparison of pre-data (solid) and post-data (dashed) transfer functions.

description. The post-move system would be expected to show significant variation from these most-probable parameter values, so, according to engineering judgment, the assigned variances for the PDFs of these uncertain parameters are relatively large. The natural frequencies are each given a coefficient of variation of 10%, and the damping ratios a coefficient of variation of 25%. The pre-data model probability distributions for these uncertain parameters becomes the *a priori* PDF for the updating of the uncertainty description using Bayes's Theorem (see Section 3.4). Hence, using $\boldsymbol{\theta} = \{\omega_1 \quad \zeta_1 \quad \dots \quad \omega_9 \quad \zeta_9\}'$ to represent the vector of uncertain modal parameters, the prior PDF is

$$p(\boldsymbol{\theta}|\Theta) = \frac{1}{(2\pi)^9 \prod_{i=1}^{18} \sigma_{\boldsymbol{\theta}_i}} \exp\left[-\frac{1}{2}(\boldsymbol{\theta} - \boldsymbol{\theta_0})' \operatorname{diag}[\sigma_{\boldsymbol{\theta}_i}](\boldsymbol{\theta} - \boldsymbol{\theta_0})\right] \tag{5.5}$$

where the $\sigma_{\boldsymbol{\theta}_i}$'s are the coefficients of variation of the uncertain parameters, and $\boldsymbol{\theta_0}$ represents the most probable parameters for the pre-data model.

The probability model for the post-data system can be determined from (3.13) and by the methods described in Beck (1996) and Beck and Katafygiotis (1998). The expression for $p(\mathcal{D}|\boldsymbol{\theta}, \Theta)$ can be found by expanding the probability distribution for the prediction error about the most probable parameter values. The most probable parameters will minimize the prediction error and maximize its "white-ness." The prediction error, e_n, at each time step n, $n \in \{1, \dots, N\}$, is given by

$$e_n = y_n - q_n(\boldsymbol{\theta}), \tag{5.6}$$

where y_n is the measured output and $q_n(\boldsymbol{\theta})$ is the output predicted by the model (and the known input). The probability of the data given the model follows the Gaussian probability distribution of the prediction errors. Hence,

$$\begin{aligned} p(\mathcal{D}|\boldsymbol{\theta}, \Theta) &= p(\{y_1, \dots, y_N\}|\boldsymbol{\theta}, \Theta) \\ &= \prod_{n=1}^{N} \left(\frac{1}{\sqrt{2\pi}^{N_o} \prod_{i=1}^{N_o} \sigma} \exp\left[-\frac{1}{2}(y_n - q_n)'\Sigma^{-1}(y_n - q_n)\right] \right), \end{aligned} \tag{5.7}$$

where N_o is the number of measured outputs, $\Sigma = \text{diag}[\sigma_i^2]$ is the diagonal matrix of prediction error variances for each channel. The natural logarithm of $p(\mathcal{D}|\boldsymbol{\theta}, \boldsymbol{\Theta})$ can be expanded about $\hat{\boldsymbol{\theta}}$, the most probable parameter values, to yield

$$p(\mathcal{D}|\boldsymbol{\theta}, \boldsymbol{\Theta}) \simeq p(\mathcal{D}|\hat{\boldsymbol{\theta}}, \boldsymbol{\Theta}) \exp\left[-\frac{1}{2}(\boldsymbol{\theta} - \hat{\boldsymbol{\theta}})' A_N (\boldsymbol{\theta} - \hat{\boldsymbol{\theta}})\right], \tag{5.8}$$

where

$$\begin{aligned}[A_N]_{ij} &= \left[\frac{\partial^2 \ln p(\mathcal{D}|\boldsymbol{\theta}, \boldsymbol{\Theta})}{\partial \boldsymbol{\theta}_i \partial \boldsymbol{\theta}_j}\right]_{\hat{\boldsymbol{\theta}}} \\ &= \frac{NN_o}{2}\left[\frac{1}{J_{\boldsymbol{\theta}}}\frac{\partial^2 J_{\boldsymbol{\theta}}}{\partial \boldsymbol{\theta}_i \partial \boldsymbol{\theta}_j}\right]_{\hat{\boldsymbol{\theta}}}\end{aligned} \tag{5.9}$$

and

$$p(\mathcal{D}|\hat{\boldsymbol{\theta}}, \boldsymbol{\Theta}) = \left(2\pi e J(\hat{\boldsymbol{\theta}})\right)^{-NN_o/2}. \tag{5.10}$$

The above expression is evaluated to determine $p(\mathcal{D}|\boldsymbol{\theta}, \boldsymbol{\Theta})$ for the post-data system using a finite difference approach, then Bayes's Theorem (3.13) can be used to determine $p(\boldsymbol{\theta}|\boldsymbol{\Theta}, \mathcal{D}) = cp(\mathcal{D}|\boldsymbol{\theta}, \boldsymbol{\Theta})p(\boldsymbol{\theta}|\boldsymbol{\Theta})$, where c is a constant chosen such that $\int_{\boldsymbol{\Theta}} p(\boldsymbol{\theta}|\boldsymbol{\Theta}, \mathcal{D})d\boldsymbol{\theta} = 1$. However, when the amount of response data from the system is large, the parameter estimates are quite precise, and $[A_n]$, which is $\mathcal{O}(N)$, dominates the $\text{diag}[\sigma_{\boldsymbol{\theta}_i}^{-2}]$ matrix from the prior PDF $p(\boldsymbol{\theta}|\boldsymbol{\Theta})$ when calculating $p(\boldsymbol{\theta}|\boldsymbol{\Theta}, \mathcal{D})$. For this application, the contribution of the prior PDF to the covariance matrix for $\boldsymbol{\theta}$ is negligible, and it is ignored for the post-data calculations.

The sensor noise and modeling error of the system, which account for the remaining prediction error of the system, can be modeled as a Gaussian-white process. This process is parameterized by its mean and variance, where the parameters describing the prediction-error process could be considered uncertain variables themselves. For this study, however, the mean of the prediction error is assumed to be zero and its standard deviation (square root of the variance) is assumed to be constant, and is chosen to be 1.0 for the pre-data model and 0.2 for the less uncertain post-data

case. These values correspond to the 2-norms of the prediction errors as given in Table 5.7.

5.4.3 Pre-data and post-data performance analysis of uncontrolled systems

The results of the pre-data and post-data analysis of the uncontrolled models for the structure are shown in Table 5.8. The total failure probability and the probable $\mathcal{H}_2$ performance are computed using the uncertain pre-data and post-data models described above. Also included in the table are the failure probabilities and $\mathcal{H}_2$ performance of the nominal systems.

The failure levels that are used for the failure probability calculations are 3 cm for the computed displacement at the accelerometers and 0.1 N for the required actuator effort. The choice of these particular failure levels is somewhat arbitrary for this structure, as they do not correspond to the levels that would indicate "failure" of the laboratory system. The displacement failure level that was chosen corresponds to nearly 1.5% of the overall height of the laboratory structure, while the actuator "failure" level of 0.1 N represents approximately 0.01% of the weight of the structure. A study of the scaling relationship between the laboratory structure and a typical civil engineering structure could be performed to determine how the quantities relate between the laboratory model and an actual structure.

For the calculated failure probabilities, the nominal pre-data model and the "robust" pre-data model performances differ by many orders of magnitude, indicating that this performance measure is very sensitive to uncertainties in the model. The post-data failure probability is close for both the nominal and robust cases, because the parameters for this system are much less uncertain, according to the post-data analysis method described above. The pre-data model performance still appears to be significantly better than the performance for the post-data model, but in this case, the probability model for the pre-data model uncertainty does not appear to adequately capture the uncertainty in the parameters. Future work could focus on the pre-data model uncertainty description.

For the $\mathcal{H}_2$ performance calculations, the pre-data model again shows significant differences between the nominal and robust cases, while the post-data calculations indicate the robust performance is quite close to the performance of the nominal (and most probable) model. Again, this is due to the larger uncertainty associated with the pre-data model than with the post-data model.

Table 5.8 Probable performance of pre-data and post-data models for the uncontrolled system.

	Nominal P_f (%)	Robust P_f (%)	Nominal $\mathcal{H}_2$	Expected $\mathcal{H}_2$
Pre-data model	3.37×10^{-7}	0.018	1.95	0.770
Post-data model	0.993	1.46	2.18	2.20

5.5 Nominal-model controller design

5.5.1 Overview

Two performance objectives are considered for controller design for the structure, the $\mathcal{H}_2$ performance and the failure probability of the system. These performance measures are both discussed in detail in Chapter 2. Controllers are designed that minimize these performance objectives for both the pre-data and post-data models of the system. The controllers are designed using only the nominal model information, then their probable robust performance is computed using the methods described in Section 5.5.4.

5.5.2 $\mathcal{H}_2$-optimal control

An $\mathcal{H}_2$-optimal controller (Doyle et al. 1989) is designed for the flexible structure. The $\mathcal{H}_2$-optimal controller uses acceleration feedback and a state estimator to minimize the weighted $\mathcal{H}_2$-norm of the control effort and the performance variables by the control synthesis method described in Doyle et al. (1989). The performance variables are the computed displacements and velocities of the structure.

For these experimental studies, the first VCA is used for excitation, and the

second VCA for the feedback control force. All three accelerometers on the lower level of the structure are used for sensing. The input time history for the structure on which the controllers are tested is the scaled 1940 El Centro NS Record, where the El Centro Record is the same input that is used in Chapter 4. For the flexible structure, the record has been lengthened by a factor of 5 in the time domain from the time history shown in Figure 4.12, which is the inverse of the time-scaling factor that is used to create the Benchmark input record. Then the ratio for the time scaling of the flexible structure input to the actual earthquake record is 1:1, which is desirable because the natural frequencies of the flexible structure are similar to those found for steel high-rise buildings.

Controllers are designed for both the pre-data and post-data nominal models of the system. Several performance weights were considered when designing the controllers, although only one controller designed for each model is displayed here. The displacement time history of the system controlled by the pre-data controller is shown in Figure 5.7, along with the Fourier transform of the measured accelerations. The displacements are obtained by integrating the acceleration response twice, detrending the data before each integration to reduce the displacement and drift errors from the integration. The displacement time history and acceleration FFT for the structure that is controlled by the post-data controller can be seen in Figure 5.8.

The performance of the $\mathcal{H}_2$ controller that is designed for the post-data model of the structure is much better than that for the pre-data model for the response of the flexural modes. Both controllers appear to attenuate the torsional response of the system effectively, as is evident in the reduction of the second peak (corresponding to the torsion mode) on the Fourier amplitude spectrum of the response. The controllers' effectiveness against the torsional modes is probably due to a combination of factors. For the torsional response, the actuator has a lot of control authority over the modeshape, so it is an effective energy dissipater. In addition, the model of the torsional modes of the structure is more accurate for the torsional modes than the flexural ones, and it changes little between the pre-data and post-data systems,

so less model uncertainty exists in the torsional modes to degrade the response. As is evident from the figures, the controllers are able to achieve only a small reduction in the response of the flexural modes of the system, particularly for the pre-data controller. One reason that the controller is not very effective against the flexural modes is that with only one actuator used for control, the controller has very little control authority in a direction perpendicular to the side containing the actuator (and this direction is close to the motion that is created by the excitation of the other VCA). In addition, the model uncertainty in the system is likely to reduce the controller effectiveness, and the parameters describing the flexural modes are more uncertain than those describing the torsional modes. As a final note, the controller designs could probably be improved if more time is spent refining the system model and the actual control design, which would both be good topics for further research.

5.5.3 Failure-probability-based controllers

In addition to the $\mathcal{H}_2$-optimal controller designs, controllers are designed for the pre-data and post-data models of the structure that minimize the probability of failure for the nominal model of the system, where failure is defined to occur when the computed displacements at the accelerometer locations on the bottom level exceed 3 cm. The probability of actuator failure is also included in the performance objective, where actuator failure is defined to occur when the actuator effort exceeds its saturation level of 0.1 V.

The responses of the closed-loop system that is controlled by the controllers that minimize the nominal failure probability of the system (i.e., the "P_{fail} controllers") are shown in Figure 5.9 for the pre-data controller and in Figure 5.10 for the post-data controller, where the system has been excited by the El Centro Record. As is apparent from these responses, the controller design for the post-data model is able to achieve much greater attenuation of the displacement response than the controller for the pre-data model. In addition, when compared with the performance of the $\mathcal{H}_2$ controllers, the displacement response for the P_{fail} post-data controller appears smaller than that for the $\mathcal{H}_2$ post-data controller. The comments on the effectiveness

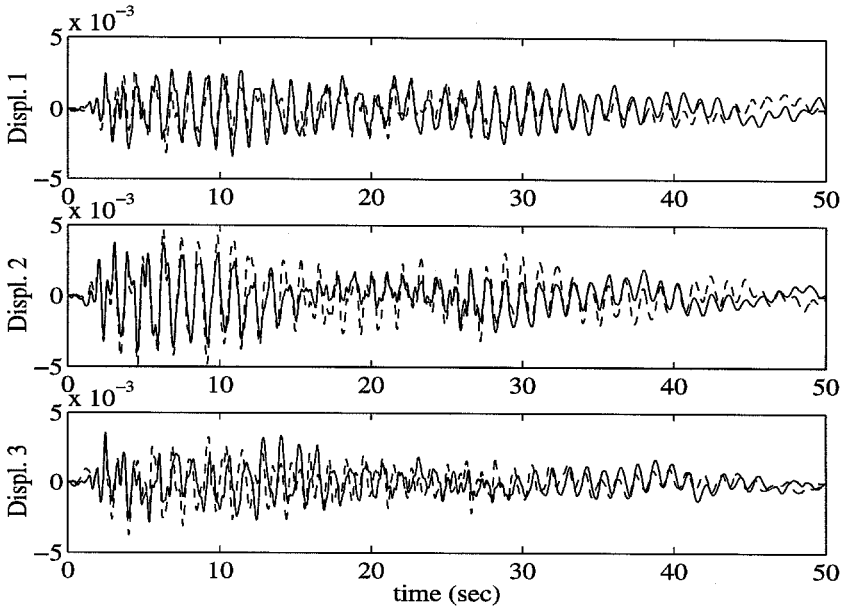

(a) Displacement time history.

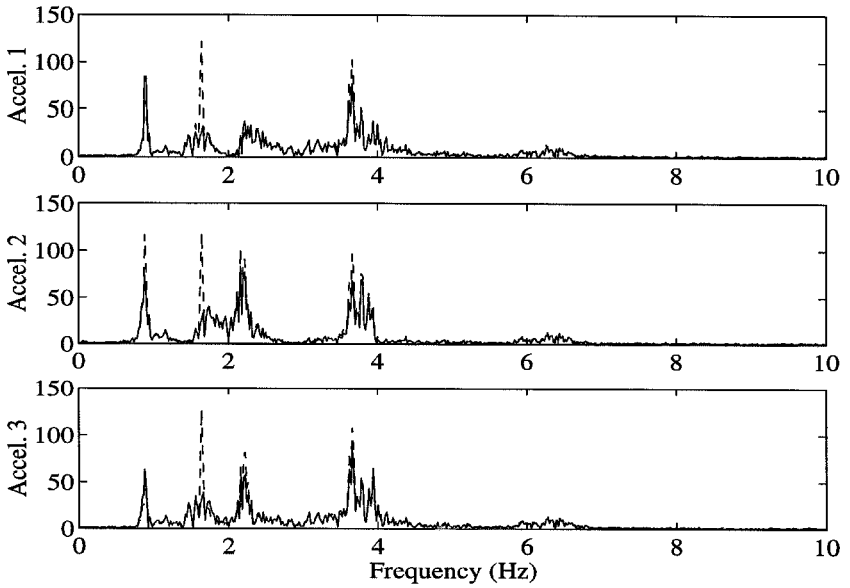

(b) FFT of measured accelerations.

Figure 5.7 Response of controlled (solid) and uncontrolled (dashed) structure to El Centro Record for the pre-data $\mathcal{H}_2$ controller.

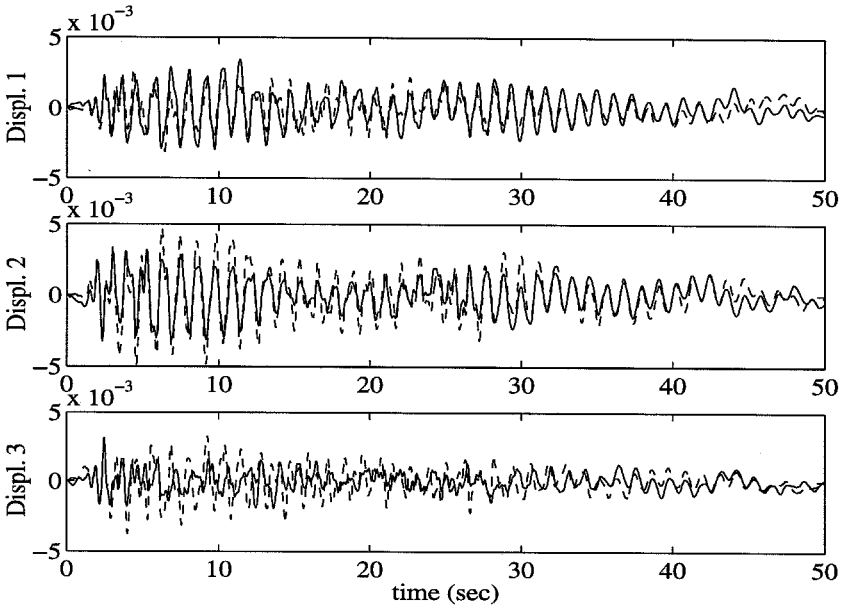

(a) Displacement time history.

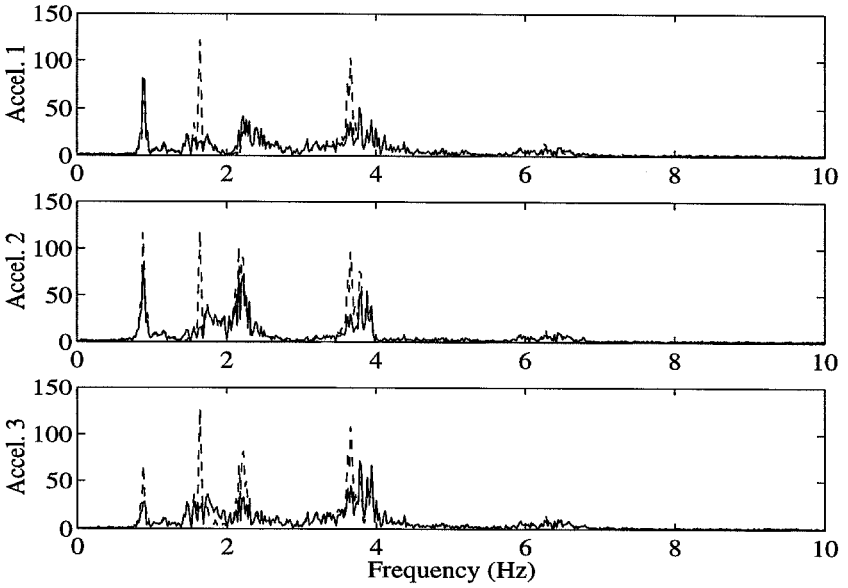

(b) FFT of measured accelerations.

Figure 5.8 Response of controlled (solid) and uncontrolled (dashed) structure to El Centro Record for the post-data $\mathcal{H}_2$ controller.

of the controller design from the $\mathcal{H}_2$ controller design section are also appropriate here.

5.5.4 Robust performance analysis of controlled systems

For the four controllers described above (pre and post–data $\mathcal{H}_2$, pre and post-data P_{fail}), the probabilistic performance measures are calculated on the basis of the post-data model. The results of the performance calculations are shown in Table 5.9. As would be expected, the post-data $\mathcal{H}_2$ controller yields the best $\mathcal{H}_2$ performance as determined by the post-data model, and the post-data P_{fail} controller yields the lowest failure probabilities on the post-data system. The pre-data controllers exhibit significantly worse performance on the post-data system than the post-data controllers do. This is not surprising, as the controllers are designed without considering the model uncertainties. Note that the pre-data P_{fail} controller's performance is computed to be even worse than the performance of the uncontrolled system.

Table 5.9 Probable performance of various controllers as computed for the post-data model of the system.

	Nominal P_f (%)	Robust P_f (%)	Nominal $\mathcal{H}_2$	Expected $\mathcal{H}_2$
$\mathcal{H}_2$ pre-data controller	0.702	0.711	2.51	2.51
$\mathcal{H}_2$ post-data controller	0.068	0.069	1.88	1.89
P_{fail} pre-data controller	4.51	4.82	2.74	2.75
P_{fail} post-data controller	0.00143	0.00795	2.15	2.16
Uncontrolled post-data model	0.993	1.462	2.18	2.20

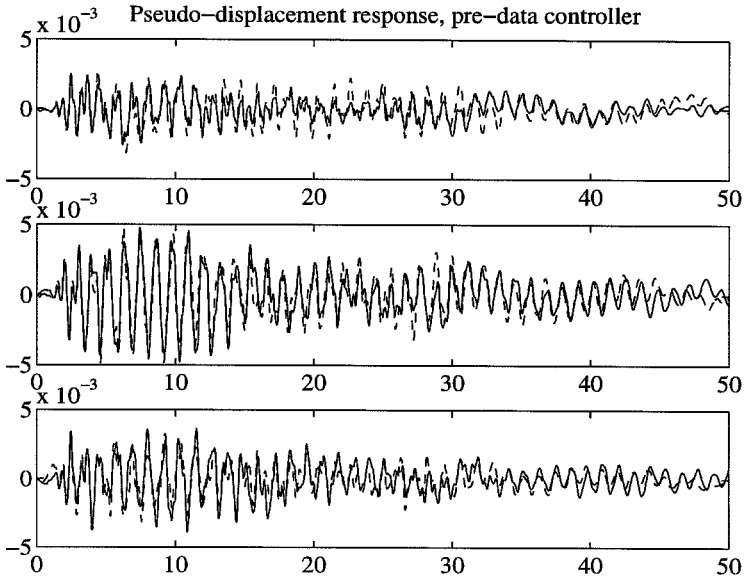

(a) Displacement time history.

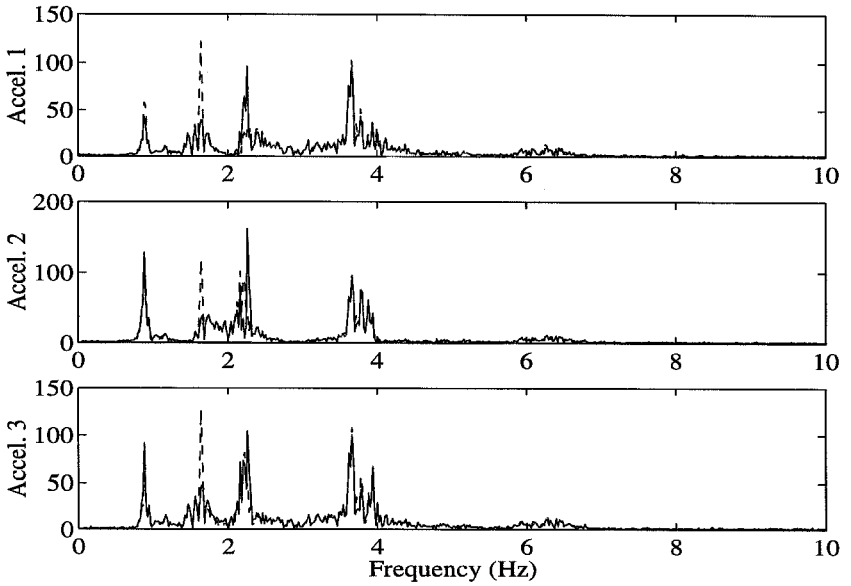

(b) FFT of measured accelerations.

Figure 5.9 Response of controlled (solid) and uncontrolled (dashed) structure to El Centro Record for the pre-data P_{fail} controller.

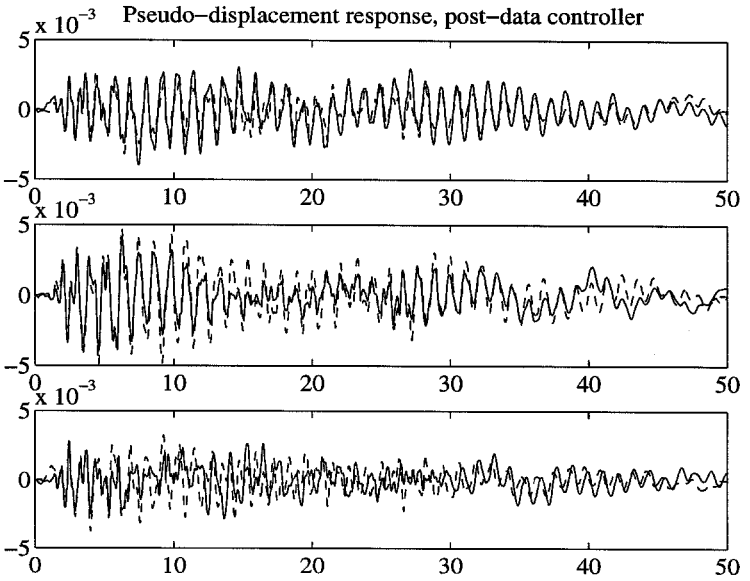

(a) Displacement time history.

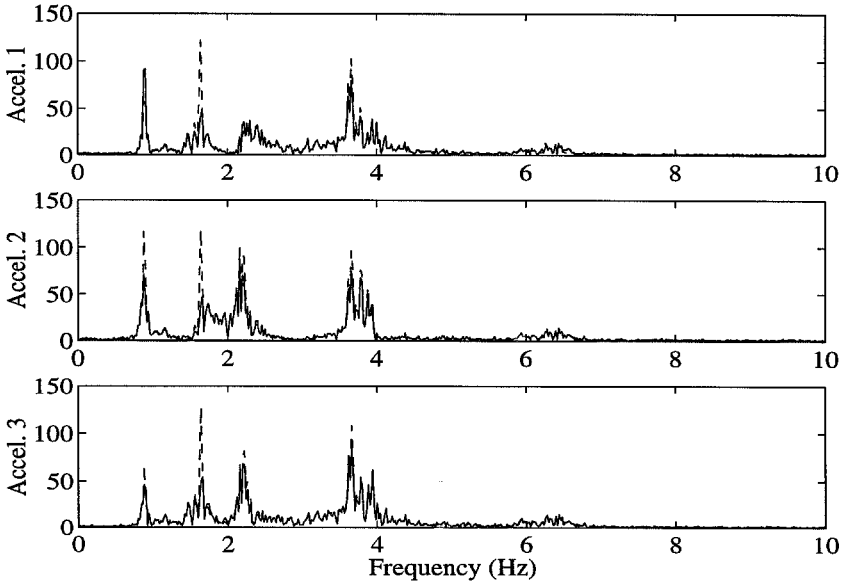

(b) FFT of measured accelerations.

Figure 5.10 Response of controlled (solid) and uncontrolled (dashed) structure to El Centro Record for the post-data P_{fail} controller.

Chapter 6

Conclusions and future work

6.1 Conclusions

The material in this thesis yields a framework for a probabilistic approach to robust control and develops the method for applications to civil engineering structures. This approach directly addresses several issues in structural analysis that are foremost in the mind of civil engineers, namely the uncertainty in the model used for control analysis and design and determining the reliability of the structural system. Specifically, the main contributions of this work to the field of structural control are

- A probabilistic robust analysis method that incorporates the probabilities of the models from the set of possible models,
- A method to determine the "total" robust reliability/failure probability of an uncertain system,
- Direct use of the reliability/failure probability as the performance objective for control design, and
- A method to incorporate new information to update the calculated performance for an uncertain system through a simple application of Bayes's theorem.

The probabilistic robust analysis method that is developed in Chapter 2 determines the *probable* performance of an uncertain system and allows the probability

of the uncertain models to be included in the robust analysis. This is an advantage over current norm-bounded robust control methods, which yield only the worst-case performance of the uncertain system as the answer to the robust analysis question, with no information as to how likely the worst case is to occur in practice. Hence, the probability-based approach adds an "extra dimension" to the robust analysis, where the extra dimension is the probability over the uncertain model set and the probable (rather than worst-case) performance measure.

A disadvantage of the probabilistic robust analysis method is that the total probability integral over the uncertain model set must be performed, which can be very expensive computationally. An efficient asymptotic expansion method is used to approximate the integral that appears to work well for the problems that have been studied. The method is particularly effective for the problems studied in this work because the peak of the integrand is generally close to the most-probable model of the system, so the most-probable model is a good initial guess for the search for the maximum of the integrand, which is required for the asymptotic expansion. In Chapter 5, the asymptotic approximation is applied to the probabilistic robust analysis of a system with 18 uncertain parameters (9 uncertain modal frequencies and damping ratios), and the computation time required is approximately an hour (run using MATLAB on a DEC/Alpha workstation). This computation time is reasonable for an analysis problem of this size, but it does preclude optimizing the performance for robust control design.

The total reliability (or failure probability) of an uncertain system can be determined from the methods outlined in Chapter 2, then used in the controller design discussed in Chapter 3. Using the structural reliability as a performance objective for the controller design is desirable from a structural engineering perspective, as the system's reliability is often the quantity used to measure structural performance.

In Chapter 3, the post-data analysis technique that uses Bayes's theorem to update the probabilities of the models in the uncertain model set is useful for modifying the description of a system's performance in the presence of new information from the system. This is important in earthquake engineering, as the actual behavior of

a structure during an earthquake is often quite different from that predicted by an initial finite element model of the system. The initial probabilities for the model uncertainty class are generally not sharply peaked near the most probable model of the system (which corresponds to the best pre-data model). Earthquake response data from a structure can be used to modify the "best" model and to make the probability distribution for the uncertain model class more highly peaked around the most-probable (post-data) model.

The post-data analysis of the probable robust performance is applied to the Caltech Flexible Structure in Chapter 5, where large differences are observed in the performance of the controllers designed for the post-data model relative to the pre-data model. The poor performance of the controllers designed for the pre-data model would presumably be improved with robust controller design. Unfortunately, the probabilistic robust control optimization described in Chapter 3 is intractable for this system. Furthermore, the performance differences between the pre-data and post-data controllers provide a strong argument for updating the controller design when new data is available from the system.

6.2 Future work

This thesis has laid out the framework for a probabilistic approach to control of uncertain civil engineering structures. Several directions exist for possible future work on the probabilistic robust analysis and control design methodology.

The first is to consider application of the control design approach to passive or semi-active systems for vibration control. The analysis methodology remains the same, and all that would be required is to choose a controller class that corresponds to the particular application, then optimize over the design parameters for the passive or semi-active system.

In addition, alternative performance measures could be considered for the structure, rather than the inter-story drift failure probability. For example, probability of instability for the uncertain system is of particular interest, as a controller design

that could lead to instability would be unacceptable.

One shortcoming of the approach that is presented herein is that the computation time required to solve the design problem for the uncertain-model controller is considerable. An area for further research is to explore whether an alternative formulation of the probabilistic analysis problem or other probability-based performance objectives and uncertainty descriptions can be found that would lead to more efficient solutions for both the analysis and control design. As experience is gained with the probabilistic robust analysis approach, computational procedures that exploit the structure of particular problems are likely to be developed.

For the Caltech Flexible Structure, several analysis and control design issues could be explored more fully under the probabilistic robust control framework. The first is to improve the modal identification method to obtain better models for the system. One idea is to use a modal identification algorithm that incorporates a physical basis for the modeshape components and modal participation factors for the closely spaced flexural modes. Then, uncertainty in the modeshape components and modal participation factors could be included more easily. Also, the effect of uncertainty in the model for the Gaussian process used to describe the modeling error and sensor noise should be studied for the structure and for other systems.

Another interesting task for the flexible structure would be to use the proof-mass actuators for control. These actuators are analogous to active mass driver actuators, which are common in civil engineering structural control applications. The proof mass actuators have more internal dynamics in the frequency range of the structural modes than do the voice coil actuators, which would provide additional control design challenges. A final task for the flexible structure (and other complicated systems) is to explore methods for making the probabilistic robust control design more tractable.

Appendix A

Two-story steel-frame building example

A.1 Overview

This appendix relates some of the details of the design procedure used to create the mathematical model of the illustrative example used in Chapters 2 and 3. The example is a model of a two-story special-moment-resisting-frame (SMRF) building, which was "designed" to satisfy the lateral drift requirements detailed in the 1994 Uniform Building Code (UBC), as well as the required capacity with respect to vertical loads. A schematic drawing of the two-story frame is shown in Figure 2.1.

The goal for the example problem is to construct a low-order modal model of the system that is consistent with a higher-fidelity model of a two-story building. The modal model is obtained for this system through the simplifying assumption that the axial deformations of the members are negligible and hence the horizontal displacements at the building joints are the same at each level. A Guyan static reduction (Cook et al. 1989; Guyan 1965) of the degrees of freedom of the higher-order model is also used to remove the rotational degrees of freedom from the equations of motion.

A.2 Selection of model parameters

The building is designed to satisfy the UBC lateral drift requirements for earthquake design, as described in Sections 2330–2334 of the UBC (1994), as well as standard

strength requirements for vertical loads found in both the UBC and the LRFD Steel Design Manual (1986). The design procedure requires first estimating the weight of the building, assuming typical building components and loading conditions. Then, the lateral forces on the building are estimated for the "design" earthquake. Next, the distribution of moments in the beams and columns at the connections is approximated using a simple analysis technique such as the portal method. Finally, the necessary beam and column moments of inertia are selected to provide adequate inter-story drift performance. A subsequent analysis is then performed to ensure that the selected moments of inertia satisfy the lateral drift requirement.

The design base shear for the structure is given by the relationship (UBC 1994)[1]

$$V = \frac{ZIC}{R_w} W, \tag{A.1}$$

where

- V is the design base shear
- Z is the seismic zone factor ($Z = 0.4$ for zone 4)
- I is the building's importance factor ($I = 1.0$)
- C is a numerical coefficient, (A.2)
- R_w is the "reduction factor" (12 for SMRF buildings)
- W is the total seismic dead load of the structure (Table A.1).

The coefficient C is given by

$$C = \min\left(\frac{1.25S}{T^{2/3}}, 2.75\right) \tag{A.2}$$

where S is the site coefficient, which depends on the soil type at the site and is taken to be 1.0 in this example, and T is the period of the building's fundamental mode of vibration. The fundamental period is initially approximated using the relationship

$$T = C_t (h_n)^{3/4}, \tag{A.3}$$

[1]Note that for this section only, the notation convention convention of Chapter 1 is not used so that the variable names in this section can match those found in the UBC (1994).

where $C_t = 0.035$ for a SMRF, and h_n is the height in feet to the n^{th} (i.e., top) floor. After the initial design is determined using this period value, the period estimate for the fundamental-mode can be updated.

The weight of the various building components are shown in Table A.1, and these weights are used to estimate the seismically effective dead load W. Referring to Figure 2.1, the heights of the columns h_c are 12 ft., and the beams span $l_b = 30$ ft. The tributary length per bay of the structure is also 30 ft.

Table A.1 Load estimates for typical building components

Component	Weight
floor slab	40 psf[a]
floor deck	5 psf
partition walls	20 psf
miscellaneous	20 psf
floor beams	75 plf[b]
girders	100 plf
columns	200 plf
total weight per tributary area	$\sim$ 120 psf

[a]psf = "pounds per square foot"
[b]plf = "pounds per linear foot"

The lateral design load for the example is found by distributing the base shear force among the building stories according to Section 2334 of the UBC,

$$F_i = \frac{(V - F_t)W_i h_i}{\sum_{j=1}^{n} W_j h_j} \tag{A.4}$$

where

V is the design base shear, (A.1)

W_i is the seismically effective weight for floor i

h_i is the *total* height of floor i

and F_t is given by

$$F_t = \begin{cases} \min(0.07TV, 0.25V), & \text{if } T > 0.7, \\ 0, & \text{if } T \leq 0.7. \end{cases} \tag{A.5}$$

The moment in each column and beam member is estimated using the portal method of analysis, and the member moments of inertia are designed based on the maximum inter-story drift ratio requirement. For a SMRF such as the example building, $R_w = 12$ is appropriate. The maximum inter-story drift ratio (i.e., ratio of inter-story displacement to story height) for a SMRF is $\varphi = 0.03/R_w = 0.0025$. To calculate the required moment of inertia, the bending moments at the connections are initially assumed to be distributed between the column and the beam such that the beam carries 70% of the moment and the columns 30% (Vance 1996). So,

$$I_b = \frac{M_{b_i} l_b}{6E(0.7\varphi)} \tag{A.6a}$$

$$I_c = \frac{M_{c_i} h_c}{6E(0.3\varphi)}, \tag{A.6b}$$

where

M_{b_i} is the moment in the beam at floor i

M_{c_i} is the moment in the columns at floor i

l_b is the length of the beam

h_c is the height of the column

E is the modulus of elasticity

φ is the inter-story drift ratio requirement.

Taking the minimum drift limit specified by the code as the only design criteria yields a design which is far too flexible; the fundamental period in this case for the two story structure is close to 0.7 sec. In addition, using wide-flange shapes from the LRFD manual (1986) whose moments of inertia corresponded to those calculated from Equations A.6a and A.6b and performing a static analysis, the moment capacities for the beams from this design are found to be exceeded when

the beams are subject to the estimated dead loads plus the lateral design loads from the earthquake. Consequently, the beam and column moments of inertia (MOIs) are increased by a factor of 2. The resulting MOIs are displayed in Table 2.1. Also shown in Table 2.1 are the drift ratios in each floor calculated for the design lateral load on the 2DOF model.

A.3 2DOF modal model of building

A mathematical model of the structure is created on the basis of these beam and column MOIs using standard methods of structural analysis (Sack 1989) and reduced using standard methods of finite element analysis (Cook et al. 1989; Guyan 1965) to yield a two-degree-of-freedom (2DOF) model of the system. In the assembly of the stiffness and lumped-mass matrices for this example, a few simplifying assumptions are made in order to reduce the number of degrees of freedom (DOFs). Axial deformations of the members are neglected, and hence so are the vertical DOFs. Since no externally generated moments are considered, the rotational DOFs of the joints were removed from the relevant equations of motion using Guyan reduction. Hence, the remaining DOFs are the horizontal displacements of the floors. A schematic representation of the 2DOF model corresponding to this two-story structure is pictured in Figure A.1. Linear viscous damping at two percent of critical is used to approximate the damping, and so the model can be transformed to classical normal modes (Caughey and O'Kelly 1965). The model parameters for the reduced-order model of the two-story example are shown in Table A.2, and the periods, damping ratios, and modeshape components are given in Table A.3, which is also shown in Chapter 2 as Table 2.2.

The equations of motion used to represent this second-order 2DOF system are

$$M\ddot{z} + D\dot{z} + Kz = f, \tag{A.7}$$

where $z(t), f(t) \in \mathbb{R}^2$, $z(t) = \left\{ z_1(t) \quad z_2(t) \right\}'$ is the nodal displacement of each floor, and $f = -M\bar{1}\ddot{x}_g$, where $\ddot{x}_g$ is the ground acceleration due to an earthquake, and $\bar{1}$

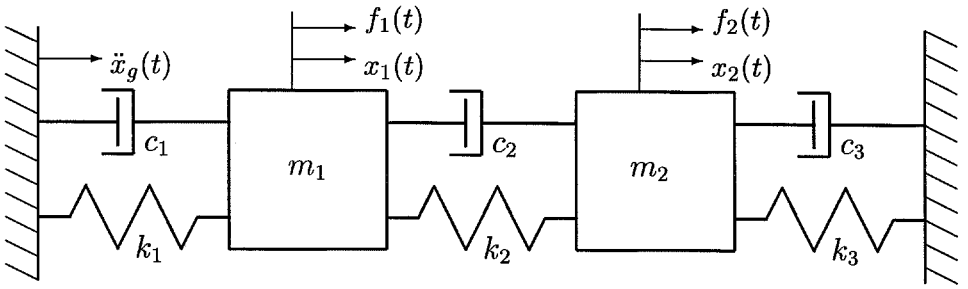

Figure A.1 A typical 2DOF system.

Table A.2 Model parameters for two-story example.

Mass Matrix	M =	$\begin{bmatrix} 303 & 0 \\ 0 & 303 \end{bmatrix}$	lb/g
Damping Matrix	D =	$\begin{bmatrix} 392 & -134 \\ -134 & 201 \end{bmatrix}$	lb-sec/in
Stiffness Matrix	K =	$\begin{bmatrix} 3.70 & -1.67 \\ -1.67 & 1.19 \end{bmatrix}$	$\times 10^5$ lb/in

is a vector of 1's. The mass, damping, and stiffness matrices are

$$M = \begin{bmatrix} m_1 & 0 \\ 0 & m_2 \end{bmatrix} \tag{A.8a}$$

$$D = \begin{bmatrix} c_1 + c_2 & -c_2 \\ -c_2 & c_2 + c_3 \end{bmatrix} \tag{A.8b}$$

$$K = \begin{bmatrix} k_1 + k_2 & -k_2 \\ -k_2 & k_2 + k_3 \end{bmatrix} \tag{A.8c}$$

are all given in Table A.2. Note that the D representing the damping matrix in the above equation should not be confused with the "D" matrix used elsewhere in the

Table A.3 Modal properties for two-story example.

Mode	Period	Frequency	Damping	Modeshape[a]	
	(sec.)	(Hz)	(%)	$\phi_1^{(r)}$	$\phi_2^{(r)}$
1	0.542	1.84	2.0	0.448	0.894
2	0.153	6.56	2.0	0.894	−0.448

[a] $\phi_i^{(r)}$ represents the i^{th} component of the r^{th} modeshape vector.

description of a linear system in state space.

Classical normal modes are enforced through proper selection of c_1, c_2, and c_4 in D, so (A.7) can be transformed to modal coordinates. Let

$$\Phi'\Phi = I \quad \text{(the identity matrix)}, \tag{A.9a}$$

$$\Phi' M^{-1} K \Phi = \Lambda = \text{diag}(\omega_i^2), \tag{A.9b}$$

$$\Phi' M^{-1} D \Phi = \Theta = \text{diag}(2\zeta_i \omega_i), \tag{A.9c}$$

and let

$$v = \Phi' z \tag{A.10}$$

be the vector of modal coordinates. Then (A.7) becomes

$$I\ddot{v} + \Theta\dot{v} + \Lambda v = \Phi' M^{-1} f = -\Phi' \bar{1} \ddot{x}_g. \tag{A.11}$$

This equation can be expressed in state space. Let $x = \left\{ v' \quad \dot{v}' \right\}'$, where $x(t) \in \mathbb{R}^4$, represent the state variable, so

$$\begin{aligned} \dot{x} &= Ax + Bw \\ y &= Cx, \end{aligned} \tag{A.12}$$

where $y(t) \in \mathbb{R}^{n_p}$ is the vector of n_p output variables and C represents the transformation from the state variables to the output variables. The output variables

contain both the variables used to compute the system performance and the measured outputs that can be fed back to the controller. When the input is ground motion due to an earthquake, the excitation is given by $w = -\bar{1}\ddot{x}_g$, where $\bar{1}$ is a 4×1 vector of 1's. For this example, y contains the inter-story drift ratios of the model, and may also represent the drift velocities as well, since the velocities are needed for the out-crossing rate calculation (see (2.12) in Chapter 2). The state matrices for the system are given by

$$\left[\begin{array}{c|c} A & B \\ \hline C & 0 \end{array}\right] = \left[\begin{array}{cc|c} 0 & I & 0 \\ -\Lambda & -\Theta & \Phi' \\ \hline \multicolumn{2}{c|}{C} & 0 \end{array}\right], \tag{A.13}$$

where C performs the appropriate scaling and transformation to yield the output variable vector y.

To obtain the inter-story drift ratios and their velocities as the performance variables, C is of the form

$$C = \frac{1}{h_c}\begin{bmatrix} 1 & 0 & 0 & 0 \\ -1 & 1 & 0 & 0 \\ 0 & 0 & 1 & 0 \\ 0 & 0 & -1 & 1 \end{bmatrix}\begin{bmatrix} \Phi \\ \Phi \end{bmatrix}, \tag{A.14}$$

where h_c is the height of each story. This expression leads to the inter-story drift performance variables

$$\begin{aligned} \varphi_1(t) &= \frac{x_1(t)}{h_c}, \\ \varphi_2(t) &= \frac{(x_2(t) - x_1(t))}{h_c}, \\ \dot{\varphi}_1(t) &= \frac{\dot{x}_1(t)}{h_c}, \\ \dot{\varphi}_2(t) &= \frac{(\dot{x}_2(t) - \dot{x}_1(t))}{h_c}. \end{aligned} \tag{A.15}$$

In the text, C may differ from (A.14), depending on the particular application.

Appendix B

Notation conventions

The following (fairly standard) symbols are used in this thesis:

- $\mathbb{R}$ represents the real numbers.
- $\mathbb{C}$ represents the complex numbers.
- $\mathbb{R}^N$ represents a real Euclidean space of dimension N.
- $\mathbb{C}^N$ represents a complex Euclidean space of dimension N.
- $\mathbb{N}$ represents the natural (counting) numbers, i.e., $\{1, 2, \dots\}$.

In addition, the following notation conventions are used throughout this thesis:

- The natural numbers are typically represented with the lower-case math-italic i, j, n, m r, and sometimes with an upper-case N, typically used to specify the dimension of a space.
- Scalars are represented with Greek letters (ω, ζ), or sometimes by lower-case math italic letters with a descriptive subscript.
- Vectors are represented as both lowercase math-italic letters (x, y) and bold-faced lower-case Greek letters ($\boldsymbol{\theta}$, $\boldsymbol{\phi}$).
- Elements of a vector are represented as subscripted math-italic letters (x_i, y_j) or subscripted bold-faced lower-case Greek letters ($\boldsymbol{\theta}_i$).

- Matrices are represented as uppercase math-italic letters (M, A), although G is reserved to describe linear systems, as is described next, and N is used as described above.

- Linear systems are represented with a math-italic G, often subscripted with a descriptive label (G_{olp}, G_{clp}).

- Uppercase Greek letters also represent matrices (Θ, Φ).

- (Abstract) sets are represented with either bold-faced upper-case Greek letters ($\mathbf{\Theta}$, $\mathbf{\Phi}$) or caligraphic upper-case letters ($\mathcal{D}$, $\mathcal{M}$).

Bibliography

American Institute of Steel Construction, Inc. (1986). *Manual of Steel Construction: Load and Resistance Factor Design* (First ed.). American Institute of Steel Construction, Inc.

Balas, G. (1990). *Robust Control of Flexible Structures: Theory and Experiments.* Ph.D. thesis, California Institute of Technology, Pasadena, California.

Balas, G. J. (1997, April). Synthesis of controllers for the active mass driver system in the presence of uncertainty. In L. Kempner and C. B. Brown (Eds.), *Building to Last: Proceedings of Structures Congress XV*, Volume 2, Portland, Oregon, pp. 1270–1274. ASCE.

Balas, G. J., J. C. Doyle, K. Glover, A. Packard, and R. Smith (1994). *μ-Analysis and Synthesis Toolbox: User's Guide.* MUSYN Inc. and The Mathworks Inc.

Beck, J. L. (1978). *Determining Models of Structures from Earthquake Records.* Ph.D. thesis, California Institute of Technology.

Beck, J. L. (1989, August). Statistical system identification of structures. In *Proceedings of the 5th International Conference on Structural Safety and Reliability*, New York, pp. 1395–1402. ASCE.

Beck, J. L. (1990). *User's Guide for Mode-ID.* Pasadena, California: California Institute of Technology. Version 5.0.

Beck, J. L. (1996, June). System identification methods applied to measured seismic response. In *Proceedings of the 11th World Conference on Earthquake Engineering*, Acapulco, Mexico.

Beck, J. L. and P. C. Jennings (1980). Structural identification using linear models

and earthquake records. *Earthquake Engineering and Structural Dynamics 8*, 145–160.

Beck, J. L. and L. S. Katafygiotis (1998). Updating structural dynamic models and their uncertainties: statistical system identification. *ASCE Journal of the Engineering Mechanics Division*. To appear.

Beck, J. L., B. S. May, and D. C. Polidori (1994). Determination of modal parameters from ambient vibration data for structural health monitoring. In *Proceedings First World Conference on Structural Control*, Pasadena, California, pp. TA3:3–TA3:12.

Beck, J. L., B. S. May, D. C. Polidori, and M. W. Vanik (1995, December). Ambient vibration surveys of three steel-frame buildings strongly shaken by the 1994 northridge earthquake. Technical Report SAC 95–04, SAC.

Benjamin, J. R. and C. A. Cornell (1970). *Probability, Statistics, and Decision for Civil Engineers*. New York: McGraw-Hill.

Box, G. E. P. and G. C. Tiao (1973). *Bayesian inference in statistical analysis*. John Wiley and Sons, Inc.

Breitung, K. W. (1989). Asymptotic approximations for probability integrals. *Probabilistic Engineering Mechanics 4*, 187–190.

Breitung, K. W. (1991). Probability approximations by log likelihood maximization. *ASCE Journal of the Engineering Mechanics Division 117*, 457–477.

Breitung, K. W. (1994). *Asymptotic Approximations for Probability Integrals*. Number 1592 in Lecture Notes in Mathematics. Berlin: Springer Verlag.

Caughey, T. K. and M. E. J. O'Kelly (1965). Classical normal modes in damped linear dynamic systems. *Journal of Applied Mechanics 32*, 583.

Chung, L. L., R. C. Lin, A. M. Reinhorn, and T. T. Soong (1989). Experiments on active control for mdof seismic structures. *ASCE Journal of the Engineering Mechanics Division 115*, 1609–1627.

Chung, L. L., A. M. Reinhorn, and T. T. Soong (1988). Experiments on active

control of seismic structures. *ASCE Journal of the Engineering Mechanics Division 114*, 241–256.

Clough, R. W. and J. Penzien (1975). *Dynamics of Structures.* New York: McGraw-Hill, Inc.

Computer Boards, Inc. (1991). *CIO-DDA06 User's Manual.* Mansfield, MA: Computer Boards, Inc. Revision 1.0.

Computer Boards, Inc. (1994). *CIO-DAS16/330 User's Manual.* Mansfield, MA: Computer Boards, Inc. Revision 2.0.

Cook, R. D., D. S. Malkus, and M. E. Plesha (1989). *Concepts and Applications of Finite Element Analysis* (Third ed.). New York: John Wiley & Sons.

Doyle, J. C., B. A. Francis, and A. R. Tannenbaum (1992). *Feedback Control Theory.* New York: Macmillan Publishing Company.

Doyle, J. C., K. Glover, P. P. Khargonekar, and B. A. Francis (1989, August). State-space solutions to standard $\mathcal{H}_2$ and $\mathcal{H}_\infty$ control problems. *IEEE Transactions on Automatic Control 34*(8), 831–847.

Dyke, S. J., B. F. Spencer, A. E. Belknap, K. J. Ferrell, P. Quast, and M. K. Sain (1994, August). Absolute acceleration feedback control strategies for the active mass driver. In *Proceedings of the First World Conference on Structural Control*, pp. TP1–51–TP1–60.

Dyke, S. J., B. F. Spencer, P. Quast, and M. K. Sain (1995). Role of control-structure interaction in protective system-design. *ASCE Journal of the Engineering Mechanics Division 121*(2), 322–338.

Dyke, S. J., B. F. Spencer, P. Quast, M. K. Sain, D. C. Kaspari, and T. T. Soong (1996). Acceleration feedback-control of MDOF structures. *ASCE Journal of the Engineering Mechanics Division 122*(9), 907–918.

Field, R. V., L. A. Bergman, and W. B. Hall (1995). Computation of probabilistic stability measures for a controlled distributed parameter system. *Probabilistic Engineering Mechanics 10*, 181–192.

Franklin, G. F., J. D. Powell, and A. Emami-Naeini (1994). *Fedback Control of Dynamic Systems* (Third ed.). Reading, Massachusetts: Addison Wesley.

Guyan, R. J. (1965). Reduction of stiffness and mass matrices. *American Institute of Aeronautics and Astronautics 3*(2), 380.

Housner, G. W. (Ed.) (1992, July). *U.S.–Italy–Japan Workshop/Symposium on Structural Control and Intelligent Systems*, Sorrento, Italy and Genoa, Italy. U.S. Panel on Structural Control Research.

Housner, G. W., L. A. Bergman, T. K. Caughey, A. G. Chassiakos, R. O. Claus, S. F. Masri, R. E. Skelton, T. T. Soong, B. F. Spencer, and J. T. P. Yao (1997). Structural control: Past, present, and future. *ASCE Journal of the Engineering Mechanics Division*. To appear.

Housner, G. W. and S. F. Masri (Eds.) (1990, October). *U.S. National Workshop on Structural Control Research*, Los Angeles, California. U.S. National Science Foundation.

Housner, G. W. and S. F. Masri (Eds.) (1993, December). *Proceedings of International Workshop on Structural Control*, Honolulu, Hawaii. U.S. Panel on Structural Control Research and Japan Panel on Structural Response Control.

Housner, G. W., S. F. Masri, and A. G. Chassiakos (Eds.) (1994, August). *Proceedings of the First World Conference on Structural Control*, Pasadena, California. International Association for Structural Control.

Housner, G. W., T. T. Soong, and S. F. Masri (1994, August). Second generation of active structural control. In *Proceedings of the First World Conference on Structural Control*, pp. Panel–3–Panel–18.

International Conference of Building Officials (1994). *Uniform Building Code*. Whittier, California: International Conference of Building Officials.

Jaynes, E. T. (1978). Where do we stand on maximum entropy? In R. D. Levine and M. Tribus (Eds.), *Maximum Entropy Formalism Conference*, Cambridge, Massachusetts, pp. 15–118. Massachusetts Institute of Technology.

Jeffreys, H. (1961). *Theory of Probability.* Oxford University Press.

Kanai, K. (1957). Semi-empirical formula for the seismic characteristics of the ground. *University of Tokyo Bulletin of Earthquake Research Institute 35*, 309–325.

Kempner, L. and C. B. Brown (Eds.) (1997, April). *Building to last: proceedings of the structures congress XV*, Volume 2, Portland, Oregon. ASCE.

Lin, Y. K. (1976). *Probabilistic Theory of Structural Dynamics.* Malabar, FL: Robert E. Krieger Publishing Company.

Lin, Y. K. and G. Q. Cai (1995). *Probabilistic Theory of Structural Dynamics: Theory and Applications.* New York: McGraw-Hill, Inc.

Lu, J. and R. E. Skelton (1997, April). Covariance control using closed loop modeling for structures. In L. Kempner and C. B. Brown (Eds.), *Building to Last: Proceedings of Structures Congress XV*, Volume 2, Portland, Oregon, pp. 1285–1289. ASCE.

Madsen, H. O., S. Krenk, and N. C. Lind (1986). *Methods of Structural Safety.* Englewood Cliffs, NJ: Prentice Hall, Inc.

Marrison, C. I. and R. F. Stengel (1995). Stochastic robustness synthesis applied to a benchmark control problem. *International Journal of Robust and Nonlinear Control 5*, 13–31.

Mason, A. B., J. L. Beck, J. C. Chen, and R. R. Ullmann (1989, May). Modal parameter identification of an offshore platform from earthquake response records. In *Proceedings Sessions Related to Seismic Engineering at Structures Congress*, pp. 217–226. ASCE.

May, B. S. and J. L. Beck (1997). Probabilistic control for the active mass driver benchmark structural model. *Earthquake Engineering and Structural Dynamics*. to appear.

Moser, A. N. (1992). *An Experimental Investigation of Modeling and Optimal Control of Modified Space Structures.* Ph.D. thesis, California Institute of

Technology, Pasadena, California. Also available as Report DYNL-92-1.

Moser, A. N. and T. K. Caughey (1991). Some experience with identification of the Caltech experimental space structure. In *Proceedings of the American Control Conference.*

Murray, R. M., E. Wemhoff, and M. Kantner (1995, May). *Sparrow Reference Manual.* California Institute of Technology. Version 2.1f. Available electronically from http://avalon/~murray/sparrow.

Nisar, A. D., S. D. Werner, and J. L. Beck (1992). Assessment of UBC seismic design provisions using recorded building motions. In *Proceedings Tenth World Conference on Earthquake Engineering*, Balkema, Rotterdam, pp. 5723–5728.

Paganini, F. (1996). *Sets and Constraints in the Analysis of Uncertain Systems.* Ph.D. thesis, California Institute of Technology.

Papadimitriou, C., J. L. Beck, and L. Katafygiotis (1997). Asymptotic expansions for reliabilities and moments of uncertain dynamic systems. *ASCE Journal of Engineering Mechanics*. In press.

Papadimitriou, K. (1990). Stochastic characterization of strong ground motion and applications to structural response. Technical Report EERL 90-03, California Institute of Technology.

Papoulis, A. (1965). *Probability, Random Variables, and Stochastic Processes.* McGraw-Hill Book Company.

Pierre, D. A. (1986). *Optimization Theory with Applications.* Mineola, NY: Dover Publications, Inc.

Press, W. H., S. A. Teukolsky, W. T. Vetterling, and B. P. Flannery (1992). *Numerical Recipes in C, the Art of Scientific Computing* (Second ed.). Cambridge University Press.

Rice, S. O. (1944). Mathematical analysis of random noise. *Bell System Technical Journal 23*, 282–332.

Sack, R. L. (1989). *Matrix Structural Analysis.* Boston: PWS-KENT Publishing Company.

Smith, H. A., S. E. Breneman, and O. Sureau (1997, April). $\mathcal{H}_\infty$ static and dynamic output feedback control of the AMD benchmark problem. In L. Kempner and C. B. Brown (Eds.), *Building to Last: Proceedings of Structures Congress XV*, Volume 2, Portland, Oregon, pp. 1280–1284. ASCE.

Smith, H. A. and J. G. Chase (1994, August). Robust disturbance rejection using $\mathcal{H}_\infty$ control for civil structures. In *Proceedings of the First World Conference on Structural Control*, Pasadena, California, pp. TP4–33–TP4–42.

Söderström, T. and P. Stoica (1989). *System Identification.* Prentice Hall.

Soong, T. T. (1990). *Active Structural Control: Theory and Practice.* Essex, England: Longman Scientific & Technical.

Soong, T. T. and M. Grigoriu (1993). *Random Vibration of Mechanical and Structural Systems.* New Jersey: Prentice-Hall.

Spencer, B. F. (1997). Special issue on benchmark structural control problem. *Earthquake Engineering and Structural Dynamics.* to appear.

Spencer, B. F., S. J. Dyke, and H. S. Deoskar (1997a). Benchmark problems in structural control, part I: Active mass driver system. *Earthquake Engineering and Structural Dynamics.* to appear.

Spencer, B. F., S. J. Dyke, and H. S. Deoskar (1997b). Benchmark problems in structural control, part II: Active tendon system. *Earthquake Engineering and Structural Dynamics.* to appear.

Spencer, B. F. and D. C. Kaspari (1994a). Reliability based optimal structural control. In *Proceedings 5th U. S. National Conference on Earthquake Engineering*, pp. 703–712.

Spencer, B. F. and D. C. Kaspari (1994b). Structural control design: a reliability-based approach. In *Proceedings of the American Control Conference*, pp. 1062–1066.

Spencer, B. F., M. K. Sain, C.-H. Won, D. C. Kaspari, and P. M. Sain (1994). Reliability-based measures of structural control robustness. *Structural Safety 15*, 111–129.

Stengel, R. F. and L. R. Ray (1991, January). Stochastic robustness of linear time-invariant control systems. *IEEE Transactions on Automatic Control 36*(1), 82–87.

Tajimi, H. (1960, July). A statistical method of determining the maximum response of a building structure during an earthquake. In *Proceedings of the Second World Conference on Earthquake Engineering*, Volume II, Tokyo and Kyoto, pp. 781–798.

The MathWorks, Inc. (1994a). *Matlab User's Guide.* Natick, Massachusetts: The MathWorks, Inc.

The MathWorks, Inc. (1994b). *Simulink User's Guide.* Natick, Massachusetts: The MathWorks, Inc.

The MathWorks, Inc. (1995). *Matlab Control System Toolbox User's Guide.* Natick, Massachusetts: The MathWorks, Inc.

Vance, V. L. (1996, June). *Effects of architectural walls on building response to ambient and seismic excitations.* Ph.D. thesis, Stanford University.

Veneziano, D., M. Grigoriu, and C. A. Cornell (1977, June). Vector-process models for system reliability. *ASCE Journal of the Engineering Mechanics Division 103*(EM3), 441–460.

Werner, S. D., J. L. Beck, and M. B. Levine (1987, February). Seismic response evaluation of Meloland Road Overpass using 1979 Imperial Valley earthquake records. *International Journal of Earthquake Engineering and Structrual Dynamics 15*, 249–274.

Yang, J. N., J. C. Wu, A. M. Reinhorn, M. Riley, W. E. Schmitendorf, and F. Jabbari (1994, August). Experimental verifications of $\mathcal{H}_\infty$ and sliding mode control for seismic-excited buildings. In *Proceedings of the First World Conference on Structural Control*, pp. TP4–63–TP4–72.

Yoshida, K. and T. Watanabe (1994, August). Robust control of structural vibrations using active dynamic vibration absorber system. In *Proceedings of the First World Conference on Structural Control*, Pasadena, California, pp. TP4–53–TP4–62.

Zhou, K., K. Glover, and J. C. Doyle (1996). *Robust and Optimal Control.* New Jersey: Prentice Hall.